Building a light driven synthetic carbon dioxide fixation cycle within microdroplets

Dissertation

zur
Erlangung des Doktorgrades
der Naturwissenschaften
(Dr. rer. nat.)

Dem Fachbereich Biologie
der Philipps-Universität Marburg
vorgelegt von

Tarryn E. Miller
aus Grand Junction, Colorado, USA

Marburg/Lahn, Deutschland, 2020

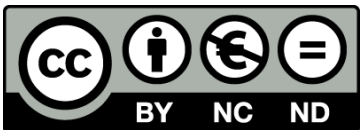

Die Untersuchungen zur vorliegenden Arbeit wurden von September 2015 bis Oktober 2020 unter der Betreuung von Herrn Prof. Dr. Tobias Jürgen Erb in Marburg am Max-Planck-Institut für terrestrische Mikrobiologie in der Abteilung Biochemie und Synthetischer Metabolismus durchgeführt.

Vom Fachbereich Biologie

der Philipps-Universität Marburg als Dissertation

angenommen am:

Erstgutachter: Prof. Dr. Tobias Erb

Zweitgutachter: Prof. Dr. Stefan Rensing

Weitere Mitglieder der Prüfungskommission:

Prof. Dr. Martin Thanbichler

Prof. Dr. Hans-Ulrich Mösch

Prof. Dr. Jean-Christophe Baret

Tag der mündlichen Prüfung: November 25th, 2020

Erklärung

Ich versichere, dass ich meine Dissertation mit dem Titel „**Building a light driven synthetic carbon dioxide fixation cycle within microdroplets**“ selbstständig ohne unerlaubte Hilfe angefertigt und mich dabei keiner anderen als der von mir ausdrücklich bezeichneten Quellen und Hilfsmittel bedient habe.

Diese Dissertation wurde in der jetzigen oder einer ähnlichen Form noch bei keiner anderen Hochschule eingereicht und hat noch keinen sonstigen Prüfungszwecken gedient.

Marburg, den 06.10.2020

Tarryn Miller

Parts of this work were created through collaboration with the Center de Recherche Paul Pascal, Bordeaux, France **and their experimental contributions are mentioned:**

Microfluidic experiments were performed with Thomas Beneyton (Center de Recherche Paul Pascal, Bordeaux, France).

Mathias Girault developed all LabView software (Center de Recherche Paul Pascal, Bordeaux, France).

Publications

Part of this work was published in the following articles:

Miller, T. E., Beneyton. T., Schwander, T., Diehl, C., Girault, M., McLean, R., Chotel, T. Claus, P., Cortina, N. S., Baret, J.C., and Erb, T. J. (2020) "Light-powered CO_2 fixation in a chloroplast with natural and synthetic parts." Science. Vol. 368, Issue 6491, pp. 649-654.

Burgener, S., Luo, S. McLean, R., **Miller, T. E.** and Erb. T. J. (2020) "A roadmap towards integrated catalytic systems of the future." Nature Catalysis. Issue 3, pp. 186–192.

Bernhardsgrütter, I. Stoffel, G. M. M., **Miller, T. E.**, and Erb. T. J. (Accepted, Current Opinion in Biotechnology) "Carboxylases for sustainable biotechnology: from mechanism to application."

I stand at the seashore, alone, and start to think.
There are the rushing waves
mountains of molecules
each stupidly minding its own business
trillions apart
yet forming white surf in unison

Ages on ages
before any eyes could see
year after year
thunderously pounding the shore as now.
For whom, for what?
On a dead planet
with no life to entertain.

Never at rest
tortured by energy
wasted prodigiously by the Sun
poured into space.
A mite makes the sea roar.

Deep in the sea
all molecules repeat
the patterns of one another
till complex new ones are formed.
They make others like themselves
and a new dance starts.
Growing in size and complexity
living things
masses of atoms
DNA, protein
dancing a pattern ever more intricate.

Out of the cradle
onto dry land
here it is
standing:
atoms with consciousness;
matter with curiosity.

Stands at the sea,
wonders at wondering: ***I***
a universe of atoms
an atom in the Universe*.*

1955, Richard Feynman, Physicist

Contents

Summary

Cells are highly integrated biological systems that perform complex tasks. These self – sustained compartments exist thermodynamically out-of-equilibrium with the environment and require a constant influx of energy to drive the internal metabolism and prevent decay to equilibrium. Photosynthetic autotrophic organisms convert light into chemical energy, which is the driving force for the transformation of inorganic carbon into organic compounds. Ultimately, the photosynthetic conversion of light energy proceeds through membrane bound protein complexes, which generate the energy-rich chemical cofactors adenosine triphosphate (ATP) and reduced nicotinamide adenine dinucleotide phosphate (NADPH). ATP and NADPH are subsequently used to fuel metabolic processes, in particular the fixation of carbon dioxide (CO_2) through the Calvin-Benson-Bassham (CBB) cycle. So far, efforts to create an artificial cell or organelle that mimics autotrophic photosynthesis have not succeeded in linking light harvesting and carbon fixation at the micron scale. In this work, microfluidics and synthetic biology were combined in an attempt to develop and optimize a functional mimic of a chloroplast in a mostly bottom-up fashion.

In this work, a photosynthetic energy module was developed based on thylakoid membranes of spinach chloroplasts, its function optimized, and then used to power different enzymatic reactions and complex metabolic networks by light. Microfluidic-based encapsulation of the photosynthetic energy module generated cell-sized droplets that can be equipped with enzymes, energized by light and analyzed for catalytic function in multiplex and real-time. The activity of the micro-droplets can be programmed and controlled by adjusting internal compositions (e.g. thylakoid membranes and enzyme concentrations) as well as using light as an external trigger.

Coupling this photosynthetic energy module with a 17-enzyme, new-to-nature CO_2-fixation cycle, created a structural and functional mimic of a chloroplast that continuously converts CO_2 into the organic compound glycolate. In essence, natural and synthetic parts have been combined to drive anabolic reactions by light at a micron scale. This platform represents a basis useful for multiple applications in both top-down and bottom-up synthetic biology approaches, while also signifying another step on the way towards creating functional mimics of living cells.

Zusammenfassung

Zellen sind hochintegrierte biologische Systeme, die komplexe Aufgaben ausführen. Diese sich selbsterhaltenden Kompartimente befinden sich fernab des thermodynamischen Gleichgewichts mit der Umwelt und erfordern einen konstanten Zufluss von Energie, um den inneren Stoffwechsel anzutreiben und die Rückkehr zurück ins Gleichgewicht zu verhindern. Photosynthetische, autotrophe Organismen wandeln Licht in chemische Energie um, die die treibende Kraft für die Umwandlung von anorganischem Kohlenstoff in organische Verbindungen ist. Letztendlich erfolgt die photosynthetische Umwandlung von Lichtenergie über membrangebundene Proteinkomplexe, die die energiereichen chemischen Cofaktoren Adenosintriphosphat (ATP) und reduziertes Nicotinsäureamid-Adenin-Dinukleotid-Phosphat (NADPH) erzeugen. ATP und NADPH werden dann verwendet, um Stoffwechselprozesse anzutreiben, insbesondere die Fixierung von Kohlendioxid (CO_2) durch den Calvin-Benson-Bassham- (CBB-)Zyklus. Bisher sind Versuche, künstliche Systeme, Zellen oder Organellen zu erschaffen, die autotrophe Photosynthese imitieren können, daran gescheitert, die Lichtsammlung und Kohlenstofffixierung im Micron-Maßstab miteinander zu verbinden. Hier wurden nun Microfluidics und synthetische Biologie kombiniert, um größtenteils „bottom-up“ eine funktionelle Chloroplasten-Nachbildung zu entwickeln und zu optimieren.

In dieser Arbeit wurde ein photosynthetisches Energiemodul basierend auf Thylakoidmembranen von Spinatchloroplasten entwickelt, dessen Funktion optimiert und dann verwendet wurde, um verschiedene enzymatische Reaktionen und komplexe metabolische Netzwerke durch Licht anzutreiben. Die Einkapselung des photosynthetischen Energiemoduls durch Microfluidics erzeugte Tröpfchen in der Größe von Zellen, die mit Enzymen ausgestattet, mit Licht angeregt und im Multiplex und in Echtzeit auf ihre katalytische Funktion analysiert werden können. Die Aktivität der „Micro-Droplets“ kann programmiert und gesteuert werden, indem die interne Zusammensetzung (z.B. Thylakoidmembranen und Enzymkonzentrationen) verändert und Licht als externer Auslöser verwendet wird.

Durch die Kopplung dieses photosynthetischen Energiemoduls mit einem neuartigen CO_2-Fixierungszyklus, bestehend aus 17 Enzymen, wurde eine strukturelle und funktionelle Nachahmung eines Chloroplasten erzeugt, der CO_2 kontinuierlich in Glykolat umwandelt. Im

Wesentlichen wurden natürliche und synthetische (Bau-)Teile kombiniert, um anabole Reaktionen durch Licht im Micron-Maßstab zu steuern. Diese Plattform stellt die Basis für viele potenzielle Anwendungen dar, die in der synthetischen Biologie für sowohl „top-down“ als auch „bottom-up“ Strategien von Nutzen sind, und ist gleichzeitig ein weiterer Schritt auf dem Weg zur Nachbildung funktionaler, lebender Zellen.

1. Introduction

1.1. Life

What is life? Scientists and philosophers have sought an answer to this question for millennia. Something that is living can be recognized with ease, however, defining *life* is indeed a complex issue. Scientists have asked questions such as: What features make something alive? Or, when does matter become alive? These large questions lack clear answers however, by dividing complex issues into smaller more manageable parts scientists can address these questions; e.g. when does a bacterial cell divide? By answering these simpler questions, scientists have begun to elucidate fundamentally what is *required* to be alive rather than specifically what it *is* to be alive. In his book titled, "What is life?," Erwin Schrödinger asked the question, "How can the events within the spatial boundary of a living organism be accounted for with physics and chemistry?" Thinking thermodynamically, he noted that life exists outside of equilibrium with its environment and that a continuous supply of energy is required to maintain life[1]. This can only be done within a confined space and therefore, life requires a boundary. In a living system, that boundary encloses what we call a cell.

Thus, life requires cells. Even viruses, while not necessarily considered alive cannot reproduce without a portion of their lifecycle existing within the confines of a cellular environment. This has been a core principle of biology[2]. A cell is an intricately organized and controlled chemical factory that exists outside of equilibrium with the environment. They are equipped with the machinery that gives them the ability to take matter and energy from the surroundings and use this to grow and eventually replicate. These self-organizing and self-regulated compartments are incredibly diverse. Nevertheless, they share certain common principles that are consistent among them. These principles are[3,4]:

> **Program** is the organized plan that is encoded in DNA. This blueprint influences the structure, components of the cell, and kinetics of the interaction of those components. The plan or program summarized in the DNA is maintained and passed on through generations and will encode for the proteins and nucleic acids that carry out the cellular functions.

Adaptation is the capacity of the living system, or cell to make modifications to the program itself. The living system exists as part of the environment around it and a program must be plastic, allowing modifications that ensure the survival of the species after changes in the environment. Modifications of the program can be achieved through mechanisms such as mutation or horizontal gene transfer, and eventual selection of these **adaptations**. Changes providing a benefit will be passed down through generations and allow for a long-term response to changes in the environment or circumstances around a living system.

Energy is required to prevent the cell from decaying to equilibrium. A consistent source of energy is required to drive the essential functions of the living system e.g. facilitation of active transport, movement, and metabolism. On earth, the primary source of this energy is derived from the sun. Through photosynthesis, energy rich chemicals are produced which are used to counteract and prevent entropic decay to equilibrium.

Metabolism is a hallmark of a living cell; it is the execution of the program. This is the complex chemistry that occurs within a cell. Through metabolism the necessary components to grow are regenerated compensating for the inevitable losses that occur within the living system. Examples of this are the (re-)synthesis of cofactors; passive or active transport of chemicals into or out of the living organism; or the repair of damaged enzymes, cofactors, and nucleic acids. In particular, carbon fixation restores the organic molecules used for both energy regeneration and as carbon building blocks for other processes in the cell. It is important that many reactions can occur simultaneously within the living system. This occurs naturally in sub cellular compartments or through the speed and selectivity of enzymes, so that enzymes do not react uncontrollably with any chemical that they come in contact with. Regulation of the program can occur through feedback or feedforward responses.

Compartmentalization. Living systems must be confined to a limited volume and in cells this this volume is enclosed with a semipermeable membrane. By defining an *in* and an *out* of a living system allows for it to exist outside of equilibrium with the environment. Inside this compartment important chemical components can be enriched allowing fundamental biochemical reactions to take place and the toxic,

deleterious components can be exported or isolated from the inside of the compartment. Diverse compartments also exist within a cell e.g. bacterial microcompartments that are enclosed with a proteinaceous shell, or a nucleus enclosed with a membrane in a eukaryotic cell.

Regulation is the immediate response to the environment in a feedback or feedforward manner to use the aforementioned program to respond to the environment. This requires the living system to perceive and immediately adapt its "behavior" on a molecular level to the world around it. Examples of this include adapting to high light conditions, new carbon source, taxis, or cell-cell communication.

Replication or self-replication is the ability of an organism to create another copy of itself. Here the program is copied and passed on to daughter cells. Reproduction is a mechanism for the living system to reset. Furthermore, this enables an organism to undergo Darwinian evolution.

These principles: program, adaptation, energy, metabolism, compartmentalization, regulation, and replication reflect both the thermodynamic and kinetic principles that govern life and cells on earth. When observing the life that exists on this planet the implementation of these principles is clear. For example, natural selection is simply adaptation and photosynthetic linear electron flow is a source of energy. These guiding principles can also be used as tools in the laboratory e.g. directed evolution. Particular adaptations in the program could be selected by creating artificial conditions for an organism to evolve[5,6]. This is enhanced by using various techniques to modify these principles including: genetic engineering that will alter the program[7]; or by using RNAi[8] or CRISPRi[9] that can regulate the cell to specific instructions on a short term. Using these techniques one can further elucidate *what is life*? To study life in this fashion is called a top-down approach, essentially taking an organized system apart, even minimizing it[10], and studying it. However, there is also what is called a bottom-up approach, which would be building more complex systems from simpler pieces to learn about the whole[11,12]. The act of (re)-building living systems can provide insights and better understanding about life and demonstrate a true understanding of the principles that govern life[13].

In Mary Shelley's book, "Frankenstein, or, the Modern Prometheus," Dr. Frankenstein reanimated a being that was built from parts of others, and in an analogous fashion, can

scientists create life from the bottom up[14]? Despite having an understanding of the principles that govern life or that are required for life, scientists have yet to build life from scratch. However, using various approaches scientists from many fields have begun to create systems, which mimic some of the processes of life including energy regeneration[15,16], compartmentalization [17], self-replication [18], metabolism [19], etc.

With a similar mindset, this work set out to create a structural and biochemical mimic of a chloroplast, requiring interdisciplinary approaches. In order to even begin to build life from the bottom up, the basic key principles that define life must be established in the lab. In an *in vitro* setting, a robust supply of chemical energy and metabolism must precede the implementation of repair and reproduction. Starting with an autotrophic pathway that generates the initial building blocks for other subsequent pathways provides a foundation that can be built upon. Here, light-driven carbon fixation was compartmentalized through the encapsulation into to cell-sized water-in-oil (w/o) droplets. This introduction will focus on the tools and components, both synthetic and natural, used to establish some of these essential pillars (specifically energy, regeneration, seclusion, and compartmentalization) in the lab.

1.2. Energy and cofactor regeneration—oxygenic photosynthesis

As Schrödinger stated, cells operate out-of-equilibrium and to sustain this state, there must be a constant flux of energy in order to enable cellular functions. Organisms across the kingdoms of life employ different strategies for this. Here, the strategy employed by photoautotrophs will be discussed. In plants, algae, and cyanobacteria there is specialized photosynthetic machinery that allows for the harvesting of light energy and its conversion into chemical energy in the form of adenosine triphosphate (ATP) and reduced nicotinamide dinucleotide phosphate (NADPH). This chemical energy can, in turn, be used to synthesize organic compounds from CO_2 through the Calvin-Benson-Bassham (CBB) cycle and eventually fueling other cellular processes, building biomass, and feeding the majority of the biosphere. The complex energy converting biological machines generate molecular oxygen by using water as an electron donor, use light to elevate the derived electrons to higher (useable) energy levels, and establish a proton motive force across a membrane. Oxygenic photosynthesis is one of the most significant evolutionary events and it resulted in the great oxygenation event that occurred 2.4 billion years ago[20,21]. This dramatic buildup of molecular

oxygen in the atmosphere had profound biological and geological consequences and ultimately enabled the life we encounter now.

In photosynthetic organisms, the components capable of photochemistry evolved alongside the CBB cycle, creating an incredibly interconnected system. The success of these combined processes led to the high level of oxygen in the atmosphere, which had detrimental consequences, some are discussed below.

Cyanobacteria are thought to be the evolutionary ancestors of chloroplasts, organelles specialized in photosynthesis located in the eukaryotic algae and plants[22,23]. In chloroplasts and photosynthetic eukaryotes, the complex molecular components capable of converting light-energy into chemical energy undergo complex processes to photophosphorylate ATP and photoreduce NADPH.

1.2.1. Linear electron flow

Oxygenic photosynthetic carbon fixation is driven by the chemical energy that is converted from light energy into ATP and NADPH and uses water as its primary electron donor. These reactions are coined the light reactions of photosynthesis. In cyanobacteria, and organisms that have taken them up as endosymbionts, these reactions are carried out by complexes housed on or near the thylakoid membrane (*Gleobacter* being the sole exception known to date[24]). In a first step of linear electron flow (LEF, Figure 1), at photosystem II (PSII), the photons are used to excite the special pair of chlorophyll, which undergoes complex charge separation and used to extract electrons from water, this occurs at the oxygen evolving complex. Here, eight photons are needed to oxidize two water molecules producing molecular oxygen and four protons on the side of the lumen. This is one of the most important reactions on the planet and is the source of all the oxygen in our atmosphere. The electrons extracted from the water are used to reduce plastoquinone to plastoquinol at the Q-site of PSII. These enter the Q-cycle at the Cytochrome b_6f complex, a plastoquinol—plastocyanin reductase, an intermediate step between PSII and PSI. Through this complex, two more protons are pumped across the thylakoid membrane and the electrons are used to reduce the soluble electron carrier protein, plastocyanin (PC). The reduced form of this protein, located on the lumen side of the thylakoid membrane interacts with the photosystem I (PSI). At PSI, light energy is used to oxidize PC (lumen) and reduce ferredoxin (stroma). PSI is astonishing in that it is capable of using light energy and the electrons from PC to create a reductant capable of generating

enough reducing potential to reduce ferredoxin. $NADP^+$ photoreduction occurs when the electrons from ferredoxin (Fdx) are transferred by action of the Ferredoxin—NADP+ oxidoreductase (FNR).

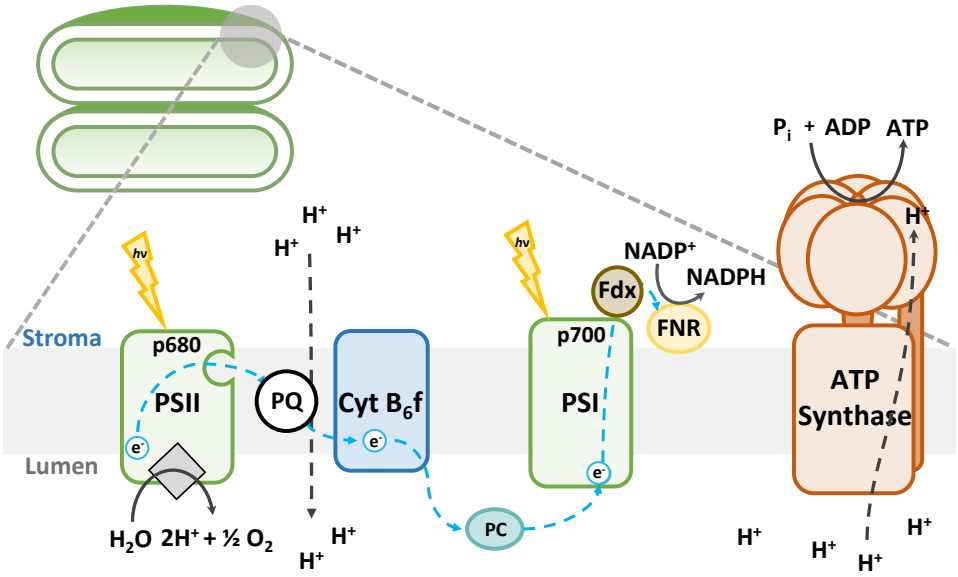

Figure 1. Schematic showing ATP and NADPH generation from linear electron flow in the thylakoid membrane. Upon excitation by light, PSII extracts electrons from water, depositing two protons per electron into the lumen, and reduces plastoquinone. The reduced plastoquinol is oxidized at the Qo site (quinol oxidation) of the cytochrome *b*$_6$*f* complex (Cyt *b*$_6$*f*) and the electrons are passed to plastocyanin (PC). During PQH_2 oxidation, two protons are deposited in the lumen. The PC will then transfer an electron to PSI that will then reduce ferredoxin (Fdx) and ferredoxin:$NADP^+$ oxidoreductase (FNR), eventually leading to the reduction of $NADP^+$, producing NADPH. The proton motive force (PMF) built through this process will be used to drive ATP synthesis through ATP synthase.

The protons that have been pumped across the membrane during this process lead to the formation of a proton motive force (PMF) that drives ATP synthesis through the F_oF_1-ATP synthase. The overall reaction of this process is:

$$8 \text{ photons} + 2\ H_2O + 2\ NADP^+ + 2.57\ ADP + 2.57\ P_i \rightarrow O_2 + 2\ NADPH + 2.57\ ATP \quad (eq.\ 1.1)$$

The resulting photon: O_2: NADPH: ATP ratio is fixed at 8: 1: 2: 2.57 due to the number of 14 subunits in the c-ring in ATP-synthase itself[25,26]. Through LEF this ratio is fixed, however other processes exist in the cell to modulate the ratio of ATP/NADPH production to meet the energy demands of the cell. In order to maintain LEF and prevent photodamage there must be a

balance in the consumption and production of NADPH and ATP. This is especially important for maintaining plasticity in the cells to compensate for varying environmental conditions and to meet cellular demands.

When comparing the NADPH and ATP demands of carbon fixation through the CBB cycle, which requires 2 NADPH for every 3 ATP (see *eq 1.2*), there is a discrepancy to the NADPH/ATP production through LEF. It has been a matter of debate if the production of ATP and NADPH through LEF is capable of meeting the demands of the CBB cycle[25,27]. However, there are mechanisms within the cell to provide extra ATP, including cyclic electron flow around PSI providing additional ATP without the concomitant generation of NADPH (discussed in Section 1.2.2).

None of this would be possible without the ancillary light-harvesting complexes (LHC) that act as antenna to increase the likelihood that energy from a photon can be used by the photosystems. These complex proteinaceous structures are filled with light active pigments like chlorophyll and photoprotective carotenoids. These undergo complex interactions with both photosystems to funnel absorbed photons to the special pairs of chlorophyll within the reaction core of each photosystem (p680 and p700, in PSII and PSI respectively). Simply put, photosynthetic antennae act much like a satellite dish, used to increase the likelihood that a photon will be captured and can be used for photochemistry. The LHC are rich in chlorophyll, on average there are 617 and 552 chlorophyll molecules per PSII and PSI reaction center, respectively[28]. This difference is due to the fact that there is slightly more PSI than PSII. In whole thylakoid preparations, the PSI/PSII was determined to be 1.13[28]. The thylakoids membranes have a very organized architecture and this ratio varies over specific parts of the membrane. On average there are 4 light harvesting complexes per PSII monomer. The chlorophyll molecules are capable of absorbing blue and red light[28].

Photoinhibition occurs when the light energy absorbed exceeds the demands of the cell. Complex regulatory mechanisms are in place to prevent the photodamage that causes photoinhibition, including non-photochemical quenching. Particular components of the light reactions are highly reactive and under such conditions, when the photons excite the reaction centers and are unable to enter into the electron transport chain can result in the formation of reactive oxygen species (ROS). In particular, O_2 will be reduced at PSI and form superoxide (O_2^-) and at PSII, O_2 will be excited from the ground state (triplet, $^3O_2$) to the singlet state ($^1O_2$).

ROS formed affects the redox state of the cell and chloroplast and it plays an important role in cell signaling and will affect protein expression[29].

As discussed above, the production and consumption of NADPH and ATP must be balanced[25]. Conditions where they are not balanced can lead to situations where the system is over reduced, which will prevent the absorbed light energy from undergoing photochemistry and result in the formation of ROS and lead to photodamage. In order to maintain plasticity through altering the NADPH and ATP production ratio is important. Cyclic electron flow can help the cell to alter the ratio in which NADPH/ATP are produced.

1.2.2. Cyclic electron flow and reduced ferredoxin

The major role of reduced ferredoxin is to reduce $NADP^+$ via FNR, however it can have other important fates within the chloroplast or cell. This can include nitrogen assimilation, amino acid synthesis, sulfur assimilation, and cyclic electron flow. Cyclic electron flow (CEF) occurs around PSI and plays an important role in the homeostasis of the cellular environment, especially under adverse conditions. In this second route for light energy utilization, electrons from ferredoxin or NADPH will reduce the plastoquinone pool, resulting in additional proton translocation at the cytochrome b_6f complex and thus generation of ATP independent of NADPH formation[30]. This modulates the ATP/NADPH energy budget and plays a role in photoprotection by preventing photoinhibition. This slows down the net oxidation by PSI and further acidifies the thylakoid lumen[31]. There are multiple routes for CEF, one of the most studied is NAD(P)H dehydrogenase (Ndh)[32-34].

Furthermore, reduced ferredoxin can be autoxidized by molecular oxygen, resulting in the formation of superoxide, a reactive oxygen species that must be detoxified. The mechanism for this is discussed in detail below.

1.2.3. Reactive oxygen species

The oxygen generated from oxygenic photosynthesis has enabled life as we know it, however, this comes at a cost. It creates a reactive environment that facilitates the generation of free radicals. In a living system, reactive oxygen species (ROS) can have harmful or even lethal effects. Organisms have evolved numerous strategies for the prevention of damage caused by ROS and many mechanisms have evolved in living systems to overcome the formation of ROS. Mutations in these systems can be fatal or significantly decrease fitness.

Oxygenic photosynthesis is a major source of ROS, forming superoxide, hydrogen peroxide, and singlet oxygen. Moreover, oxygen is an important electron acceptor, which allows photosynthetic organisms to drain excess electrons that will lead to photoinhibition and damage to PSI. Many mechanisms both prevent the creation of ROS and deal with ROS that are generated. The antioxidant capacities of the cell involve many proteins including multiple super oxide dismutases, ascorbate peroxidases, glutathione reductase, and catalase. In one example, when Fdx_{rd} reduces oxygen it forms superoxide through the Mehler reaction, which is then detoxified. This set of reactions is also called the water-water cycle:

Photooxidation at PSII	$2\ H_2O \rightarrow O_2 + 4\ e^- + 4\ H^+$
Reduction of O_2 at PSI	$2\ e^- + 2\ O_2 \rightarrow 2\ O_2^{\cdot -}$
SOD catalyzed	$2\ O_2^{\cdot -} + 2\ H^+ \rightarrow H_2O_2 + O_2$
Peroxidase catalyzed	$H_2O_2 + 2\ AH_2 \rightarrow 2\ AH + 2\ H_2O$
Cofactor regeneration	$2\ AH + 2\ e^- + 2\ H^+ \rightarrow 2\ AH_2$
Overall reaction	$2\ H_2O + O_2 \rightarrow O_2 + 2\ H_2O$

When molecular oxygen acts as the terminal electron acceptor, photophosphorylation will occur without the generation of NADPH. Therefore, the water-water cycle influences the formation and balance between ATP and NADPH[35,36].

All of these enzymes serve important roles in the cell and prevent over-reduction of the insoluble and soluble electron carriers and maintain LEF activity. This maintains proper poising of redox states throughout the components of the electron transport chain, preventing photodamage.

1.3. Metabolism—Carbon dioxide fixation

An essential requirement of life on earth, directly or indirectly, is the conversion of inorganic carbon into organic carbon molecules, or, in other words, the conversion of non-living matter to living matter. The fixation of carbon serves as the basis for all life and in that sense, it could be argued to be the most important biosynthetic process on earth. This important molecular process affects the global climate and efforts to improve or exploit this process are ongoing[6,37].

Autotrophic carbon fixation occurs through six naturally occurring pathways and in the recent past, synthetic pathways have been developed[38]. The organic matter fixed through these pathways is catabolized in order to generate energy rich cofactors used to drive cellular functions like metabolism, locomotion, growth, and replication.

1.3.1. Calvin-Benson-Bassham (CBB) Cycle

Arguably, the most important carbon fixing pathway is the Calvin-Benson-Bassham (CBB) cycle[39]. Naturally, the CBB cycle occurs in oxygenic photosynthetic organisms like plants, algae, and cyanobacteria, but also many chemo-litho-autotrophic, chemo-organo-autotrophs, as well as (photo-)heterotrophic bacteria[40]. In the primary producing organisms, the pathway is used to fix and reduce CO_2 into carbohydrates. In photosynthesis, this process is called the dark reactions and will eventually reduce CO_2 into organic molecules such as starch or sucrose, building biomass. This serves as a longer-term energy storage that can be catabolized by the cell (and eventually other organisms) to fuel other cellular processes.

The CBB cycle can be divided into three phases: carboxylation, reduction, and regeneration (Figure 2). In the carboxylation step, the enzyme ribulose 1,5-bisphosphate carboxylase/oxygenase, RuBisCO, will carboxylate ribulose 1,5-bisphosphate (RuBP) to 3-phosphoglycerate (PGA). The reduction phase, comprised of several enzymes, will use the NADPH and ATP generated from the light reactions to reduce PGA to glyceraldehyde 3-phosphate (G3P). Five out of six of the G3P are used to regenerate RuBP and one can be siphoned off (Figure 2) to eventually produce sucrose or enter biosynthetic pathways directly. The overall reaction for the CBB cycle is:

$$3\ CO_2 + 6\ NADPH + 6\ H^+ + 9\ ATP \rightarrow G3P + 6\ NADP^+ + 9\ ADP + 3\ H_2O + 8\ P_i \qquad (eq.\ 1.2)$$

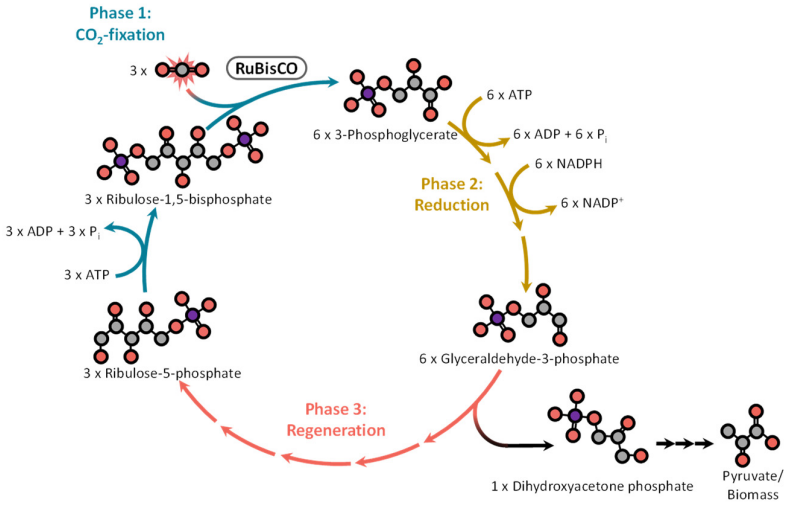

Figure 2. Simplified schematic of the Calvin-Benson-Bassham cycle. The three phases of the pathway (carboxylation, reduction, and acceptor regeneration) are indicated. Ribulose-1,5-bisphosphate will be carboxylated and eventually a single, 3 carbon sugar phosphate can be withdrawn to enter central metabolism.

1.3.1.1 Photorespiration

The CBB cycle relies solely on the enzyme RuBisCO for carboxylation and as the name suggests, this enzyme can also perform an oxygenation reaction resulting in the formation of 2-phosphoglycolate. This metabolite is toxic and must be removed from the cell, through an energetically expensive process called photorespiration. Moreover, this side reaction competes with carboxylation and will occur around one third of the time under physiological conditions[41]. While the enzyme itself has a higher preference to use CO_2 as a substrate, the atmosphere, as a result of the light reactions has a high concentration of O_2 compared to that of CO_2 (21% vs. 0.0412%)[42,43]. The differences in the solubility of these gases also have an effect on the overall carboxylation vs. oxygenation ratio. Furthermore, temperature affects the solubility of these gases and as the global temperature continues to rise due to human activity this effect will become more pronounced because the ratio of dissolved [CO_2] to [O_2] will continue to decrease. Note, the increase in atmospheric CO_2 does not overcome this effect. Therefore, losses in productivity due to an increase of photorespiration in phototrophs will continue to increase. Nature has employed several strategies to compensate for this, including high expression of RuBisCO and carbon concentrating mechanisms (e.g. C4 photosynthesis, pyrenoids, and carboxysomes). Scientists have employed various strategies to decrease losses through photorespiration including engineering the carboxysome into plants[44] and engineering more efficient pathways for photorespiration[45,46].

1.3.2. Synthetic CO_2 fixation cycles

Meeting the food and energy demands of a growing global population requires novel solutions. Modern agricultural techniques e.g. using fertilizer and irrigation has dramatically improved crop yield likely shifting the limitation in productivity to carbon fixation. Efforts to improve carbon fixation by altering both the light-dependent reactions and the dark, or light-independent reactions have shown promise[47,48]. The limitations of RuBisCO make it a target in efforts to improve carbon fixation. Attempts at directly improving RuBisCO through altering the speed or specificity have achieved marginal improvements[49,50]. Therefore, creating RuBisCO independent pathways could offer interesting solutions to improve carbon fixation. To that end, synthetic cycles for the fixation of carbon dioxide that bypass RuBisCO entirely have been designed, developed, and established[38,51]. This visionary approach, takes advantage of all of the enzymes that have been discovered to date providing many opportunities for diverse solutions and expanding the repertoire of carbon fixing pathways.

One solution is the 17-enyzme Crotonyl-CoA Ethylmalonyl-CoA 4-hydroxybutyryl-CoA cycle, or CETCH cycle, that has been established *in vitro* (Figure 3). This pathway employs reductive carboxylases called enol-CoA carboxylases/reductases (ECRs), which have unequaled high rates of catalysis and efficiency of carboxylation and do not react with oxygen[52-55].

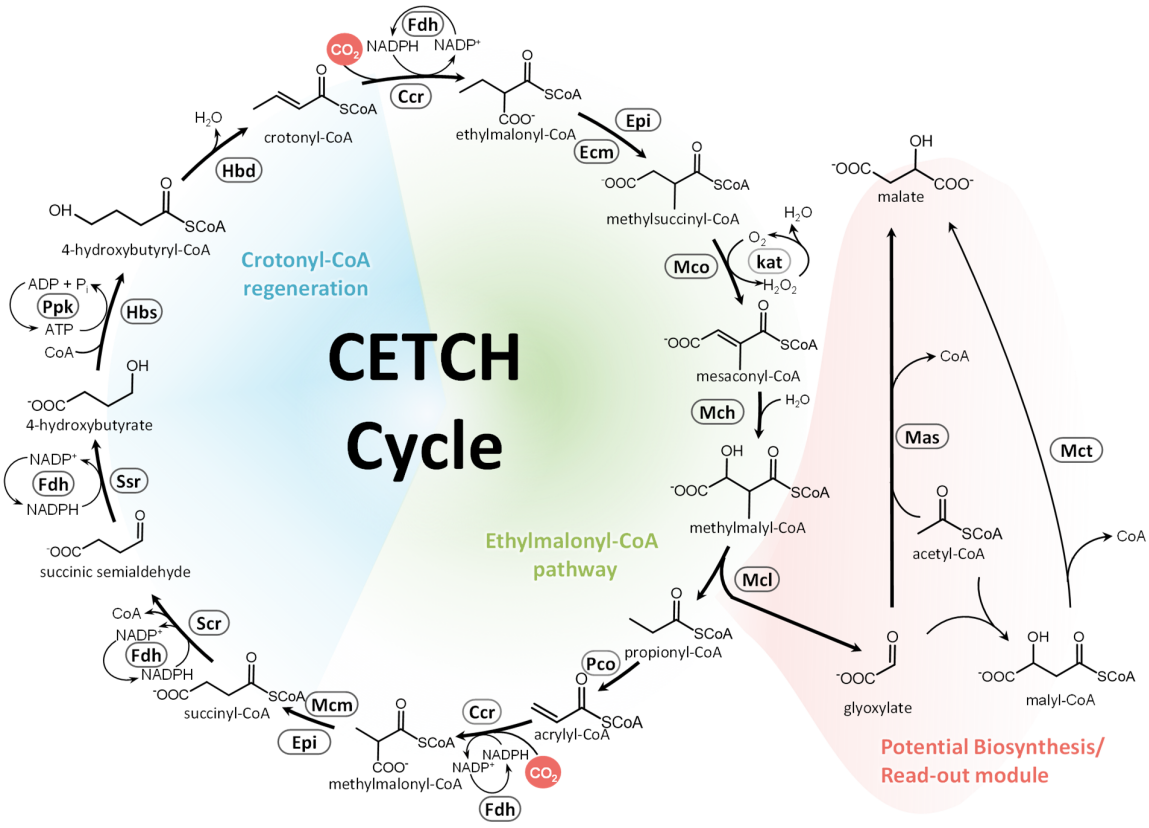

Figure 3. The synthetic CO_2 fixation pathway, CETCH 5.4 The portions of the cycle based on the ethylmalonyl-CoA pathway are indicated in green; crotonyl-CoA regeneration module in blue, and biosynthesis/readout module in salmon[38].

The CETCH cycle is based on the natural ethylmalonyl-CoA pathway, which is employed in some bacteria for acetyl-CoA assimilation[53]. This linear pathway is converted into a cycle through the addition of four enzymes that regenerate the starting substrate (crotonyl-CoA). Through several rounds of optimization, some enzymes were replaced and engineered to accept novel substrates. In initial attempts to establish the CETCH cycle *in vitro,* the cycle would not complete a full turn and methylsuccinyl-CoA accumulated. This indicated methylsuccinyl-CoA dehydrogenase (Mcd) was rate limiting. Mcd catalyzes the oxidation of methylsuccinyl-CoA and requires an electron acceptor, for the *in vitro* experiments

ferrocenium was added to act as an electron acceptor. In these conditions (low ferrocenium, high NADPH), the ferrocenium would be oxidized by NADPH to ferrocene. Naturally, after oxidizing methylsuccinyl-CoA this enzyme will eventually reduce the quinone pool through electron transport flavoprotein ubiquinone oxidoreductase (Etf:QO) via the soluble electron carrier, electron transport flavoprotein (Etf). This entire module was not reconstructed in the lab however, the Mcd was rationally engineered to use molecular oxygen as an electron acceptor, creating methylsuccinyl-CoA oxidase (Mco). The reduction of oxygen will produce H_2O_2, and catalase was added to prevent oxidative damage. After this substitution, the CETCH cycle was capable of performing two turns. The addition of an output module further improved the cycle performance because the depletion of the glyoxylate produced from the CETCH cycle should drive the Mcl reaction. However, the addition of an output module had unwanted side reactions. Correcting for this required the addition of enzymes that are capable of correcting dead-end side products for metabolic proofreading. Furthermore, this required changing one of the core enzymes, which also performed an unwanted side reaction. This substitution replaced the step performed by the biotin dependent carboxylase, propionyl-CoA carboxylase (Pcc), with two enzymes. One is another engineered enzyme to act as a propionyl-CoA oxidase (Pco) reducing O_2. The oxidation of propionyl-CoA forms acrylyl-CoA, which in turn is carboxylated by the crotonyl-CoA carboxylase/reductase (Ccr) to form methylmalonyl-CoA. In combination, these enzymes resulted in a cycle capable of fixing CO_2 *in vitro*. In a living system, combinations of enzymes and biochemical pathways have been optimized overtime to function congruently. The CETCH cycle combined enzymes from many different organisms and since they were not combined in nature they had not evolved to function synchronously and enviably had unintended crossreactivity with other substrates. Operation of a synthetic cycle required artificially correcting and optimizing the pathway for successful functionality.

The *in vitro* CETCH cycle can continuously fix carbon dioxide, however this requires the regeneration of ATP and NADPH. One enzyme in particular, 4-hydroxybutyryl-CoA synthetase (Hbs) requires a high ATP/ADP ratio for the reaction to proceed. Meaning, ATP must continuously be regenerated to maintain this high ratio. Regeneration of these cofactors relied on polyphosphate kinase (Ppk) and an engineered formate dehydrogenase (Fdh), which required the addition of polyphosphate and formate, respectively. The capacity for energy regeneration is limited to the amount of added formate and polyphosphate. Furthermore, Fdh will oxidize formate to CO_2 in order to regenerate NADPH; decreasing the net carbon fixed by

the CETCH cycle. Coupling CETCH to an alternative energy source such as the light-driven regeneration of NADPH and ATP from photosynthetic linear electron flow would achieve a truly carbon negative synthetic CO_2-fixing pathway.

In its final form, CETCH relies on enzymes from all domains of life and engineered enzymes that together can perform the essential task of carbon fixation. This solution for carbon fixation relies on biochemical and molecular biological discoveries, that combined create a seventh autotrophic CO_2 fixing cycle that has not evolved in nature. The final net reaction is summarized in the following chemical equation:

$$2\ CO_2 + 3\ NADPH + 2\ ATP + FAD \rightarrow \text{glyoxylate} + 3\ NADP^+ + 2\ ADP + 2\ P_i + FADH_2 \qquad (eq\ 1.3)$$

1.4. Compartmentalization

Compartmentalization is an essential feature of a living system that allows the spatial and temporal control of biological processes. The boundary of living cells is a semipermeable membrane composed of a lipid bilayer, allowing for the enrichment of specific components while isolating the internal space from waste products or toxic molecules. Internally, a cell often has other compartments that serve essential functions. Examples include the chloroplast, mitochondria, pyrenoids, bacterial microcompartments, and more. The barrier enclosing these internal compartments can vary[56-58]. Internal compartments allow for specific division of labor and isolation of reactions that may be toxic for the cell. They may even allow to maintain specific conditions for certain tasks or reactions to take place. Without a boundary, the essential components of life would diffuse to concentrations too low for cellular functions to reliably occur. Building life from the bottom up requires some compartmentalization and there are several technologies that are suited for this.

One method, microfluidics, has created many opportunities for research in physics, chemistry and biology. Specifically, using these miniaturized fluid devices allows for the high-throughput formation of large quantities of monodisperse microdroplets. Their characteristics are easily controlled allowing the creation of uniform droplets in both size and content. Droplet-based microfluidics has been used to perform quantitative measurements in very small reaction volumes[59], for complex sorting[60], extremely high-throughput screening efforts[61,62], and in bottom-up synthetic biology[63,64]. These closed compartments can vary in structure and size and be used to model cellular processes and dynamics. Techniques have been developed to form various types of compartments including water-in-oil (w/o) droplets[65] and liposomes

(e.g. small, large, or giant unilamellar liposomes)[63,66,67]. Liposomes, possessing a lipid bilayer, more similarly reflect a cell than w/o droplets which have a simpler boundary at the interface of the water and oil. Liposomes can be created using different lipid types which vary in properties[68]. W/o droplets do not model the membrane in complexity the way liposomes do; however, they still form a closed reaction volume resembling a cell in size.

Often, w/o droplets are manufactured using a T-junction or a flow focusing microfluidic chip[59]. The size of a droplet can be controlled by adjusting the flow rates while manufacturing. The w/o droplets must be stabilized with a surfactant to prevent coalescence[69]. Depending on the surfactant used, the head groups can be functionalized[70]. It is possible that components within droplet, or even the oil, can diffuse between the two phases (aqueous and oil) depending on the properties of the components, oil, and surfactant.

This work used microfluidics to generate monodisperse w/o droplets to act as individual reaction chambers that could be controlled in volume and allowed for reactions to take place in a defined space. Since they are reproducible and monodispersed they can be used for quantitative and qualitative studies and comparisons at such small volumes that resemble cells in size.

1.5. Aims

This work set out to combine an artificial CO_2 fixing pathway with light derived energy and eventually develop a synthetic system analogous to chloroplasts. Using a bottom-up approach, photosynthetic membranes were co-encapsulated together with the CETCH cycle in cell-sized water-in-oil (w/o) droplets to mimic a chloroplast, both in structure and metabolic function. In order to achieve this a stepwise development of specific modules was required:

1. **Energy**
    a. *Light driven generation of NADPH and ATP*
    Development of the energy module required the isolation of photosynthetically active membranes. The rate of photophosphorylation and photoreduction was to be determined in respect to alterations and additions of soluble electron carriers, substrates, and antioxidants. The stability of the membranes needed to be characterized and conditions optimized to improve the function and lifetime of these membrane preparations.

2. **Metabolism**
    a. *Powering carbon fixing reactions in vitro*
    After the development of a functional *in vitro* energy module the NADPH and ATP generated had to be used to power enzymatic reactions. Therefore, enzymes that use either ATP or NADPH or both were needed. The carboxylases, propionyl-CoA carboxylase and crotonyl-CoA carboxylase/reductase of the ethylmalonyl-CoA pathway were selected for this purpose.
    b. *Powering carbon fixing pathways for the continuous reduction of CO_2*
    Once the energy module could be coupled to different enzymatic reactions, the complexity of the system could be increased by expanding it to an entire CO2 fixing pathway. This required optimization for both the CO2-fixation and energy modules to operate harmoniously. Towards that end, the original CO2 fixation pathway had to be modified.
3. **Compartmentalization:**
    a. *Development of a functional microfluidic platform*
    With the eventual goal of encapsulating the combination of the energy module and the CETCH cycle in cell-sized droplets, a suitable microfluidic platform had to be developed. Taking a similar approach as above this was achieved in a stepwise fashion. Firstly, the energy module has to be encapsulated, tested and optimized for the drastic down-scale in volume. The light driven generation of NADPH was demonstrated in droplets. Using this system thousands of droplets could be created and monitored in real time
    b. *Coupling photosynthetic membranes with individual reactions*
    Next, the photosynthetic droplets needed to be tested in the context of co-encapsulated single enzyme reactions. The single enzymes tested were glyoxylate reductase (Ghr), Crotonyl-CoA carboxylase/reductase, and propionyl-CoA synthase (Pcs).
    c. *Encapsulating all of the components for light driven continuous CO_2 fixation*
    Finally, the entire CETCH cycle was coupled to the photosynthetic membranes and co-encapsulated into cell-sized water-in-oil droplets. The activity was confirmed in real time by monitoring the dynamic equilibrium of individual droplets overtime and the contents of the droplets were measured by HPLC-MS for both CoA ester intermediates and the output product glycolate. This set-up provided a high throughput platform to study the dynamics, controllability and function of the CETCH cycle in multiplex. Using this system cycle, variants were compared side by side

2. Results

2.1. Establishment of the energy module

In photosynthesis, complex proteins located on the thylakoid membranes convert light energy into chemical energy. Light reactions of photosynthesis are intimately connected with the dark reactions, the CBB cycle for CO_2-fixation *in vivo*. These processes have evolved congruently for billions of years and balance between them is tightly controlled and regulated. This interconnectivity poses a challenge for utilizing this incredible light driven energy regeneration ability to drive non-canonical reactions and reaction cascades *in vivo*. This complexity lies at every step of the biological process from the DNA up to the biochemistry of enzymes, e.g. difficulty for genetic modification, stoichiometry of enzyme expression, repair, and balancing of redox equivalents. One major hurdle is that due to the complexity and interconnectivity in these primary producing organisms the "rewiring" of the metabolism proved to be difficult. Therefore, to exploit this natural "power-plant" to drive synthetic carbon fixing cycles, photosynthetically active membranes themselves were isolated and established for the light driven regeneration of ATP and NADPH *in vitro*.

2.1.1. $NADP^+$ photoreduction *in vitro*

The thylakoid membranes of *Chlamydomonas reinhardtii* and *Spinacia oleracea* were isolated via density centrifugation[33,71-74]. Eventually, *S. oleracea* thylakoids were used exclusively due to the ease of isolation and stability of the membranes. Crude extracts were able to regenerate NADPH and ATP without the supplement of soluble electron carriers. However, when using purified and washed membranes it was important to add ferredoxin (Fdx). To determine the optimal concentration of ferredoxin, $NADP^+$ photoreduction was measured at 340 nm using a Cary 60 spectrophotometer with various Fdx concentrations. $NADP^+$ photoreduction was observed upon illumination; with 100 µmol photons m^{-2} s^{-1} of white light, the addition of 5 µM of Fdx was optimal (Figure 4A & C). The difference in reduction rates was negligible between Fdx from *C. reinhardtii* (Fdx1) and *S. oleracea (*Fdx2*),* which have 75% sequence identity. Purified ferredoxins showed the typical absorption maxima for 2Fe-2S clusters[75] (Supplemental Figure S1). Initially, ferredoxin:$NADP^+$ reductase (FNR) was also added to the reaction mixture at 10 µM (further discussion in Section 2.2.2).

The NADP⁺ photoreduction occurred in a light dependent manner and could be regulated by alternating light dark cycles (Figure 4B). At 100 µmol photons m^{-2} s^{-1} these thylakoid preparations catalyzed the light-dependent reduction of NADP⁺ to NADPH at a specific activity of 3.41 ± 0.01 µmol min^{-1} $µg^{-1}$ total chlorophyll (chlorophyll A and B, referred to as Chl; Figure 4D), which is comparable to values measured by others (Supplementary Table 1).

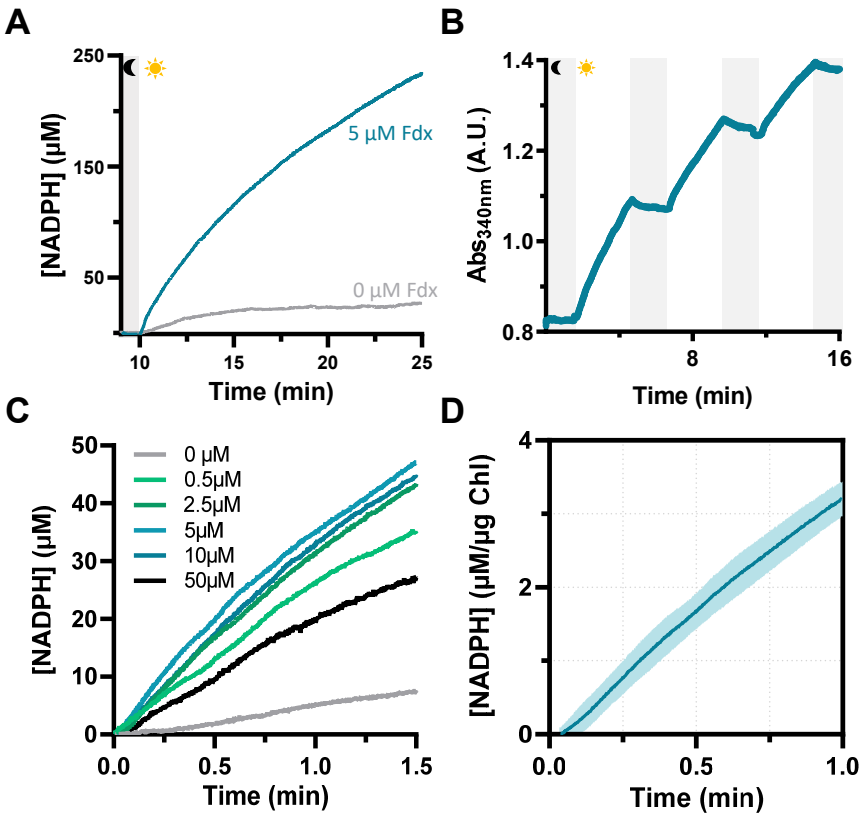

Figure 4. Characterization of the light-driven NADP⁺ photoreduction by thylakoid membrane-based energy modules. (**A**) NADPH production is dependent on light and externally added ferredoxin (**B**) NADPH photoreduction is controlled by alternating light dark cycles. (**C**) NADP⁺ photoreduction: Titration of ferredoxin concentrations. NADPH production is dependent upon the addition of external ferredoxin. The highest rates of NADP⁺ photoreduction were achieved with the addition of ferredoxin between 2.5-10 µM. Shown are representative examples of NADPH production rates at 100 µmol photons m^{-2} s^{-1}, 10 µg total chlorophyll a + b (Chl) and varying ferredoxin concentrations. (**D**) NADP⁺ photoreduction by photosynthetic membranes NADPH production rate normalized to µg of Chl (line is the mean value with shaded area corresponding to ± standard deviation, N = 6). Rate of NADP⁺ photoreduction was determined from the first minute after the light had been turned on (100 µmol photons m^{-2} s^{-1}).

2.1.2. ATP photophosphorylation *in vitro*

Thylakoid membranes also catalyzed the regeneration of ATP from ADP, both in the light and the dark. The ATP that was generated in the dark can be attributed to the membrane bound adenylate kinases[76], which catalyze the reaction:

$$2\ \mathrm{ADP} \rightleftarrows 1\ \mathrm{AMP} + 1\ \mathrm{ATP} \qquad (eq\ 2.1)$$

The ATP regeneration in the dark was quantified at 1.2 ± 0.2 µM min^{-1} $µg^{-1}$ Chl, which could be suppressed by using an adenylate kinase specific inhibitor, diadenosine pentaphosphate (DAPP) [33,77] (Figure 5). When exposed to light, ATP production from ADP increased 6-fold (6.5 ± 0.5 µM min^{-1} $µg^{-1}$ Chl) and in a sample containing DAPP resulted in a light- (and ATPase) dependent ATP synthesis rate of 5.4 ± 0.5 µM min^{-1} $µg^{-1}$ Chl (Figure 5). This is comparable to previous studies using chloroplast and thylakoid extracts (Supplementary Table 1). Indicating that the energy module could be capable of generating sufficient ATP and NADPH to drive CO_2 fixation with the CETCH cycle.

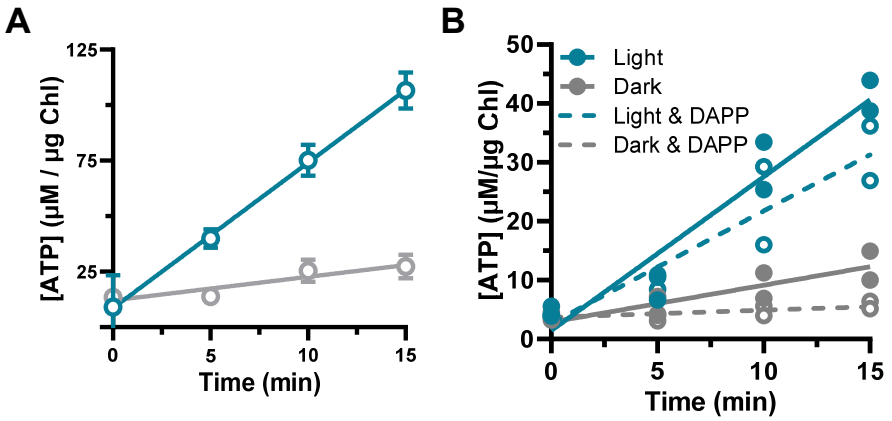

Figure 5. Characterization of the light-driven ADP photophosphorylation by thylakoid membrane-based energy modules. (**A**) ATP production is dependent on light, with some background reaction in the dark due to membrane bound adenylate kinase (**B**) Light-driven ATP formation and dark-control in the presence of the adenylate kinase inhibitor DAPP (teal and grey, respectively; open circles indicate samples with DAPP added). The addition of DAPP decreases ATP formation both in the dark and in the light (lines shown are linear fits, 2 biological replicates, 60-70 µmol photons m^{-2} s^{-1}), presumably due to inhibition of the background reaction of membrane-bound adenylate kinase.

2.1.3. Optimization, stability, and mitigation of ROS

In chloroplast and thylakoid extracts, the enzymes responsible for CEF are unstable and will lose activity quickly[33]. Without a contribution from CEF, the LEF production ratio of ATP:NADPH should be 1.28:1. After 30 minutes in the light without the addition of DAPP a ATP:NADPH ratio was determined to be 0.8 and with the addition of DAPP it was 1.6 (Figure 6A). The exact reason for this discrepancy was not specifically elucidated, however, this could be due to not all membranes being completely intact or limitations on the electron acceptor side. The measured NADPH production and O_2 evolution ratio match the expected ratio of 2:1 (Figure 6B & C). This would be an indication that the membranes were not fully intact and some protons would be leaking. However, this would need to be experimentally confirmed.

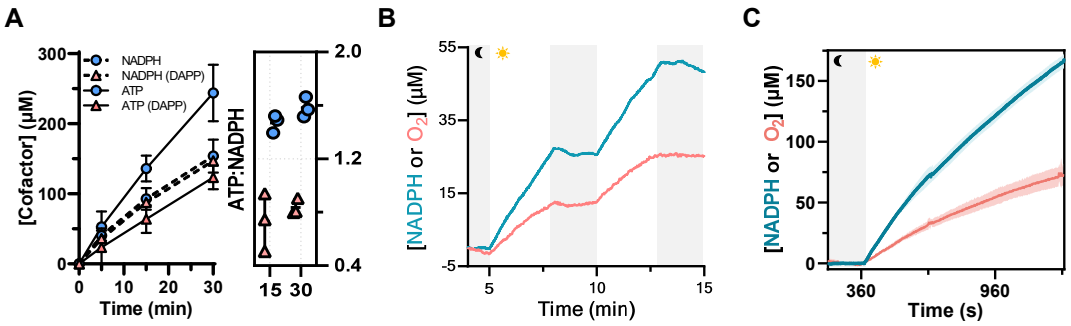

Figure 6. Characterization and stoichiometry of light-driven ATP and NADPH regeneration by thylakoid membrane-based energy modules. (**A**) Stoichiometry of cofactor regeneration: ATP (solid lines) and NADPH (dashed lines) production in the presence (coral triangles) and absence of DAPP (blue circles), and the calculated ATP to NADPH ratio at 15 and 30 minutes after light exposure (60 µmol photons m^{-2} s^{-1}). (**B**) Relative molar $NADP^+$ photoreduction and O_2 evolution curves over light/dark cycles. The O_2 production occurs in a 1:2 molar ratio with NADPH, the same ratio that occurs under physiological conditions. (**C**) NADPH production with O_2 evolution curves at 60 µmol photons m^{-2} s^{-1}. Lines are the average of three replicates and the standard deviation is shown in the shaded area.

The specific activities of thylakoid membranes varied slightly between individual preparations (Figure 7B). Thylakoid membranes were stably maintained in the dark for at least two hours at room temperature and at least 24 hours when maintained on ice with no observable loss of NADPH productivity upon illumination (Figure 7A). Membrane preparations could be stored at -80 °C for more than a year without notable loss of activity (Figure 7B), demonstrating their

long-term usability as a thylakoid membrane-based energy module for subsequent experiments.

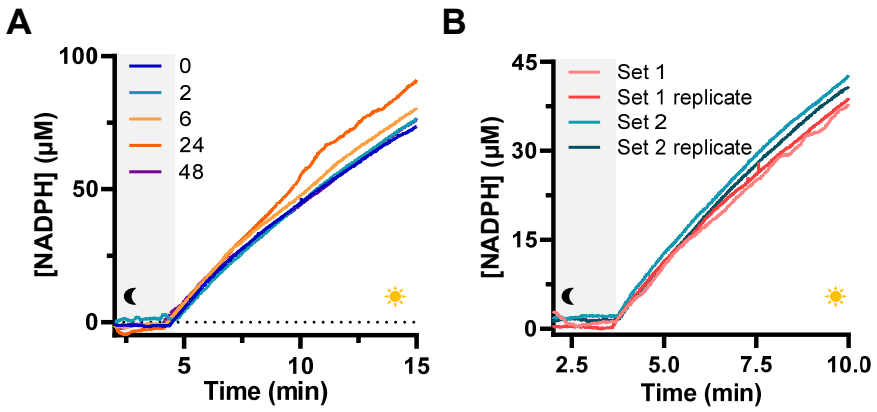

Figure 7. Stability of thylakoid membrane-based energy modules. (**A**) Stability of thylakoids in the dark: NADPH production of the energy module was maintained in the dark for 1 and 2 hours (at room temperature) or 6, 24, and 48 hours, respectively (at 0 °C, 60 µmol photons m^{-2} s^{-1}). (**B**) Reproducibility of energy module preparations: NADPH production rates of thylakoids are consistent between different thylakoid preparations. Two replicate experiments from two different thylakoid preparations, one of which had been stored at -80 °C for over a year, are shown (at 23 °C, 60 µmol photons m^{-2} s^{-1}).

The light intensity used affected the lifespan of the thylakoids. In general, lower light intensities were inversely proportional to thylakoid lifespan (Figure 8A & B). Photosynthetic activity was assayed at three light intensities (30, 60, 300 µmol photons s^{-1} m^{-2}) by measuring O_2 evolution. At 60 µmol photons s^{-1} m^{-2} the O_2 evolution was the highest, however after 3500 seconds the oxygen levels were surpassed by that of thylakoids illuminated with 30 µmol photons s^{-1} m^{-2}. Initially, thylakoids illuminated with 300 µmol photons s^{-1} m^{-2} out-performed thylakoids illuminated with 30 µmol photons s^{-1} m^{-2}, however the oxygen level quickly decreased, indicating a loss of function.

Adding antioxidative substrates and enzymes increased the lifetime of the thylakoids. Chloroplasts contain two ascorbate peroxidases, one being membrane bound[78]. In order to preserve the activity of ascorbate peroxidases, ascorbate was included in every step during the purification of the thylako*ids*[79]. The activity of three superoxide dismutases (Sods) was assayed using the method based on nitro blue tetrazolium (NPT) and the production of superoxide

from xanthine oxidase[80]. In this indirect activity assay, the oxidation of NPT is prevented by Sod activity. The oxidation was monitored at 560 nm. Sod A and B were overproduced and purified from *E. coli,* and compared to the commercially purchased Bovine Sod had lower activity, therefore the bovine Sod was used in subsequent experiments. The native *E. coli* catalase (Cat) was overexpressed and purified from *E. coli*. The addition of these enzymes allowed for the *in vitro* system to prevent oxidative damage from the many sources of ROS including from the photosystems themselves. Addition of superoxide dismutase and catalase to scavenge reactive oxygen species (ROS) resulted in prolonged thylakoid membrane activity (Figure 8A).

The importance of the addition of the antioxidative enzymes Sod and Cat was demonstrated by measuring O_2 evolution in the presence and absence of Cat and Sod at 60 and 300 µmol photons s^{-1} m^{-2} conditions. The O_2 evolution was higher at 60 µmol photons s^{-1} m^{-2} versus 300 µmol photons s^{-1} m^{-2}. Furthermore, the activity was maintained longer in conditions containing Cat and Sod (Figure 8A). In the subsequent experiments, SOD and catalase were always included and light intensities between 50-60 µmol photons m^{-2} s^{-1} were used to minimize the formation of ROS that would be damaging the photosynthetic apparatus while providing sufficient rates of NADPH regeneration (Figure 8B).

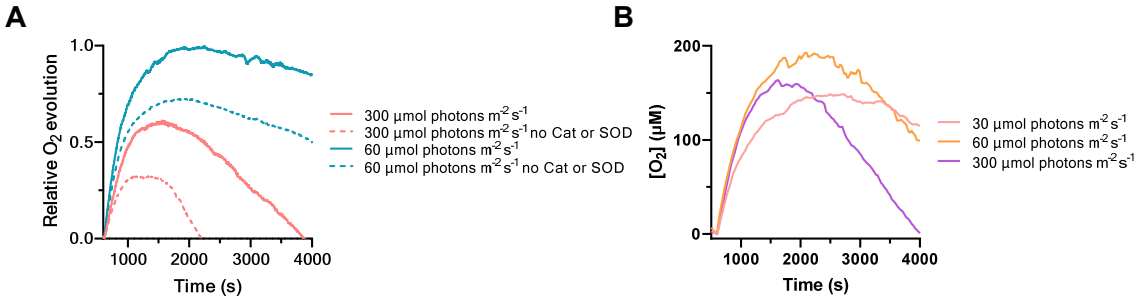

Figure 8. (**A**) Relative O_2 evolution at 60 or 300 µmol photons m^{-2} s^{-1} in a reaction buffer either with or without catalase (Cat) and superoxide dismutase (Sod). (**E**) A similar experiment as in (**B**) but an even lower light condition is shown. All conditions contained Sod and catalase. At 30 µmol m^{-2} s^{-1} the O_2 evolution was slower but was maintained longer.

In summary, these efforts created a functional photosynthetic energy module that could be used to regenerate ATP and NADPH in light. The thylakoid preparations could be cryopreserved for long periods and were consistent in their behavior. Adding antioxidative

proteins and substrates showed a benefit for the activity. Using low light intensities would maintain activity for longer periods while generating ATP and NADPH sufficiently.

2.2. Coupling metabolism to energy generation

2.2.1. Individual light powered CO_2-fixation reactions

To test if the ATP and NADPH generated through LEF from the photosynthetic membranes could be used to drive individual biochemical reactions the energy module was coupled to two different CO_2-fixing enzymes, namely crotonyl-CoA carboxylase/reductase (Ccr) and propionyl-CoA carboxylase (Pcc), which require NADPH and ATP, respectively (Figure 9). In the case of Ccr, product formation was strictly light-dependent with a CO_2-fixation rate of 5.2 ± 0.2 µM min^{-1} $µg^{-1}$ Chl (Figure 9B). Pcc showed a light-dependent CO_2-fixation rate of 5.1 ± 0.2 µM min^{-1} $µg^{-1}$ Chl (Figure 9B). There was a low, light-independent carboxylation by Pcc that occurred at a rate of 0.8± 0.1 µM min^{-1} $µg^{-1}$ Chl, due to the adenylate kinase activity of the thylakoids (see above). Notably, these carboxylation rates are more than three orders of magnitude higher than recent efforts to couple enzymatic CO_2-fixation to isolated PSII (approx. 6.9·104 molecules h^{-1} per PSII reaction center compared to 34 molecules h^{-1} per PSII reaction center, Supplementary Table 2), highlighting the capability of the thylakoids to efficiently energize catalytic transformations.

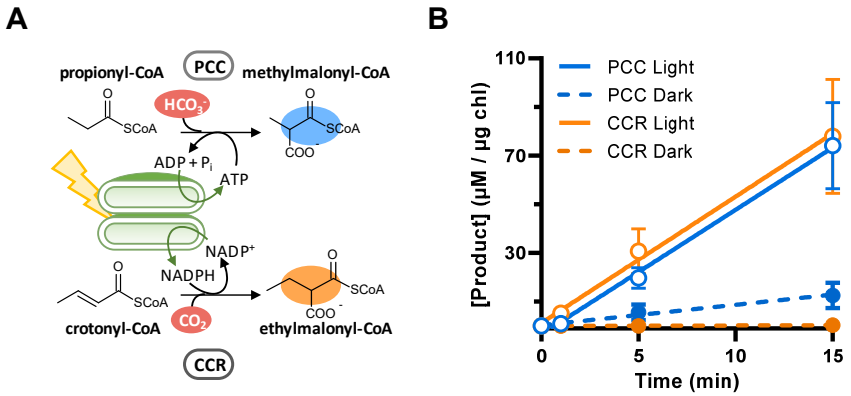

Figure 9. Light-driven cofactor regeneration by thylakoid membrane-based energy modules. (**A**) Scheme of thylakoid energy module-driven carboxylation reactions of propionyl-CoA carboxylase (Pcc) and crotonyl-CoA carboxylase/reductase (Ccr) utilizing light-produced ATP and NADPH, respectively. (**B**) Reactions coupled to thylakoid energy module (2.5 or 5 µg Chl and 60 µmol photons m^{-2} s^{-1}) (N=6).

2.2.2. Metabolism: Light driven CO_2-fixing cycles

Within living cells, biocatalysis and metabolism occur in networks or cycles. Mostly, carbon fixation occurs by adding a carbon to a longer backbone. Eventually, a pathway intermediate will be split creating an organic molecule that can be used for biosynthetic routes and another product that will be used to regenerate the substrate for the carboxylation, thus forming a cycle. Combining the thylakoid energy module with a complete metabolic cycle for the fixation of CO_2, would allow for the continuous fixation of carbon dioxide by light. To that end, the energy module was combined with the core enzymes of the CETCH cycle (version 5.4, see Figure 3 in Section 1.3.2.) and a glyoxylate/hydroxypyruvate reductase from *Escherichia coli* (Ghr)[38]. To demonstrate that the light dependent regeneration of NADPH and ATP could be extended to sustain entire metabolic cycles, all CETCH cycle enzymes were added to the thylakoid reaction mixture. After light exposure, samples were taken throughout, and the formation of the CoA thioester intermediates and their incorporation of ^{13}C-labeld CO_2 were analyzed by HPLC-MS. The expected incorporation of the ^{13}C label is shown in Supplemental Figure S2.

Initial efforts to operate the CETCH cycle (CETCH version 5.4) together with the energy module failed, and the expected CoA ester intermediates were not produced (Figure 10A-D). This indicated some sort of negative interaction of system components. To assess this problem, supernatant from pre-illuminated thylakoids was used as the reaction buffer for the CETCH enzymes. For this, the reaction buffer contained everything except the CETCH enzymes and substrates, only ADP and $NADP^+$ were added and illuminated for 45 minutes. Subsequently, the thylakoids were spun down at 3000 x g for 3 minutes and the CETCH enzymes were added to the supernatant. The reaction sequence was started by addition of propionyl-CoA and samples were taken. The results are depicted in Figure 10E and show that thylakoids were capable of generating sufficient NADPH and ATP to turn the cycle 3 times. Through an iterative process, several issues with the combination of the thylakoids and CETCH module were determined. Particularly there was a negative interaction between FAD dependent enzymes in the cycle with NADPH formation.

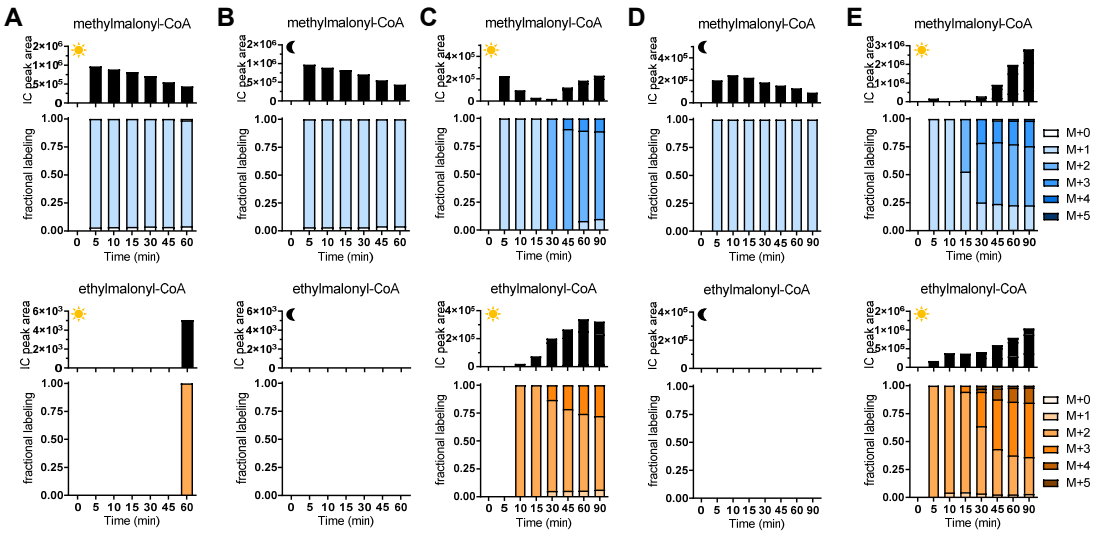

Figure 10. Initial experiments to couple the CETCH cycle to the thylakoid energy module (in bulk). To couple the CETCH cycle to the thylakoid energy module, enzymes of the CETCH cycle plus Ghr from *E. coli* were mixed with thylakoids. Propionyl-CoA was added and the reaction mixture was illuminated (100 µmol photons m^{-2} s^{-1}). Operation of the CETCH cycle was assessed by following the ^{13}C-labelling patterns (see Supplementary Figure 2) and CETCH cycle metabolites methylmalonyl-CoA and ethylmalonyl-CoA as previously described[38]. (**A-B**) Labelling pattern of CETCH v6.0 coupled to p (50 µg Chl mL^{-1}) starting with 150 µM propionyl-CoA. Both conditions were supplemented with an addition of 10 µM ferredoxin-$NADP^+$ reductase (FNR), with added 15 µM FAD (1:1.5 molar ratio, for the contribution of FAD and FNR on the system see Figure 11). Very little difference between the light (**A**) and dark (**B**) operated cycles was observed and ethylmalonyl-CoA was only detected after 60 minutes in the light. (**C-D**) Labelling pattern of CETCH v6.0 coupled to the thylakoid energy module (70 µg chl mL^{-1}) in the absence of FNR starting with 150 µM propionyl-CoA (see Supplementary Fig. 6 for details on the effect of FNR and its interplay with Mco and free FAD). When additional FNR was left out of the reaction mixture, the cycle operation increased under illumination (**C**), demonstrated by the ^{13}C-labelling pattern and formation of ethylmalonyl-CoA. The dark control (**D**) did not show any significant label incorporation and no ethylmalonyl-CoA formation. (**E**) Positive control demonstrating that supernatant of a thylakoid reaction (with 20 µg Chl) illuminated for 45 minutes is able to provide sufficient NADPH and ATP to subsequently operate the CETCH cycle v6.0 for several rounds, suggesting some negative interactions of CETCH cycle v5.4 and the thylakoids.

There seemed to be a link between the flavin adenine dinucleotide (FAD)-dependent enzymes methylsuccinyl-CoA oxidase (Mco) and propionyl-CoA oxidase (Pco) interfering with thylakoid productivity, likely due to the formation of ROS and unbound FAD in the enzyme preparations. The latter is capable of directly oxidizing NADPH through the interaction with FNR (see also Figure 10A, 10B, 11B, 11A). This interaction was simplified by returning to experiments containing only thylakoids. In literature, experiments using chloroplast extracts often have added external FNR. However, here additional FNR did not increase activity further (Figure 11A). When unbound FAD was added the NADPH production rate actually decreased. If a system contained FNR and FAD was added later, the NADPH was directly oxidized and the NADPH production would halt. Therefore, free FAD in the system appeared to cause direct oxidation of NADPH through the interaction with FNR (Figure 11B). Naturally, FNR exists in two states—a soluble and a membrane associated state. FNR will become dissociated from the membrane under stress conditions that lead to the formation of super oxide. When this occurs FNR will switch from an NADPH producer to an NADPH consumer[81], which was apparently the case in the *in vitro* system.

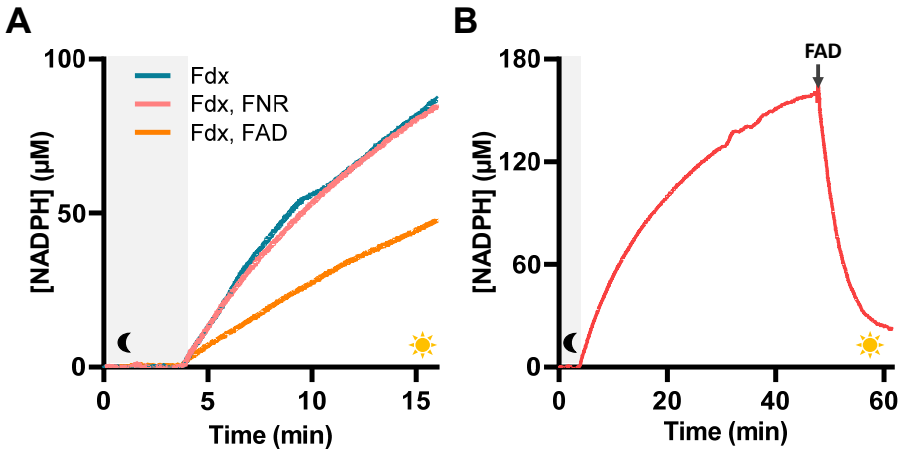

Figure 11. Negative effect of Mco and free FAD on NADP⁺-dependent photoreduction by thylakoids: (**A**) NADP⁺ photoreduction monitored on a spectrophotometer at 340 nm by thylakoids starts upon illumination (60 µmol photons m^{-2} s^{-1}). Fdx is required for NADP⁺ photoreduction (Figure 4A) and adding 5 µM FNR did not improve the NADPH production rate from thylakoids (10.3 µM min^{-1} with only Fdx and 9.9 µM min^{-1} with Fdx and FNR, calculated from the first 2.5 minutes of illumination). However, adding excess FAD (14 µM) decreases this rate (4.3 µM min^{-1}). **(B)** NADPH is produced in the presence of FNR and Fdx (5 µM each) but inhibited upon the addition of FAD (14 µM) even under constant illumination.

The flavin adenine dinucleotide (FAD)-dependent enzymes methylsuccinyl-CoA oxidase (Mco) and propionyl-CoA oxidase (Pco) were often prepared with additional FAD (in a 1:1.2 molar ratio of protein to FAD). Compared to their native counterparts, these engineered enzymes would only loosely bind FAD and during purification lose a significant amount of FAD. Furthermore, each of these oxidases would directly produce ROS by using molecular oxygen as a substrate. The effects caused by free FAD and ROS formation were minimized by changes in the CETCH cycle and the enzyme purification protocols. In the case of Pco, it could easily be replaced with Pcc, but due to the side reaction with acetyl-CoA as discussed in Section 1.3.2 this would require an alternative output module. An output module helps to pull the reaction catalyzed by malyl-CoA lyase (Mcl) and thus forcing the cycle to turn forward. Different output modules were tested and eventually Ghr was chosen, which directly withdrew glyoxylate from the cycle (creating CETCH cycle version 6.0, Figure 14A), and having the additional benefit of an ease of detection of glycolate.

However, replacing Mco with a methylsuccinyl-CoA dehydrogenase (Mcd) was much more difficult. In natural systems, the conversion of methylsuccinyl-CoA to mesaconyl-CoA is catalyzed by Mcd. Mcd is a FAD–dependent acyl-CoA dehydrogenase, which is coupled via electron transfer flavoproteins (Etf) to the membrane-located ubiquinone pool through the membrane bound electron transfer flavoprotein-ubiquinone oxidoreductase (Etf:QO, Figure 12). During the development of the CETCH cycle, Mcd alone and in combination with its cognate Etf was not sufficient to operate the CETCH cycle[38]. This required engineering of a Mco that was ultimately used in CETCH v5.4 (Figure 3). The efforts for replacing Mco with Mcd are outlined below.

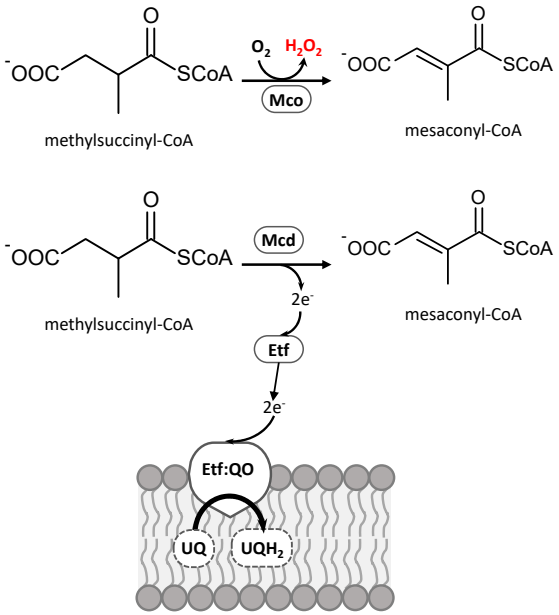

Figure 12. Mco and Mcd reaction: Mco catalyzes the reduction of methylsuccinyl-CoA and uses O_2 as an electron acceptor. Naturally, this reaction proceeds with multiple enzymes involved in electron transport to eventually link the reaction to the quinone pool.

Electron transfer flavoprotein-ubiquinone oxidoreductase is a membrane anchored protein that contains an FAD, 4Fe-4S cluster, and a ubiquinone binding site [82]. This plays an important role in a cell or organelle, its activity includes linking fatty acid oxidation to the respiratory chain. Through this enzyme electrons from Etf will reduce ubiquinone to ubiquinol in two one-electron transfer steps[81] (Figure 12). Etf:QO was cloned from *Rhodobacter sphaeroides* 2.4.1 into pET-16b with an N-terminal strep II tag. Etf:QO was overproduced in *E. coli* and purified from the insoluble fraction (Supplemental Figure S3). The interaction of the protein with the thylakoid membranes was assessed by incubating Etf:QO with purified membranes and subsequent washing. After three washing steps samples were taken and analyzed by SDS PAGE and subsequently blotted using an anti-his antibody. Even after the washes a slight band of Etf:QO was visible, indicating an association with the membrane (Supplemental Figure S4. For a control the similar sized enzyme, citrate synthase from *Synechocystis* sp. PCC 6803, was used and after washing there was no association with the membrane fraction. This enzyme was active without additional quinone (Figure 13). Purification of this enzyme was rather laborious and had limited yields. Higher expression was achieved with the Etf:QO from *P. migulea* and was still capable of accepting the electrons from the Etf from *R. sphaeroides* (Figure 13A, B, & C). Replacing Mco with Mcd, its cognate electron transfer protein (Etf), as

well as an Etf-ubiquinone oxidoreductase (creating CETCH cycle version 7.0) further improved glycolate formation from CO_2 and light. After addressing these issues, the CETCH cycle could be run with either Mco or Mcd (Figure 13D and 14B, C, & D).

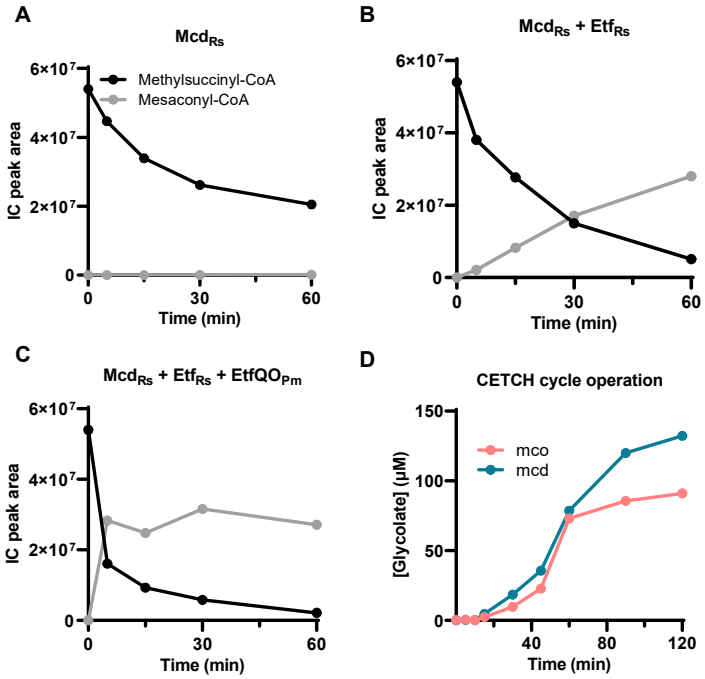

Figure 13. Developing a functional Mcd reaction for CETCH v7.0: Mco can impair the thylakoid energy module productivity through ROS and free FAD (Supplementary Fig. 5a), we aimed to replace Mco in the CETCH cycle with a functional Mcd reaction. (**A**) Mcd (6.75 µM**)** from *Rhodobacter sphaeroides* (Mcd_{Rs}) alone does not catalyze the conversion of methylsuccinyl-CoA (starting with 250 µM, shown in black) into mesaconyl-CoA (grey). The decrease of methylsuccinyl-CoA in the reaction mixture is due to spontaneous CoA-thioester hydrolysis. (**B**) Mcd in combination with 6.25 µM of its cognate Etf from *R. sphaeroides* (Etf_{Rs}) is able to form mesaconyl-CoA, likely due to re-oxidation of Etf in the presence of O_2. (**C**) Addition of 6.25 µM Etf-ubiquinone oxidoreductase from *Pseudomonas migulea* ($EtfQO_{Pm}$) increases the conversion of methylsuccinyl-CoA into mesaconyl-CoA by Mcd_{Rs} and Etf_{Rs} more than tenfold. (D) Replacing Mco in CETCH v6.0 with Mcd_{Rs}, Etf_{Rs}, and $EtfQO_{Pm}$ (3, 8, and 1 µM respectively) creates CETCH v7.0. Comparison of glycolate formed from CETCH v6.0 (Mco-based) and CETCH v7.0 (Mcd-Etf-EtfQO-based) using Ppk and Fdh as regeneration systems and starting with 2 mM NADP+ and 0.5 mM ADP. (**D**) Replacing Mco in CETCH v6.0 with Mcd_{Rs}, Etf_{Rs}, and $EtfQO_{Pm}$ (3, 8, and 1 µM respectively) creates CETCH v7.0. Comparison of glycolate formed from CETCH v6.0 (Mco-based) and CETCH v7.0 (Mcd-Etf-EtfQO-based) using Ppk and Fdh as regeneration systems and starting with 2 mM $NADP^+$ and 0.5 mM ADP.

Subsequently, the coupled system produced 156 µM glycolate from 120 µM acceptor molecule (Figure 14B, C, & D).

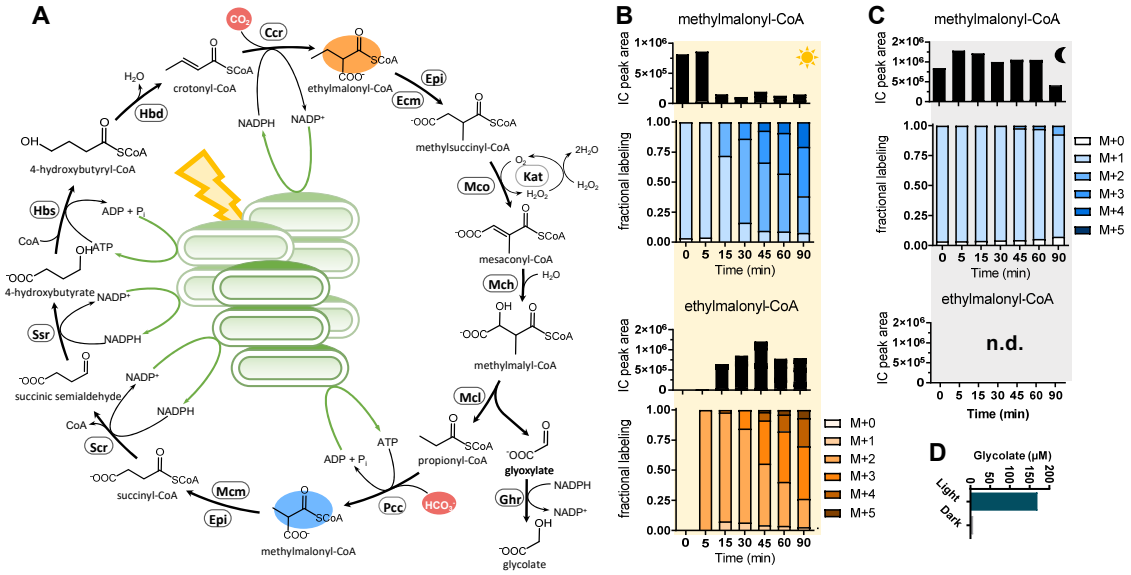

Figure 14. Light-driven, continuous fixation of CO_2 into organic acids (**A**) Scheme of CETCH version 6.0 for the conversion of CO_2 into glycolate coupled to the thylakoid energy module. (**B-C**) ^{13}C-labeling patterns and total levels of methylmalonyl-CoA (blue) and ethylmalonyl-CoA (orange) over time, starting the CETCH cycle with 80 µM propionyl-CoA. (**B**) CETCH cycle version 6.0 directly operated by 125 µg Chl mL^{-1} the thylakoid energy module under constant illumination (60 µmol photons m^{-2} s^{-1}). Shown is the extracted ion peak area and the fractional labeling of ethylmalonyl-CoA, as well as methylmalonyl-CoA (in shades of orange and blue, respectively, see Supplementary Fig. 4 for explanation of the labeling pattern) (**C**) same as in (**B**) but in the dark, showing that light is required to operate the cycle. Ethylmalonyl-CoA is not produced in the dark when starting from propionyl-CoA (n.d., not detected). (**D**) Glycolate production in the light and the dark by CETCH version 6.0.

2.3. Compartmentalization through encapsulation

Compartmentalization is a fundamental part of life, providing an "in" and an "out" allows the cell to maintain an out-of-equilibrium state. Droplet based microfluidics has emerged as a useful method for creating cell-like mimics in the lab[68]. Here independent monodisperse droplets were generated, which encapsulated both the CO_2-fixing module and the photosynthetic membranes and could be illuminated to drive the continuous fixation of CO_2 (Figure 15). The droplet activity was triggered by using white light, switching the droplets from a "sleeping" state to an active state, which was monitored by NADPH fluorescence and on a single droplet level. In the end, the microdroplets were capable of continuously fixing CO_2 for several hours. The microfluidic platform allowed for the high throughput generation of droplets and multiplexing of experiments. Perturbations of cycle components could be tested side-by-side and in real time. This system was developed in a stepwise fashion, which is outlined below.

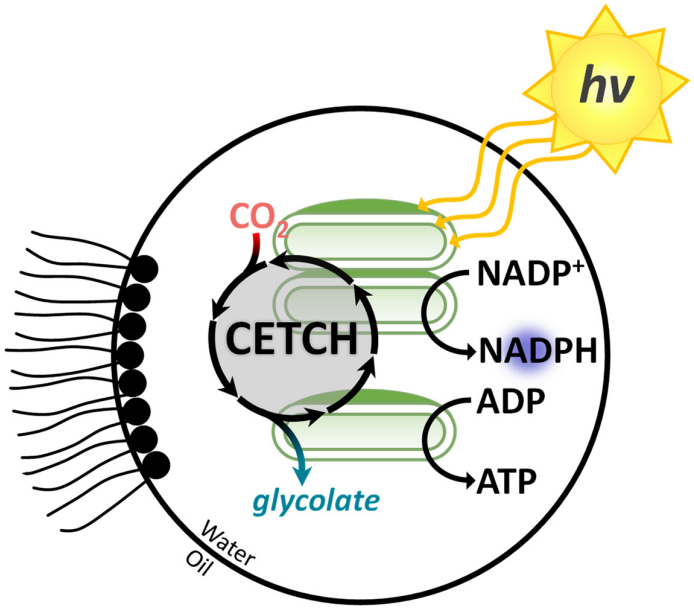

Figure 15. Photosynthetically active microdroplets. Scheme of the thylakoid energy system co-encapsulated with CETCH in microdroplets. Light triggers the thylakoid energy module activity to produce NADPH and ATP to drive carbon fixation. NADPH production is monitored by NADPH fluorescence (365 nm) of individual droplets. Populations of droplets can be distinguished from one another through the addition of a barcoding dye.

2.3.1. Development of a functional microfluidic platform

The microfluidic platform developed was modified from Beneyton *et al.*[19]. Here, microfluidic chips were used to generate water-in-oil droplets, approximately 300 pL in volume (Supplemental Figure S5 A). The droplets would fill a chamber, where individual droplets could be measured and tracked overtime. The chamber was observed with a fluorescence microscope that had been equipped with a white LED to illuminate the droplets (Supplemental Figure S5 B). To scale this system up and generate many different droplet populations simultaneously required using multiple dropmaker devices in parallel. This led to different populations of droplets in one experiment with uniform size (Supplemental Figure S5 C). These various droplet populations were distinguished using a coding dye (Supplemental Figure S5 D). The dye used was sulforhodamine B and could be excited at 550 nm. Droplet activity was monitored using NADPH fluorescence. NADPH was excited using a 365 nm diode (Supplemental Figure S5 E). Conditions for the measurement of NADPH had to be established that minimized bleaching and damage to the membranes. For this, a shutter was installed to minimize the time the chamber was excited with the 365 nm diode. For each experiment, the time between images was considered and adapted to minimize exposure while maximizing information.

Image analysis software was developed by Mathias Girault to extract data from each droplet[83]. The location and radius of individual droplets was determined from a bright field image of the chamber. After which, the barcode of the droplet was determined, this could be used to sort the droplets by population. The NADPH level of each droplet over time is extracted from the NADPH fluorescence images taken throughout the experiment. This process is outlined in Supplemental Figure S6.

Initially, the photosynthetic microdroplets were optimized using the energy module alone. This was done through encapsulating the thylakoids and reaction mixture (Figure 16 & 17). In initial experiments, it was clear that the thylakoids were functional within the droplets and when the droplets were illuminated would produce NADPH. However, during the manufacture of the droplets the thylakoids would settle in the reservoir solution overtime, leading to variances in the thylakoid composition of the microdroplets. Furthermore, the thylakoids would aggregate in the droplet overtime (Figure 16B). To address this, 330 mM sorbitol was added as an osmolyte to the reaction mixture, this prevented the thylakoids from settling in the syringe and aggregating in the droplets. Increasing the sorbitol concentration

to 700 mM further improved the lifetime of the thylakoids in the droplets (Figure 16A). After this, droplets could be manufactured with consistent in compositions and droplet-to-droplet variation in NADPH production was largely determined by statistical fluctuations of the number of encapsulated thylakoid granules (Supplementary Figure S7).

The energy module was further characterized and optimized for operation in micro-droplets. The effect of varying light intensities on NADP+ photoreduction was assessed. $NADP^+$ photoreduction increased with higher light intensities from 50 to 200 µmol photons m^{-2} s^{-1}, above which NADPH production rates decreased again, likely due to photodamage (Supplemental Figure S8). As shown in bulk experiments, the NADP+ photoreduction was operable and stable over light-dark cycles (Figure 18D & Supplemental Figure S9), demonstrating that the energy module could be switched on and off in individual droplets.

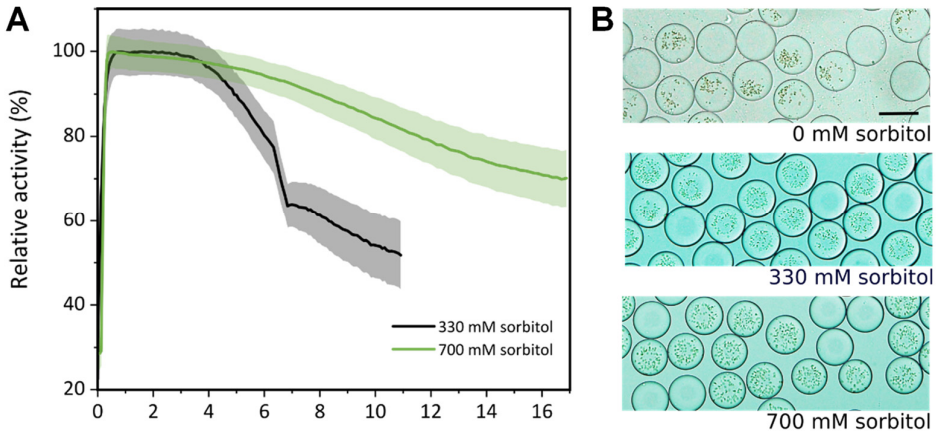

Figure 16. Thylakoid stability in droplets. (A) Relative thylakoid activity ($[NADPH]/[NADPH]_{max}$) over time under continuous illumination (100 µmol photons m^{-2} s^{-1}) using either 330 mM or 700 mM sorbitol in the reaction buffer. The relative activity is defined as the NADPH concentration normalized to its maximum value. (**B**) Droplets imaged after an overnight experiment (14-16 hours). The increasing sorbitol concentration prevents aggregation and improves the distribution of the thylakoids.

After this initial optimization, multiplexing was used to study the activity of the droplet-encapsulated thylakoid energy module. $NADP^+$ photoreduction in droplets was strictly dependent on illumination and directly correlated to the amount of thylakoids added, following a correlation with chlorophyll content (Figure 17). A maximum photoreduction rate

of 2.0 ± 0.1 (95% confidence interval) NADPH µmol min^{-1} $µg^{-1}$ Chl at 50 µmol photons m^{-2} s^{-1} was observed, which was comparable to rates obtained earlier in bulk experiments.

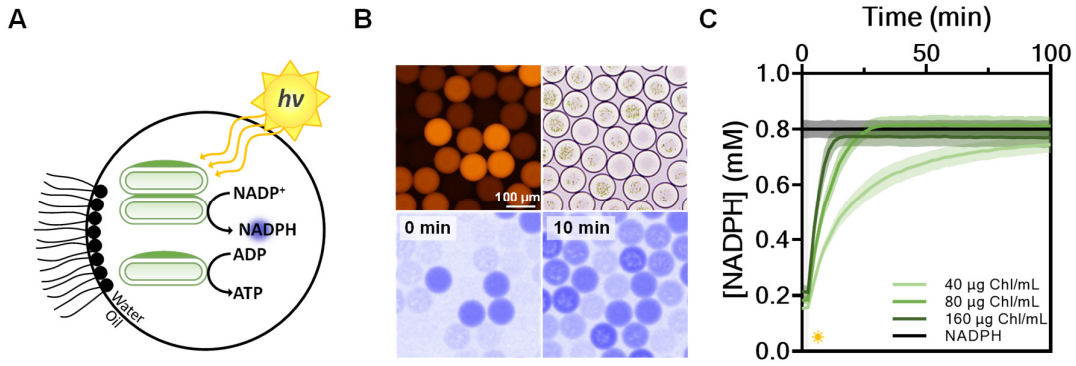

Figure 17. Encapsulation of a functional thylakoid energy module in micro-droplets. (A) Scheme of the energy module system encapsulated in micro-droplets. Light triggers thylakoid activity to produce NADPH and ATP. NADPH production is monitored by NADPH fluorescence (365 nm) of individual droplets. Populations of droplets can be distinguished from one another through the addition of a barcoding dye. **(B)** Microscopic pictures of a representative 4-bit emulsion of droplets containing four different thylakoid concentrations. First row, left to right: barcode fluorescence, bright field. Second row, left to right: NADPH fluorescence at time point 0, NADPH fluorescence after ten minutes. A time-lapse video of the increasing NADPH fluorescence is available as **Movie S1**. **(C)** NADPH concentration versus time of micro-droplets with varying thylakoid concentrations.

2.3.2. Coupling the energy module with individual biochemical reactions

In a next step, the capability of the energy module to power individual enzymatic reactions inside the droplets was tested by co-encapsulation of enzymes and substrates. First, the enzyme Ghr that catalyzes the NADPH-dependent reduction of glyoxylate to glycolate (Figure 18A) was tested. A 120 µg Chl mL^{-1} reaction mixture that also contained 8.2 µg mL^{-1} Ghr, 5 mM glyoxylate, 0.8 mM $NADP^+$, was illuminated with 50 µmol photons m^{-2} s^{-1}. After 75 minutes of illumination the droplets were dissolved and quenched and analyzed using HPLC-MS. In illuminated droplets a concentration of 4.7 mM glycolate was determined while no production of glycolate was detectable in the dark control indicating that the energy module was operating and producing NADPH only under irradiation with light.

Control over the metabolism and activity of the droplet could be achieved using an external trigger and by changing the internal compositions e.g. changing the concentration of thylakoids. However, the properties of the droplet could also be controlled by varying the substrate and enzyme concentrations. Modifications in internal components resulted in distinct dynamic NADPH equilibrium states that were reached under continuous light. Differences in this dynamic equilibrium could be seen between various populations of droplets that had different internal components (Figure 18B & C), reflecting the real-time cofactor production and consumption rates in the different populations of droplets. Furthermore, by modifying the external trigger for example using light-dark cycles could temporally regulate cofactor regeneration and enzyme kinetics in droplet populations (Figure 18D).

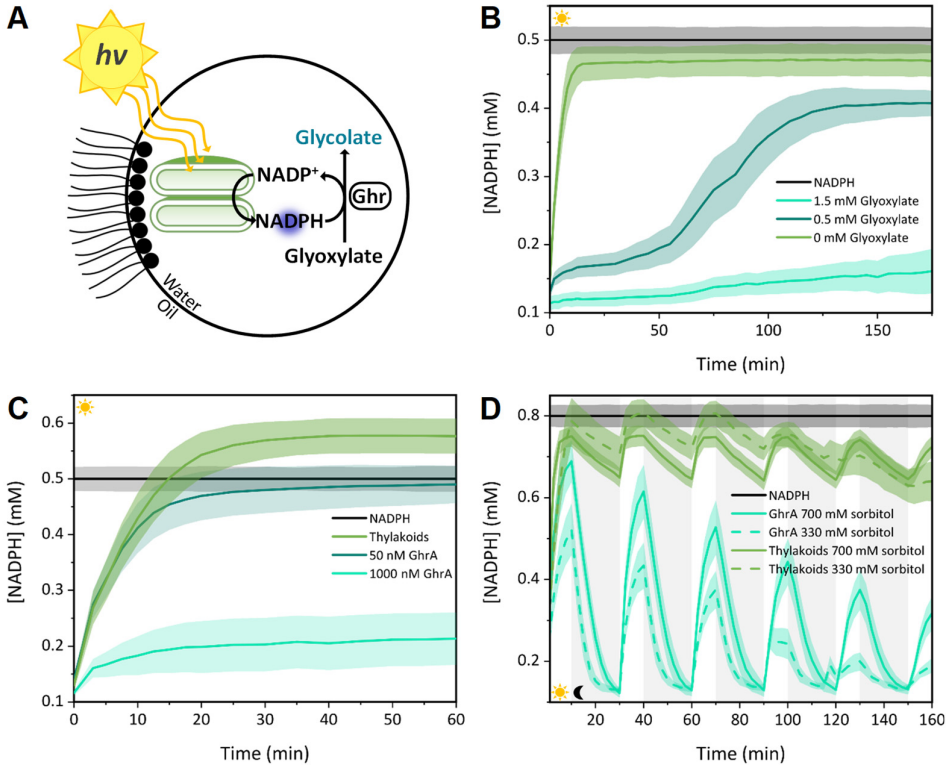

Figure 18. Coupling the NADPH-dependent reduction of glyoxylate to the thylakoid energy module in droplets demonstrates how metabolic activity and energy levels can be controlled in droplets externally. By coupling the NADPH-dependent reduction of glyoxylate to the energy module in droplets we demonstrate the control that can be achieved in droplets by varying the internal content and externally regulating the droplet by illumination. (**A**) Scheme of the Thylakoid/Ghr coupled system in microdroplets (as found in the main text). The light triggers the energy module activity to produce NADPH, which is used by Ghr to catalyze the reduction of glyoxylate into glycolate. (**B**) NADPH concentration over time

under continuous illumination (100 µmol photons m^{-2} s^{-1}) for different glyoxylate concentrations (0.5, 1.5 mM and 150 µg Chl mL^{-1}). As substrate is consumed, the NADPH level increases. (**C**) NADPH concentration over time under continuous illumination (50 µmol photons m^{-2} s^{-1}) for different concentrations of the enzyme Ghr, added at 0, 50, & 1000 nM with 65 µg Chl mL^{-1}. Different dynamic equilibrium states can be observed; as the concentration of Ghr increases, the maximum NADPH level reached decreases. Both (**B**) and (**C**) show how the internal composition can be modified to control the activity in the droplets. (**D**) Thylakoid energy module (120 µg Chl mL^{-1}) is coupled to Ghr (30 nM) and NADPH concentration is observed over time under fluctuating light conditions (50 µmol photons m^{-2} s^{-1} and dark). When the light is on, the thylakoid energy module produces NADPH, and in the dark the oxidation of NADPH catalyzed by Ghr can be observed. This is a method for synchronizing the activity in droplets and could be useful in future kinetic studies in droplets. An increase of thylakoid stability is observed in droplets containing 700 mM sorbitol (solid line) in contrast to droplets containing only 330 mM sorbitol (dashed line), where the thylakoid activity collapses after three light/dark cycles. NADPH concentration of all populations was corrected for the non-catalytic oxidation observed in the NADPH-only control. A time-lapse video of oscillations is available as **movie S2**.

The homogenous behavior of droplet populations allowed for the programming of the metabolism within the droplets. Modifying the contents of the droplets enabled the creation of "reaction compartments" with a predictable behavior. This was demonstrated by creating a patterned emulsion of two populations of droplets differing in thylakoid content as well as Ghr concentration. This binary emulsion was activated by illumination, resulting in distinct NADPH production rates, depending on the thylakoid concentration in the two droplet populations. In a subsequent dark phase, NADPH was consumed at distinct rates that were correlated to different Ghr loading of the two populations (Figure 19 & Supplementary video 3), demonstrating the high level of spatial, temporal, and synchronized control over individual reaction compartments that can be achieved with this platform. Similar results were also obtained for other droplet-encapsulated enzymes that required ATP- and/or NADPH, namely Ccr and propionyl-CoA synthase (Pcs) (Figure 20 and 21). With Ccr a single-enzyme CO_2-fixation rate of 6.4 µmol min^{-1} mg^{-1} Chl was measured in the droplets. Without any further optimization, these rates were more than two orders of magnitude higher than recent reports of coupling photosystem II (PSII) reaction centers to pyruvate carboxylase[16], comparable to values reached for PSII-coupled photoelectrochemical hydrogen production (notably without CO_2 fixation[84], and reaching levels measured for isolated whole chloroplasts (Supplementary Table 2).

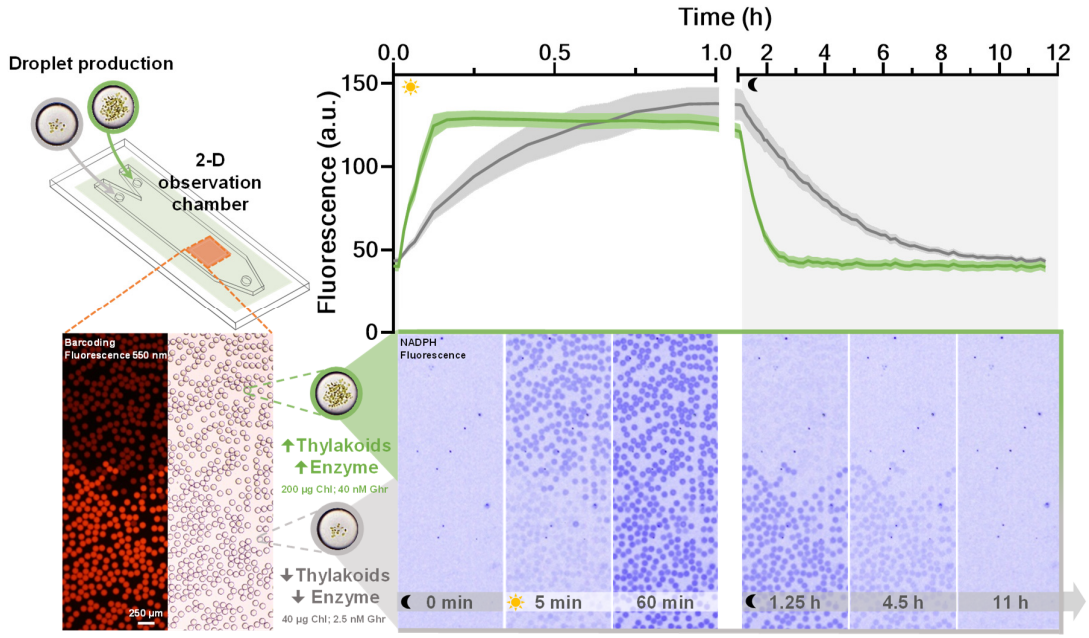

Figure 19. Time and space control of metabolic activity in droplets. A binary emulsion of droplets with two different thylakoid and Ghr concentrations was created. A spatial pattern was created by filling the droplets into an observation chamber, with each population filling approximately half of the chamber. The plot shows relative NADPH fluorescence over time under fluctuating light conditions (dark, 50 µmol photons m^{-2} s^{-1}, dark) for both droplet populations, with the same color coding. A time-lapse video of NADPH fluorescence is available as **movie S3**.

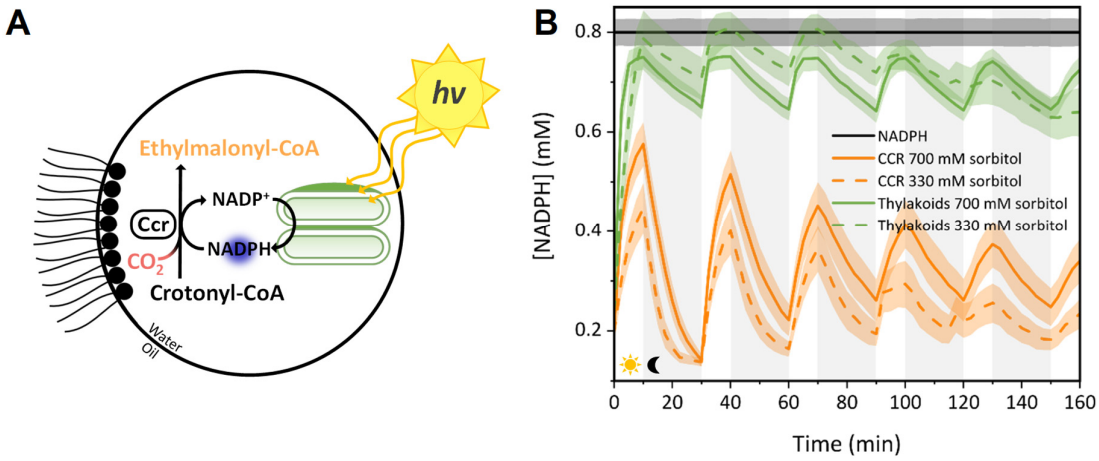

Figure 20. Coupled single carboxylase reaction to the thylakoid energy module and controlled with an external signal. (**A**) Scheme of the energy module/Ccr-coupled system in microdroplets. Light triggers Thylakoid-dependent production of NADPH, which is used by crotonyl-CoA carboxylase/reductase (Ccr) to catalyze the reductive carboxylation of crotonyl-CoA to ethylmalonyl-CoA. (**B**) NADPH concentration over time under light (50 µmol photons m^{-2} s^{-1}) and dark cycles of thylakoids (120 µg Chl mL^{-1}) coupled to Ccr (42 nM) in microdroplets. Thylakoids in microdroplets is shown in green, Ccr coupled to thylakoid energy in microdroplets is shown in orange. Similar to the Ghr coupling experiment seen in Figure 18D, a stabilizing effect of increased sorbitol can be observed (solid lines represent droplets containing 700 mM sorbitol and dashed lines 330 mM). NADPH concentration of all populations was corrected for the non-catalytic oxidation observed in the NADPH-only control (0.8 mM NADPH).

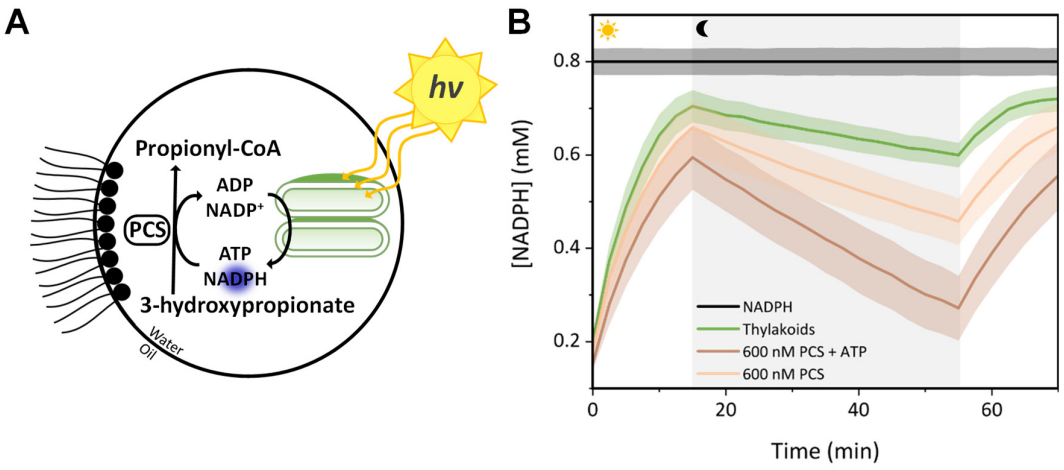

Figure 21. Propionyl-CoA Synthase coupled to thylakoid energy module (**A**) Scheme of the energy module/Pcs-coupled system in microdroplets. Light triggers thylakoid activity to produce NADPH and ATP, which are used by propionyl-CoA synthase (Pcs) to catalyze the synthesis of propionyl-CoA from 3-hydroxypropionate. (**B**) NADPH concentration over time under fluctuating light (50 µmol photons m^{-2} s^{-1})-dark cycles of the thylakoids (82 µg Chl mL^{-1}) coupled to the Pcs reaction (with 100 nM Pcs, 5 mM CoA, 5 mM 3-hydroxypropionate, 0.8 mM $NADP^+$, and 1.2 mM ATP or ADP). Thylakoid energy module in microdroplets is shown in green, Pcs coupled to the energy module in microdroplets is shown in orange, Pcs coupled to the energy module and additional ATP in micro-droplets is shown in brown. In droplets that contain additional ATP, more NADPH oxidation can be observed, indicating that ATP production (or ADP inhibition) is limiting the Pcs reaction. NADPH concentration of all populations was corrected for the non-catalytic oxidation observed in the NADPH-only control (black line).

2.3.3. Encapsulating all components for continuous light driven CO_2-fixation

Having created photosynthetic micro-compartments able to power single enzyme reactions, the next aim was ultimately the encapsulation and screening of different variants of the CETCH cycle inside thylakoid energy module-containing droplets to demonstrate the full capabilities of the platform. Through the step from single reactions to the full cycle required optimization, two specific cases are outlined below.

2.3.3.1. The tale of coenzyme B_{12} and ascorbate

Multiple enzymatic candidates exist for the reduction of glyoxylate. For the above experiments, GhrA from *E. coli* was used; however, this exhibits a relatively high K_M for gloxylate[85]. For this reason, other candidate enzymes were tested, including GhrB from *E. coli*. Tests with GhrB coupled to the full CETCH cycle were unsuccessful. These experiments were performed with different independent droplet populations in parallel containing: a control with NADPH and a CETCH cycle that lacked Ccr; $NADP^+$, the thylakoids, and a CETCH cycle that lacked Ccr; and lastly, droplets with $NADP^+$, thylakoids, and a functional CETCH cycle. From the fluorescence, NADPH oxidation was apparent in the control droplets where there should have been no NADPH oxidization. The problematic components were elucidated to be GhrB in combination with B_{12} and ascorbate (Figure 22). In the full CETCH experiments excess coenzyme B_{12} was added along with ascorbate. These components undergo a reaction with one another, where the B_{12} is reduced by ascorbate and will get reoxidized by oxygen forming H_2O_2 [86]. There are two issues with this, the hydrogen peroxide can damage the B_{12} and it will also form the oxidized form of ascorbate, dehydroascorbate. Dehydroascorbate is prone to delactonation [87], which results in the formation of 2,3-diketoglugonic acid. The latter is similar in structure to a known substrate of GhrB, 2,5-Didehydro-D-gluconate[85]. It was likely that GhrB would use 2,3-diketoglugonic acid as a substrate, consuming the NADPH in the droplets and preventing the CETCH cycle from functioning

Nevertheless, both the mutases, Mcm and Ecm, require coenzyme B_{12} and could not be replaced. Therefore, GhrA was used in subsequent experiments. Additionally, the mutases would be incubated with to coenzyme B_{12} for 30 minutes prior to their addition to the reaction mixture. These measures solved the issue of wasteful NADPH consumption.

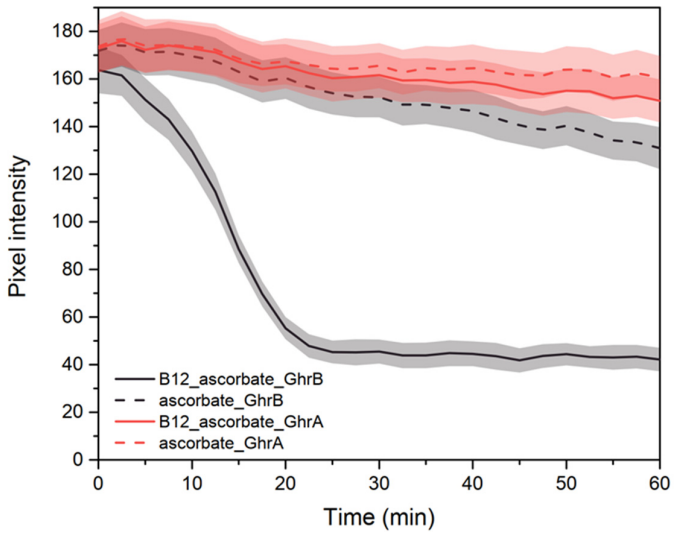

Figure 22. GhrB interaction with the B_{12} and ascorbate mixture. Reaction mixtures containing various combinations of glyoxylate reductases, B_{12}, and ascorbate. In the droplet population containing B_{12}, ascorbate, and GhrB NADPH oxidation was dramatic and 1 mM of NADPH was consumed within 25 minutes. There was a slight oxidation in droplets containing GhrB and ascorbate alone.

2.3.3.2. Promiscuous hydratases and CoA ester stability

Manufacturing large quantities of droplets takes time and in certain experiments up to 1 hour. During this incubation period the "sleeping" reaction mixture would undergo changes. Usually, in bulk experiments propionyl-CoA would be added and the starting substrate for the cycle and therefore in CETCH v6.0, the first reaction taking place is propionyl-CoA carboxylation. This step is catalyzed by Pcc, requiring ATP and results in the formation of methylmalonyl-CoA. Methylmalonyl-CoA will be further transformed into succinyl-CoA by the mutase Mcm before reaching the first NADPH requiring reaction that is catalyzed by succinyl-CoA reductase. As discussed in Section 2.1.2, thylakoids can produce ATP in the dark independent of photosynthetic electron transport via membrane bound adenylate kinases. Over this hour of incubation, ATP would be produced by the adenylate kinases be used by Pcc to carboxylate propionyl-CoA and eventually converted to succinyl-CoA. Succinyl-CoA is particularly vulnerable to hydrolysis and overtime the substrate pool for the CETCH cycle would be depleted through hydrolysis of succinyl-CoA. This would decrease the overall production of glycolate when the light was turned on. To address this, other starting points for the CETCH cycle were considered.

Although crotonyl-CoA was the best candidate there was an intrinsic hydratase activity associated with the thylakoid preparations that converted crotonyl-CoA into 3-hydroxybutyryl-CoA (Figure 23). This was addressed by the introduction of an additional enzyme, a crotonase from *P. aeruginosa* (PhaJ)[88] to provide metabolic proof-reading[89]. Higher production of glycolate was achieved when starting at crotonyl-CoA versus propionyl-CoA after incubation for 1 h (Figure 24).

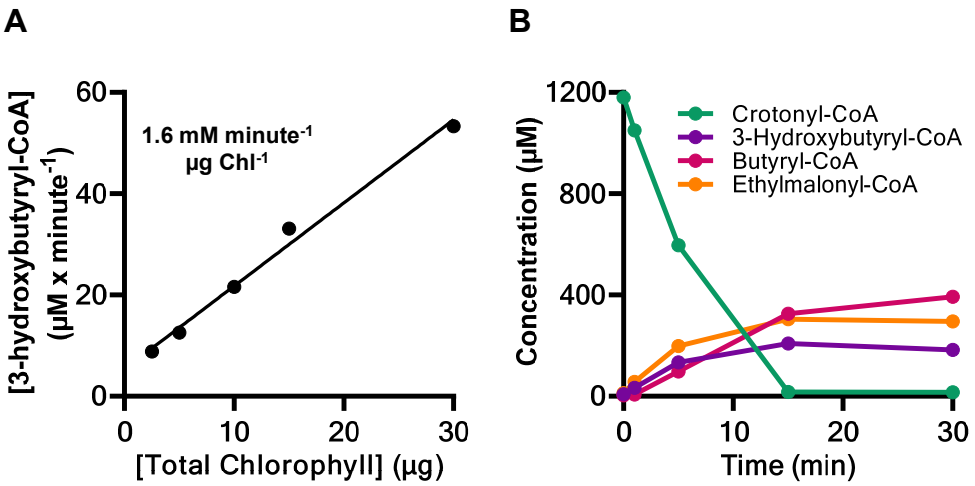

Figure 23. 3-hydroxybutyryl-CoA formation by thylakoids. (**A**) Incubation of the thylakods with 1.2 mM crotonyl-CoA in the dark leads to formation of 3-hydroxybutyryl-CoA. 3-Hydroxybutyryl-CoA formation is light-independent and linear to the thylakoid concentration at a rate of 1.6 ± 0.1 µM minute^{-1} µg^{-1} Chl (Y = 1.642X + 5.356, R^2 = 0.99) The reaction mixture included 5 µM Fdx, 310 nM SOD, 1.2 µM Cat, 1.85 µM Pcc, and 1.29 µM Ccr and various concentrations of thylakoids (2.5, 5, 10, 15, and 30 µg Chl). (**B**) The same reaction conditions but under illumination (60 µmol photons m^{-2} s^{-1}) and in the presence of Ccr (1.29 µM). Thylakoid-dependent conversion of crotonyl-CoA (green) into 3-hydroxybutyryl-CoA (purple) is still significant compared to the conversion catalyzed by Ccr (orange). Shown is a reaction containing 10 µg Chl.

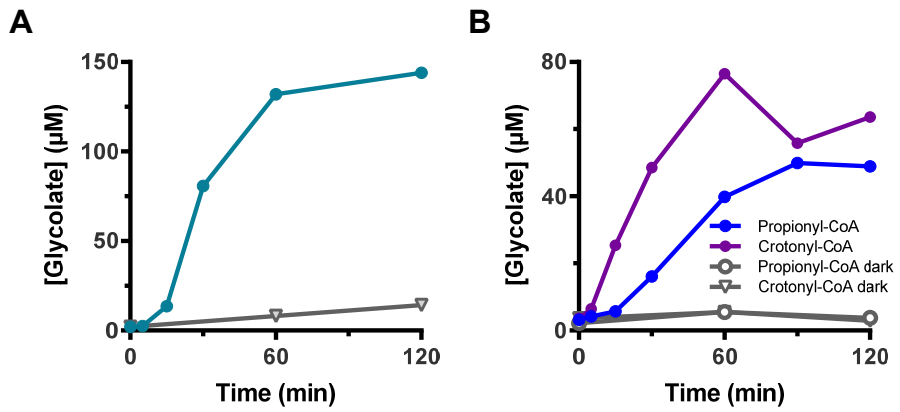

Figure 24. Optimizing preparation of microdroplets for operating the CETCH cycle with the thylakoid energy module. During encapsulation, the reaction mixture incubates for about one hour in the dark and at room temperature. To assess the effect of prolonged incubations of the reaction mixture before illumination, we measured glycolate production rates of CETCH v7.0 coupled to energy module in bulk with simulated conditions during encapsulation. (**A**) Glycolate formed starting from 120 µM propionyl-CoA when reactions are illuminated directly after mixing (teal line) or kept in dark conditions (grey line). (**B**) Glycolate formed when starting from both propionyl-CoA (blue) and crotonyl-CoA (purple) (120 and 90 µM, respectively) after one hour incubation in the dark. Samples were taken at 0, 5, 15, 30, 60, 90, and 120 minutes after illumination (60 µmol photons m^{-2} s^{-1}) or at 0, 60, and 120 minutes after the initial 1-hour incubation for samples that remained in the dark. These results from a representative experiment suggest that, with prolonged incubation times, starting from crotonyl-CoA leads to higher production rates compared to starting from propionyl-CoA. This might be explained by adenylate kinase activity producing ATP in the dark, which allows propionyl-CoA carboxylase (Pcc) to carboxylate propionyl-CoA to methylmalonyl-CoA, which is subsequently converted into succinyl-CoA. Succinyl-CoA is prone to spontaneous hydrolysis, likely lowering overall productivity of the system. As a result, we used crotonyl-CoA, and not propionyl-CoA as described by Schwander *et al.*[38], to prepare CETCH- and energy module-containing microdroplets, mimicking the chloroplast.

After these additional optimization steps of the droplet operating conditions, the co-encapsulation of both the CETCH cycle and the energy module achieved continuous fixation of CO_2. Different CETCH cycle versions were encapsulated together with the energy module and the dynamic equilibrium of NADPH was monitored (Figure 25). This allowed for a direct quantification of the behavior of different CETCH variants in hundreds of micro-

compartments side-by-side and in real time, which would not have been possible in bulk experiments (Figure 25A, 25B, 26B, & 26C). Droplets with CETCH based on Mcd (version 7.0) maintained energy module activity longer than droplets containing CETCH based on Mco (version 6.0) (Figure 25). Supply of an additional ATP regeneration module (Ppk and polyphosphate) did not increase activity further (Figure 26B & 25C), suggesting that cofactor regeneration was not limiting productivity of the integrated photosynthetic system, but rather the concentration, and/or interplay of the individual components within the system, such as the stability of CoA-thioester intermediates (Figure 24). Without further optimization, this integrated system was able to produce 47 ± 5 μM glycolate from CO_2 over 90 minutes in droplets (Figure 26D). Thus, while overall productivity of the highly complex system was lowered compared to Ccr alone, it still outperformed other efforts using only single enzymes[16]. For the full CETCH cycle, a light to carbon conversion efficiency of about 3.5% within the micro-compartments could be calculated (NADPH consumption rate of CO_2 reduction divided by the measured maximum rate of $NADP^+$ photoreduction achieved in droplets). Overall these results demonstrated that it is possible to interface natural and synthetic biological modules in thousands of cell-sized compartments to create new-to-nature photosynthetic entities that have the potential to outcompete natural photosynthesis (i.e. because of a more efficient CO_2-fixation metabolism that does not suffer from photorespiration).

Using microfluidics to combine the natural photosynthetic machinery with a synthetic CO_2-fixation pathway, we created a light-driven micro-compartment that in essence mimics a chloroplast. Functional coupling of a synthetic pathway, such as the CETCH cycle, to the native photosynthetic machinery to create a new-to-nature photosynthetic process provided an experimental and technical challenge.

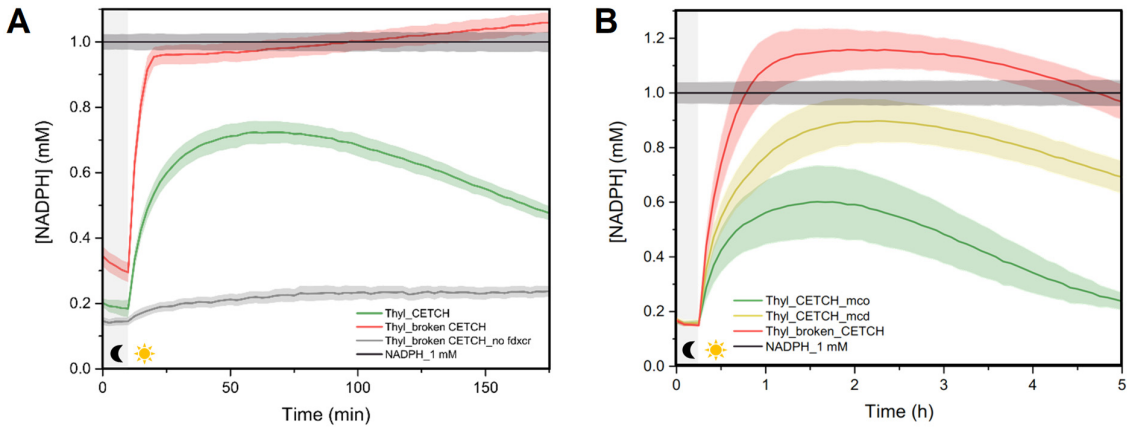

Figure 25. Dynamic equilibrium monitoring of various versions of the CETCH cycle powered by the thylakoid based energy module. (**A**) Different versions of CETCH v6.0 coupled to thylakoids (70 µg Chl mL^{-1}) in microdroplets. Droplets containing a functional thylakoid based energy module, 1 mM $NADP^+$ and a functional CETCH v6.0 (with Mco, green line), as well as control droplets containing the energy module, 1 mM $NADP^+$ and all enzymes of CETCH v6.0 except Ccr (red line), droplets containing the energy module, 1 mM $NADP^+$, all enzymes of CETCH v6.0 except Ccr and no ferredoxin (grey line), as well as control droplets containing 1 mM NADPH. The dynamic equilibrium level of NADPH (indicating thylakoid energy module activity) decreases after 100 minutes in droplets containing a functional CETCH v6.0 cycle. (**B**) Comparison of CETCH v6.0 (with Mco, green line) as shown in (**A**) and CETCH v7.0 (with Mcd, yellow line). Droplets with CETCH v7.0 maintain the dynamic equilibrium level of NADPH longer than droplets with CETCH v6.0, which is likely due to the use of Mcd instead of Mco.

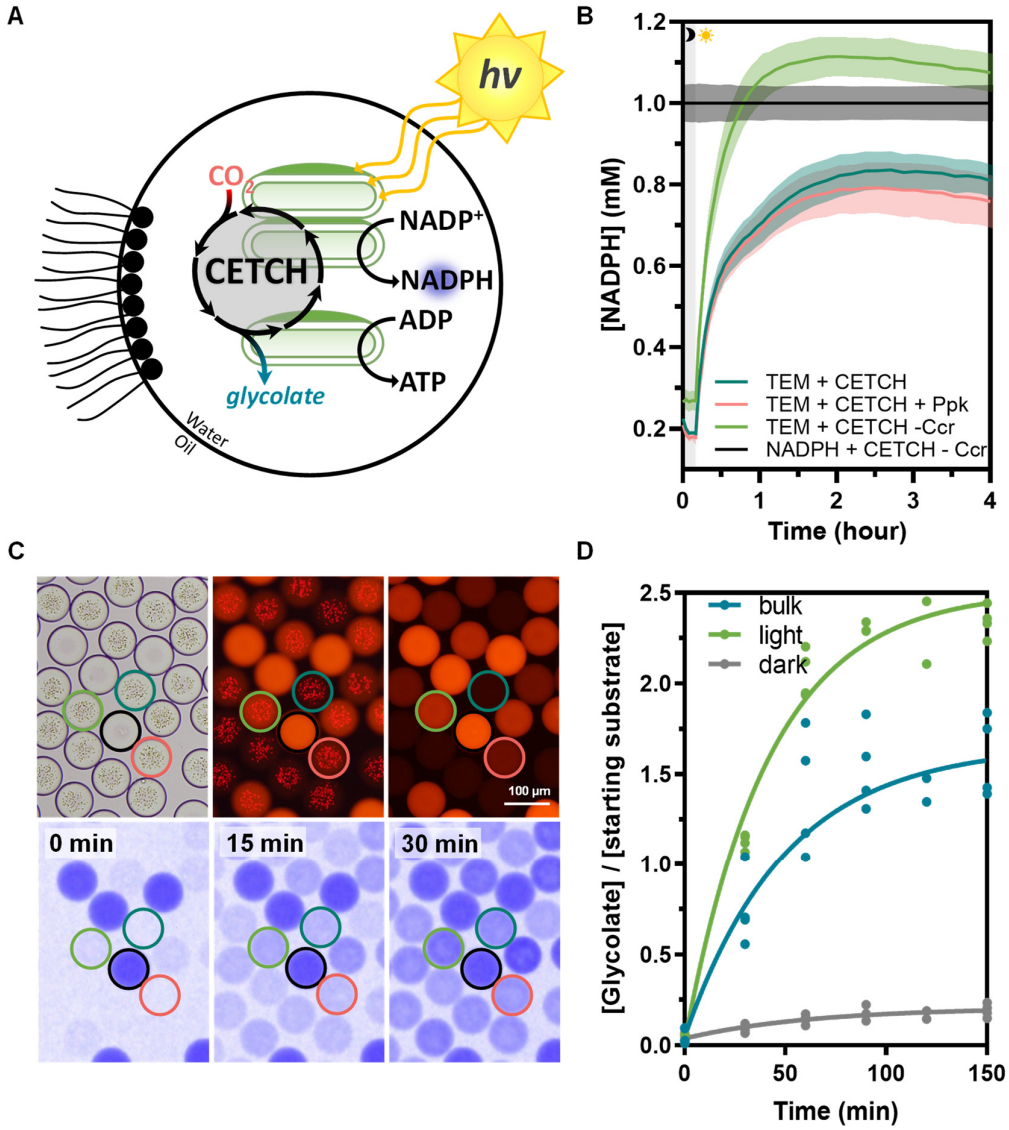

Figure 26. Light-driven, continuous fixation of CO_2 into organic acids by CETCH version 7.0 coupled to the thylakoid energy module in micro-droplets. (**A**) Scheme of the CETCH version 7.0 coupled to the thylakoid energy module operating inside micro-droplets. (**B**) Dynamic equilibrium states of NADPH fluorescence of four populations of droplets: Droplets containing the thylakoid energy module (60 µg Chl mL^{-1}), 1 mM $NADP^+$ and CETCH version 7.0 (teal line), droplets containing the thylakoid energy module, 1 mM $NADP^+$ and an additional ATP regeneration system (Ppk and polyphosphate, coral line), as well as control droplets containing 1 mM NADPH and all CETCH version 7.0 components except for Ccr (black line), and control droplets containing the thylakoid energy module, 1 mM $NADP^+$ and all CETCH version 7.0 components except for Ccr (green line). (**C**) Images of the droplets from (B) using the same color coding; first row, left to the right: bright field, thylakoid fluorescence with overlap from the coding dye, coding dye; second row, left to the right: NADPH fluorescence before illumination, after 15 minutes, and after 30

minutes illumination (scale bar corresponds to 100 μM). A time-lapse video is available as **movie S4**. (**D**) Glycolate formed per acceptor molecule (sum of crotonyl-CoA and 3-hydroxybutyryl-CoA) over time in droplets and in bulk solution. The light and dark curves represent droplets maintained in the light and in the dark. The bulk curve shows an experiment with the same reaction mixture but on the micro-tube scale, kept in the dark for the duration of droplet manufacture. The bulk solution and the droplets were simultaneously exposed to light for parallel comparison.

3. Discussion and general outlook

3.1. Design and realization of CO_2 fixing microdroplets

This work outlines the creation of microdroplets with a controllable metabolism, in which light drives the generation of NADPH and ATP that are used to energize the continuous fixation of CO_2 via the synthetic CETCH cycle. Here parts of living cells and synthetic modules were combined within independent and monodisperse metabolically active droplets that are capable of synthetic photosynthesis. These cell sized droplets house a functional light- driven metabolism, which appears to be the most miniaturized realization of such complex reactions in artificial compartments that lie within the size range of normal plant cells (10-100 µm)[90].

To create the functional metabolism within these droplets, first, a light-driven energy module had to be established and optimized. The basis for the light driven energy module was thylakoid membranes extracted from the chloroplasts of spinach. After determining the optimum concentrations of reaction components, the membranes were capable of using water as an electron donor to generate molecular oxygen, NADPH, and ATP in the light, demonstrating that the membranes were intact and functional. A functional energy module required osmolytes, antioxidative components, cofactors, and soluble electron carriers to be added. Using low light intensities were found to prolong thylakoid activity while simultaneously producing sufficient amounts of NADPH and ATP to power a complex set of biochemical reactions at high enough rates.

Secondly, the energy module needed to be successfully coupled to a synthetic CO_2 fixation pathway comprising 17 individual enzymes. This entailed modifying the previously described version of the CETCH cycle (v5.4)[38], exchanging and adding several enzymes and also replacing the output module. Initially, the energy module was used to power two individual carboxylation reactions, catalyzed by Pcc and Ccr, which use ATP and NADPH, respectively. Subsequently, this was expanded to the entire non-natural CO_2-fixing CETCH cycle, which required optimization to operate alongside the thylakoid membrane energy module. Optimizing operation conditions required modifying buffer and enzyme components as well as improving certain enzyme preparation methods. Eventually, the entire 17 enzyme comprising CETCH cycle could be powered by light allowing the continuous conversion of CO_2 into glycolate.

Lastly, a platform for the miniaturization, automation, and encapsulation was developed to create hundreds to thousands of photosynthetic reaction compartments. Each of these droplets could be individually controlled in their activity and when active, could maintain a non-equilibrium state for several hours. Compartmentalization of these modules into cell-sized droplets was achieved using microfluidics. The platform was developed such that both the CETCH cycle and the energy regeneration system could operate synchronously within water-in-oil droplets independent from the environment. Here, thousands of droplets were created that had individual characteristics and could be controlled and monitored in parallel. The droplet activity was triggered using light, switching it from a "sleeping" state to an active one. Testing individual reactions, i.e. Ghr, Pcs, and Ccr, within the droplets demonstrated that the properties of the droplets could not only be controlled by external signal but also by altering their internal composition. By specific loading of the contents of the "reaction compartment" and using light, the droplets could be programmed and activated in a predictable fashion and used to study both the thylakoid and enzyme activity. This and the high throughput capability of the platform was used to test cycle variants for the improvement of the cycle. Under continuous light the droplets reached a steady state, a dynamic equilibrium that was used to compare different operating conditions side by side. In the end, the droplets were capable of the continuous fixation of CO_2 by two new versions of the CETCH cycle (v6.0 and ultimately v7.0) using light as the sole source of energy.

3.2. Comparison to other complex systems

These efforts are notably different from recent and similar work to recapitulate complex metabolisms in droplets or other cell-free systems for energy regeneration. In these recent examples either PSII or bacteriorhodopsin were commonly used in combination with ATPase to drive ATP synthesis[15,16,91]. In particular Lee *et al.* designed a system where ATP generation could be turned on and off using light. In Lee *et al.* both PSII and proteorhodopsin were embedded in liposomes together with an ATPase. Red light was used to build a PMF across the liposome membrane to generate ATP. Proteorhodopsin is a green-light activated bidirectional proton pump that is dependent on pH. Therefore, contingent on the pH of the system and the PMF built, green light could be used to actually pump protons out of the liposome and deplete the PMF, halting the production of ATP. This small photosynthetic liposome was put inside a giant unilamellar liposome where the controllable ATP production was linked actin polymerization and depolymerization. When the actin filament was growing

it physically pushed against the artificial membrane, resulting in morphological changes. Thus, energy generation was employed to control an artificial cytoskeleton, which could potentially be used to facilitate a controlled merging of different types of reconstituted liposomes as well as for the development of division and replication in artificial systems in the future.

Water served as the electron donor for PSII however, PSII also requires an electron acceptor and for this Lee *et al.* employed the artificial electron acceptor, phenyl-p-benzoquinone. If PSII no longer has electron acceptors available, its activity would come to a halt therefore, phenyl-p-benzoquinone would actually limit the entire system. Adapting these liposomes for continuous ATP generation would require the incorporation an artificial Q-cycle, allowing the reduced phenyl-p-benzoquinone to be re-oxidized within the system, for the efficient regeneration of the electron acceptor.

Lee *et al.* also powered the carbon fixation reaction converting pyruvate to oxaloacetate catalyzed by pyruvate carboxylase. When comparing the CO_2-fixation and ATP production from Lee *et al.*, to the rates achieved in the photosynthetic micro droplets in this thesis were 100 and even 1000 times higher (Supplemental table 1 & 2). Additional comparisons to other synthetic methods and rates measured for natural systems are also shown in Supplemental table 1 & 2. Overall, this work achieved similar ATP and NADPH production rates for isolated thylakoid membranes as were described in literature but somewhat lower rates compared to intact chloroplasts. In general, the productivity of isolated membranes is usually higher than with reconstituted systems. Using a combination of PSII and PSI generates both NADPH and ATP. The concomitant consumption of NADPH by CETCH enzymes should constantly re-supply electron acceptors for PSII, allowing for the continuous generation of ATP and NADPH via the photosynthetic electron transport chain. Furthermore, the generation of ATP and NADPH allows for more complex sets of reactions to take place inside the compartments. Moreover, reduced ferredoxin is also provided which could be partially diverted to enzymatic reactions that require lower redox potential electron donors. Overall, using the entire photosynthetic electron transport chain provide the means to power diverse biosynthetic reactions or reaction cascades.

In a similar microfluidic platform, Beneyton *et al.* used inverted membrane vesicles (IMVs) derived from *E. coli*, which housed NADH oxidase to regenerate NAD^+ required for a minimal

metabolism that converted glucose-6-phosphate into phosphogluconolactone[19]. The droplets were capable of maintaining an out-of-equilibrium state as long as there was glucose-6-phosphate available to be consumed. After the substrate ran out the droplets would return to a "sleeping" state that could be restarted when additional substrate was picoinjected into the droplets. Naturally, the NADH that was oxidized would be used by the membranes to generate a PMF and finally drive ATP synthesis. It would be interesting to use the natural ability for the IMVs to generate ATP and use it to expand the minimal metabolism with an ATP dependent reaction like protein biosynthesis[92]. The system presented by Beneyton *et al.* had several differences in comparison to the system described in this work, which uses light derived NADPH and ATP to drive a much more complex metabolism. In the study presented here the trigger to start the metabolism came from light and did not require any additional picoinjection. In theory, using light one could achieve an almost perpetual regeneration of NADPH and ATP that can be used to run synthetic CO_2 fixation in a droplet. Furthermore, by using an anabolic biosynthetic cycle the minimal metabolism was not limited by a substrate. The combination of these membrane systems could achieve interesting results and provide the means to generate NADH alongside NADPH.

3.3. Further optimization

To truly take advantage of a limitless supply of energy, such as light, the system harvesting that energy must be stable over long periods. The chloroplast mimic described here, showed evidence of damage and would lose activity overtime. Damage to both the photosynthetic apparatus and to some of the CETCH enzymes did occur. Detailed characterization of the membranes could elucidate weak points in the energy module and promote additional improvements. Using photosynthetic fluorescence and quantum yield measurements, the PSI and PSII activity could be studied and used to further optimize their operation conditions. Likewise, finding membranes that have a more stable and robust photosynthetic apparatus could increase the time that membranes are active. Specifically, purifying thylakoids from organisms like thermophilic *Synechococcus* strains or *Chlorella ohadii*, which have been shown to survive in extreme conditions like high-light[93,94], could be a promising approach. Another strategy would be to immobilize the thylakoid membranes in a physical scaffold like a silica gel, since several such methods have demonstrated their utility in preserving purified thylakoid activity. Changing the buffer conditions could also improve activity; compounds like glycine betaine have been shown to provide a protective benefit to the membranes. The

ultimate solution would be to implement repair mechanisms for the photosynthetic apparatus itself. Such efforts would serve a dual purpose, increasing the lifetime of the membranes and simultaneously escalating the overall life-like complexity.

Additionally, oxidative stress still seems to have deleterious effects, when comparing the dynamic equilibrium of droplets that contain CETCH v6.0 and CETCH v7.0, which differ only in the enzymes that catalyze the oxidation of methylsuccinyl-CoA. Droplets containing CETCH 6.0 that utilized Mco appeared to lose activity faster than those that used the Mcd/Etf/Etf:QO system. Adding in more antioxidative enzymes could further mitigate the damage from ROS and improve all-over activity. One such enzyme could be a soluble ascorbate peroxidase. Another option could be to add glutathione and a glutathione regeneration system. Furthermore, the addition of IMVs from *R. sphaeroides* engineered to over-express their native Etf:QO could decrease ROS by providing an effective route for electron transport from methylsuccinyl-CoA to the quinone pool. Moreover, the IMVs from *R. sphaeroides* also possess photosynthetic activity that could be used to produce additional ATP.

3.4. Potential applications

The efforts described in this work have led to the successful creation of a platform that can be used to reconstruct, control, and study complex reaction networks in a cell-like environment. This has far-reaching applications in bottom-up and top-down synthetic biology. On the one hand, the microfluidics platform has the potential to aid and lead metabolic engineering efforts by prototyping and optimizing metabolic reaction cascades prior to their transplantation *in vivo*. Being able to test and optimize the behavior of complex pathways and their interplay with native cell extracts could help to overcome the limitations of common practice in metabolic engineering and synthetic biology that still rely on the laborious construction and analysis of individual strains[95]. The ideal stoichiometry of enzymes can easily be determined to fine-tune expression levels for *in vivo* implementation. Furthermore, the enzyme functionality is tested in conditions that more closely resemble the cell or organelle environment. For example, the B_{12} dependent mutases are functional in a buffer that contains 10 mM ascorbate, which would be representative of a chloroplast stroma, indicating that if the enzymes were intact in the chloroplast they could be active despite the negative interaction of B_{12} and ascorbate. Current technical developments, especially of combinatorial screening methods[96] and bar-coding techniques to encode reaction conditions in microfluidics-based

high-throughput screenings[97] will further enhance multiplexing capabilities and guide efforts for implementing the CETCH cycle and other new-to-nature pathways into living cells.

Furthermore, equipping the droplets with light activated energy supply also provides the means of control. These microreactors are activated with an external trigger and thousands of droplets can be synchronized, potentially simplifying the microfluidic techniques that are needed for a particular experiment. For example, if one were analyzing enzyme kinetics this circumvents the need for picoinjection of substrates or cofactors to initiate the reaction. Here, all that is needed is light to initiate metabolic activity in the droplets.

This platform also represents an effort in cell-free or *in vitro* metabolic engineering for the production of biochemicals. This strategy provides an advantage over traditional metabolic engineering because it can overcome a number of restraints that are imposed by living cells. In such *in vitro* systems, higher product titers can be achieved, because energy resources that would normally go to cell maintenance (growth, replication, etc.) can be diverted to product synthesis. Additionally, the *in vitro* platform can be used to reach product concentrations that would potentially be toxic to the living cell. Moreover, with these systems, a diverse set of feedstocks can be used that would otherwise require additional processing or specialized transporters to enter the cell. Without these limitations, the potential metabolic reaction space can be expanded to pathways that would normally not be possible in the cellular environment. Limited efforts in this field have sought to use CO_2 as a feedstock[98,99]. While much of the research has focused on using classical feedstocks, such as glucose, *in vitro* metabolic engineering has not been exploited for the utilization of inorganic carbon as raw material until recently. In this respect, the encapsulated CETCH cycle provides glycolate as a starting molecule for downstream applications, which can easily be converted into intermediates of the central carbon metabolism, potentially feeding into diverse biosynthetic routes [100].

3.5. From droplets to minimal cells

These efforts exemplify how natural and synthetic biological modules can be mixed and matched to create highly integrated systems from the bottom-up, showing life-like functions. Specifically, these efforts recapitulate three of the pillars of life: energy, metabolism, and compartmentalization. This ‘synthetic chloroplast’ possesses the essential characteristics of photosynthesis that allows it to create biological building blocks from inorganic carbon, providing the basis to develop a self-sustained, completely synthetic ‘designer’ metabolism in

this artificial organelle. The glycolate that is produced in these droplets can be used as a substrate for additional downstream reactions or pathways and serve as the basis of metabolism. Expansion of this rudimentary metabolism with other metabolic modules could be used to form a variety of different molecules necessary to sustain the various processes in a cell (e.g. amino acid biosynthesis).

The life-like complexity can be increased by the future implementation of other life characteristics, such as self-repair, reproduction, as well as information processing and regulatory circuits. This will further contribute to the realization of synthetic organelles and cells that approach a grade of organization and integration similar to their natural counterparts. By adding transcription and translation the artificial cell would be provided with an executable program. Furthermore, these already established pillars can be improved, for example through repair mechanisms, expanding the metabolic module to produce other building blocks like amino acids, and the method of compartmentalization could be changed to allow for the barrier to be a more life-like semi-permeable lipid bilayer. Examples of these systems have been demonstrated *in vitro* or in other artificial cells. More specifically, examples of compartmentalization[105], quorum sensing[101,102], information processing through DNA or RNA, advanced transcription-translation (TX-TL) circuits[103-108], cytoskeleton mimics[109], cell division[110], or complex *in vitro* metabolic networks [38,111-114] have been developed. Combining all of these life-like systems could model the sophistication of a cell within a simplified system created of minimal parts. This would be an astonishing achievement while simultaneously providing a new tool for scientists to address what are the fundamental principles required for life.

In the future, different sizes of microdroplets could be patterned and tested, including patterning the droplets in layers to test self-shading, or in a pattern that resembles a leaf. The implementation of droplet-to-droplet communication could allow for further division of labor and compartmentalization of different metabolic pathways alongside each other in an organized fashion. Further expanding and increasing the life-like complexity in a bottom-up fashion.

3.6. Outlook and closing remarks

The successful creation of an artificial cell would demonstrate an unprecedented understanding of life. Feynman wrote, “[w]hat I cannot create, I do not understand.” Despite

having an understanding of the core principles required for life, scientists have yet to reverse engineer life in the lab. However, there is a strong foundation of knowledge and tools already available to be used to build life-like structures. Using these tools, this work created a structural and functional mimic of a chloroplast, which is a stepping stone in these efforts. The process of (re)-building life will provide new insights and a better understanding of life's guiding principles. (Re)-building living systems will demonstrate whether or not we truly understand life's mechanisms.

Overall, the system described in this work is a bridge between *in vitro* development to *in vivo* implementation, serving as a model for sophisticated cells using minimal parts. At this interface invaluable knowledge can be garnered from complex metabolic pathways that can be used for the eventual implementation of these pathways *in vivo* or be used to continue to build cell mimics from the bottom up.

Pressing and difficult challenges exist for civilization, scientists, and policy makers and we must act collectively to create an effective stratagem to tackle them. With an ever increasing population, meeting the energy and food demands as well as mitigating climate change become more and more imperative. Estimates for food demand will exceed the current capacity of agriculture by 2050[115,116]. Human activity continues to impact the global CO_2 level[117]. However, synthetic biology and bottom up biotechnology can be a significant contributor in the search for solutions to these critical issues. One can take inspiration from one of biology's most elegant innovations, that of photosynthesis and see CO_2 as a feedstock for the production of valuable commodities. High value and high energy compounds that are produced from CO_2 can create a carbon neutral future. The combination of sustainable energy generation and novel biological solutions make this idea feasible. The chemical conversion of CO_2 into organic compounds often requires harsh conditions like high temperature or high pressure[118]. In contrast, enzymes can operate at standard temperatures and pressures and produce molecules of interest with high specificity. This work as well as that of many others represent novel solutions for the enzymatic conversion of CO_2. The described platform can be used to directly produce high value products or be used to optimize pathways for the fixation of CO_2 *in vivo* or *in vitro*.

The platform created here can be used to streamline the testing and evaluation of these novel biotechnological solutions. Here the utility of the platform was demonstrated by powering a

synthetic CO_2 fixing pathway and that it could be used for side by side comparison of droplets containing varying perturbations of the CETCH cycle. This can be expanded to more variations and even new cycles like HOPAC and CHYME, which can speed the creation of robust CO_2 fixing cycles[38].

By creating a robust photosynthetic energy source, the active membranes' ability to convert light energy into chemical energy could provide an almost limitless supply of chemical power to drive these reactions. This would require that the membranes were stabilized further to increase their lifetime. An alternative solution would be to link these pathways directly to photovoltaic systems to drive these reactions.

Overall, we have tools that empower us to solve the most pressing issues of the world today. It is our job to use this knowledge and these tools to create novel, innovative, and transformative solutions. Harnessing the sun to capture carbon dioxide can be part of a solution to a sustainable future. Because after all, "life and civilization will continue as long as the sun shines[119]!"

4. Materials and methods

4.1. Materials

Chemicals were purchased from Sigma-Aldrich (Munich, Germany) and CARL ROTH GmbH (Karlsruhe, Germany). Sulforhodamine B and 1H, 1H, 2H, 2H-perfluoro-1-octanol were purchased from Sigma. $Na^{13}CO_3H$ was obtained from Cambridge Isotope Laboratories Inc. (Tewksbury, USA) and 3-hydroxypropionate was bought from TCI Deutschland GmbH (Eschborn, Germany). Fluoro-silane (Aquapel) was purchased from Aquapel Glass Treatment (Pittsburgh Glass Works LLC Pittburgh, PA, USA). Coenzyme A was purchased from Roche Diagnostics. Biochemicals and materials for cloning and expression were obtained from Thermo Fisher Scientific (St. Leon-Rot, Germany), New England Biolabs GmbH (Frankfurt am Main, Germany), and Macherey-Nagel GmbH (Düren, Germany). Carbonic anhydrase was bought from MP Biomedicals (Illkirch, France). Primers were obtained from Eurofins MWG GmbH (Ebersberg, Germany). Synthesized genes were obtained from Eurofins MWG GmbH (Ebersberg, Germany) or BaseClear B.V. (Leiden, Netherlands). Materials and equipment for protein purification were obtained from GE Healthcare (Freiburg, Germany), Bio-Rad (Munich, Germany) or Merck Millipore GmbH (Schwalbach, Germany).

4.2. CoA-Thioester synthesis

Crotonyl-CoA and propionyl-CoA were synthesized from their respective anhydrides according to D. Peter *et al.*[120]. (*S*)-methylsuccinyl-CoA and mesaconyl-CoA were synthesized via the mixed anhydride method starting from the free acids and obtaining a racemic mixture of 2-(*S*)-methyl and 3-(*S*)-methyl-thioester. Ethylmalonyl-CoA and methylmalonyl-CoA were enzymatically produced with either crotonyl-CoA carboxylase or propionyl-CoA carboxylase starting from crotonyl-CoA or propionyl-CoA according to Schwander *et al.* and Peter *et al.* [38, 120]. All CoA-thioesters were purified using a HPLC (1260 Infinity, Agilent Technologies GmbH) with a Gemini® 10µm NX-C18 110 Å Column (Phenomenex, Aschaffenburg, Germany) as described previously[38,120]. The concentration of CoA-esters was quantified by determining the absorption at 260 nm (ε = 22.4 mM^{-1} cm^{-1} for unsaturated and ε = 16.4 mM^{-1} cm^{-1} for saturated CoA-thioesters).

4.3. Cloning and mutagenesis

Chlamydomonas reinhardtii ferredoxin, spinach ferredoxins, and spinach ferredoxin:NADP$^+$ oxidoreductase (FNR) lacking the transit peptides were codon optimized for enzyme production in *E. coli* by Eurofins Genomics Germany GmbH (Ebersberg, Germany). They were cloned into pET-16b, pET-28b, or pASK-IBA7 with the addition of an N-terminal Strep-tag. A *C. reinhardtii* FNR expression plasmid was provided by Dr. Winkler and described in Rumpel et al.[121]. The *Rhodobacter sphaeroides* 2.4.1 electron transport flavoprotein-ubiquinone oxidoreductase was cloned from genomic DNA (using the forward 5'-TAT ACA TAT GAC CGA GCA GAC TCC C and reverse 5'-TAT AGG TCT CGG ATC CTC ACA TGT TGG GAT AGT TCG primers) into pET16b vector containing a Strep-tag using NdeI and BamHI. The PCR product was cut with BsaI and NdeI to avoid the naturally occurring internal BamHI sites. The *Pseudomonas migulae* electron transport flavoprotein-ubiquinone oxidoreductase was codon optimized and synthesized by BaseClear B.V. (Leiden, Netherlands).

4.4. General protein production and purification

4.4.1. General heterologous production and purification of enzymes

Enzymes were produced in *Escherichia coli* strains BL21(DE3), BL21(DE3) AI, Rosetta 2 (DE3) pLysS, C41(DE3) pLysS pRKisc, and BL21(DE3) ΔiscR. Cells were grown in terrific broth at 37 °C using the appropriate antibiotic for selection (100 μg/ml ampicillin, 50 μg/ml kanamycin, 34 μg/ml chloramphenicol, 20 μg/ml Streptomycin, 10 μg/ml tetracycline, and 50 μg/ml spectinomycin). Unless otherwise noted, when an OD_{600} = 0.7-1.0 was reached the culture was cooled to 23°C and induced by the addition of 500 μM IPTG (Isopropyl-D-β-thiogalactopyranoside) or 200 μg/L anhydrotetracycline. When using *E. coli* BL21(DE3) AI as an expression host 0.02 % (w/v) L-arabinose was additionally added. After 14-18 hours the cells were harvested for 12 min at 6,600 × g at 4 °C. Unless immediately purified, cell pellets were frozen and stored at -20° or -80° C. Unless otherwise specified, His-tagged enzymes were purified by resuspending the cell pellet 1:2 (w/v) ratio in Buffer L (50 mM HEPES pH 8.0 or 20 mM Tris-HCl pH 8.1, 500 mM NaCl, 5 mM $MgCl_2$, 10% glycerol, and DNAse) and lysed by ultrasonication. The lysate was clarified by ultracentrifugation (1 hour at 100,000 × g) and the resulting supernatant was filtered through a 0.45 or 0.2 μm filter. Lysate was loaded onto a HisTrap FF (GE Healthcare, Freiburg, Germany) and unspecifically bound protein was removed with a buffer containing: 50 mM HEPES-KOH pH 8.0 or 20 mM Tris-HCl pH 8.1, 500 mM NaCl, and 75 mM imidazole. The protein was eluted in 50 mM HEPES-KOH pH 8.0

or 20 mM Tris-HCl pH 8.1, 500 mM NaCl, and 500 mM imidazole. The eluted protein was either desalted in a buffer containing: 50 mM HEPES-KOH pH 8.0 or 20 mM Tris-HCl pH 8.1, and 150 mM NaCl with a HiTrap 5 ml Desalting (GE Healthcare, Freiburg, Germany) column or by gel filtration using a HiLoad 16/600 Superdex 200 pg (GE Healthcare, Freiburg, Germany) size exclusion column equilibrated with a buffer containing: 50 mM HEPES-KOH pH 8.0 or 20 mM Tris-HCl pH 8.1, and 200 mM NaCl. Elution fractions were concentrated with Amicon Ultra-4 centrifugal filters (Merck Millipore, Darmstadt, Germany). Purified proteins were stored in 30-50% Glycerol at -20°C or -80°C and the concentration was determined on a Nanodrop 2000 (Thermo Scientific, St. Leon-Rot, Germany) from extinction coefficients calculated on ProtParam, unless otherwise specified.

Recombinant production and purification of 4-hydroxybutyryl-CoA dehydratase (Nmar0207), 4-hydroxybutyryl-CoA synthetase (Nmar0206), and 2-(*S*)-methylsuccinyl-CoA oxidase (Mco) was purified as described in Schwander et al[38]. However, the resulting protein solution was flash frozen and stored at -80°C. This increased the stability of some of the enzymes from days or weeks to months [38]. Codon optimized propionyl-CoA synthase (Pcs) was produced and purified according to Bernhardsgrütter *et al.* [122].

4.4.2. Recombinant protein production and purification of *Chlamydomonas* and Spinach ferredoxins

Ferredoxins were produced in C41(DE3) pLysS pRKisc, or BL21(DE3) ΔiscR cultures were grown to an OD_{600} of 0.7-0.9 and cooled to 23 °C and induced by the addition of 500 µM IPTG and ammonium ferric citrate was added (260 mg per liter of growth media). Cells were harvested after 14-18 h as described above. Cell pellets were resuspended in a lysis buffer (50 mM HEPES-KOH pH 7.8, 150 mM NaCl, 2 mM DTT, and 10% glycerol) at 2 mL per gram of pellet. The cells were lysed and clarified as above. The supernatant was loaded onto a StrepTrap HP (GE Healthcare, Freiburg, Germany) equilibrated with the lysis buffer or a buffer without the glycerol. The unbound protein was washed with the same buffer. Elution was carried out in the same buffer with the addition of 2.5 mM desthiobiotin. The resulting protein was concentrated as described above, but quantified using the following extinction coefficients: *Chlamydomonas* ferredoxin, 8.38 mM cm^{-1} at 420 nm [75]; *Spinacia oleracea* ferredoxin, 9.68 mM cm^{-1} at 420 nm [123].

4.4.3 Recombinant protein production and purification of *Chlamydomonas* and Spinach Ferredoxin NADP+ reductase (FNR)

Strep-tagged FNR from both *S. oleracea* and *C. reinhardtii* were produced in BL21(DE3) as described above. Cells were lysed in a buffer containing 50 mM HEPES-KOH pH 7.8, 150 mM NaCl, and 10% glycerol. Lysis and clarification were performed as above and loaded onto a StrepTrap HP (GE Healthcare, Freiburg, Germany). It was washed with a buffer containing 50mM HEPES-KOH pH 7.8 and 150 mM NaCl and eluted in a buffer containing 2.5-5 mM desthiobiotin. The protein was concentrated in an Amicon and 40% glycerol was added as a cryoprotectant prior to freezing. The concentration for both *C. reinhardtii* and Spinach FNR were determined using the extinction coefficient, 10.74 mM cm^{-1} at 456 nm [124].

4.4.4 Electron transport flavoprotein-oxidoreductase (ETF:QO) protein production and purification

ETF:QO enzymes were produced in BL21(DE3) or C41(DE3) harboring both the pLysS, and the pRKisc plasmid for iron-sulfur cluster formation[125]. Cells were grown, induced, and harvested according to the basic protocol above. The enzyme was purified based on a modified method from Usselman *et al.*[126]. Cell pellets were resuspended in 1:3 ratio (w/v) in buffer A (50 mM Tris-HCl pH 7.6, 500 mM NaCl, and 0.1 mM DTT), prior to lysis and 10 µg/mL DNAseI was added. Cells were lysed by French press or ultrasonication and the insoluble fractions were harvested by ultracentrifugation for 1 hour at 100,000 × g. The supernatant was removed and the resulting pellet was washed in buffer A and centrifuged again. A rough protein concentration of the pellet was determined with the Pierce™ Rapid Gold BCA Protein assay kit (Thermo Scientific). The pellet was resuspended in buffer A to approximately 20 mg protein/mL. The pellet was solubilized by adding dodecyl-β-D-maltoside at a ratio of 2.5:1 (w/w) of protein to dodecyl-β-D-maltoside and shaking for 90 minutes at 8°C. The solution was centrifuged for a third time for 1 hour at 100,000 × g and the resulting supernatant was diluted 10-fold in buffer A, filtered with a 0.45 µm syringe filter, and loaded onto a StrepTrap HP or HisTrap FF ($_{rs}$ETF:QO and $_{pm}$ETF:QO, respectively). The washing and elution of the enzymes was done according to the protocols above for His and Strep-tagged proteins.

4.5. Chloroplast isolation

Chloroplasts were isolated from young spinach purchased from the local market or grocery store using a modified method from[33, 74]. Spinach leaves were stored in the dark at 4-8 °C until use. The leaves were washed and the large stems were removed and buffer was added at a ratio

of 1 g plant material to 1 mL cold buffer (330 mM sorbitol, 50 mM HEPES-KOH pH 7.6, 5 mM $MgCl_2$, 0.1% (w/v) bovine serum albumin) and blended using a standard kitchen immersion blender. The resulting solution was pressed through a piece of fine mesh cotton fabric and the filtrate was centrifuged for 10 min at 3000 × g. The pellet was gently resuspended in buffer (300 mM sorbitol, 50 mM HEPES-KOH pH 7.6, 5 mM $MgCl_2$, 2 mM EDTA, and 10 mM sodium L-ascorbate,), using a fine paint brush to remove any clumps. This was overlaid on an 80/40% percoll gradient (80%: 80% v/v percoll, 10 mM sodium L-ascorbate, 300 mM sucrose, 66 mM MOPS-KOH pH 7.6 and 40%: 40% v/v percoll, 10 mM sodium L-ascorbate, 300 mM sucrose, 25 mM MOPS-KOH pH 7.6). The fractions containing thylakoids and intact chloroplasts were pooled and diluted in buffer and centrifuged for 10 min at 3000 × g. The pellet was resuspended in osmotic shock buffer (10 mM HEPES-KOH, 10 mM $MgCl_2$, 10 mM sodium L-ascorbate). Thylakoids were flash frozen with 10% DMSO as an osmoprotectant and stored at -80°C until use. The thylakoid/chloroplast solutions were maintained in darkness.

Before use, thylakoids were stored on ice and washed 2-3 times in a buffer containing: 0, 330, or 700 mM sorbitol, 10 mM HEPES-KOH pH 7.6, 10 mM $MgCl_2$, and 10 mM sodium L-ascorbate. The chlorophyll content of the resulting solution was determined according to Porra 2002 [127].

4.6. Assays of thylakoid activity

4.6.1 Spectrophotometric observation of $NADP^+$ photoreduction and the ferredoxin titration.

Thylakoid activity was assayed by monitoring NADPH production spectrophotometrically in a 5 mm quartz cuvette at 340 nm on a UV-Vis spectrophotometer (Cary 60 UV-Vis, Agilent Technologies GmbH). In a reaction volume of 0.7 mL, thylakoids were added to reach a total of 10 μg of chlorophyll to a reaction buffer containing: 50 mM HEPES-KOH pH 7.8, various ferredoxin concentrations, 3 mM ADP, 5 mM of K_2HPO_4, 3mM $NADP^+$, 10 mM sodium L-ascorbate, 10 mM KCl, 5 mM $MgCl_2$, 1.5 μM *E. coli* catalase, and 52 U mL^{-1} of bovine superoxide dismutase and illuminated with white light at 50-100 μmol photons m^{-2} s^{-1}. Initially, various ferredoxins (SpFdx1, SpFdx2, & CrFdx1) were tested with minimal differences in activity. Ultimately, for the ferredoxin titration 0, 2.5, 5, 10, 25, and 50 μM of CrFdx1 was assayed. The concentration of NADPH was calculated using an extinction coefficient of 6.22 mM cm^{-1}.

4.6.2 ATP/NADPH ratio

The ATP/NADPH production ratio was determined using a similar reaction mixture (0.7 mL) listed above, with the inclusion of 700 mM sorbitol. The NADPH production was monitored spectrophotometrically in a 5 mm quartz cuvette at 340 nm on a UV-Vis spectrophotometer (Cary 60 UV-Vis, Agilent Technologies GmbH) and the concentration was determined. To trigger thylakoid activity, a white light was used at 60 μmol photons m^{-2} s^{-1}. Samples for ATP measurements were taken at 0, 5, 15, 30 minutes after illumination and quenched with 5% formic acid. The samples were immediately measured by HPLC-MS as described below. The concentrations were calculated using a standard curve. Standard solutions were made using commercially available ATP prepared in a buffer reflective of assay conditions for accurate concentration calculation.

4.6.3 ATP production rate

The ATP production rate was determined in a reaction buffer (0.2 mL) containing: 50 mM HEPES-KOH pH 7.6, 10 mM sodium L-ascorbate, 700 mM sorbitol, 5 mM $MgCl_2$, 5 mM K_2HPO_4, 10 mM KCl, 5 μM of CrFdx1, 2 mM $NADP^+$, 2 mM ADP, 1.5 μM of catalase, and 52 U mL^{-1} of bovine superoxide dismutase, and if DAPP was added, it was at 20 μM. Thylakoids were added at 2.5 μg and 10 μg chlorophyll and assayed both in the dark and in the light at 60-70 μmol photons m^{-2} s^{-1}. Samples were taken at 0, 5, 10, and 15 minutes and quenched with a final concentration of formic acid of 5%. ATP was measured with HPLC-MS by the method described below. The concentrations were calculated using a standard curve. Standard solutions were made using commercially available ATP prepared in a buffer reflective of assay conditions for accurate concentration calculation.

4.6.4 Oxygen evolution and NADPH production

Simultaneously, the rates of O_2 evolution and NADPH production were measured in an assay volume of 0.7 mL in a reaction buffer containing: 50 mM HEPES-KOH pH 7.6, 10 mM sodium L-ascorbate, 700 mM sorbitol, 5 mM $MgCl_2$, 5 mM K_2HPO_4, 10 mM KCl, 5 μM of CrFdx1, 3 mM $NADP^+$, 2 mM ADP, 1.5 μM of catalase, 52 U mL^{-1} of bovine superoxide dismutase, and 30 μM DAPP. Thylakoids were added at a total of 10 μg chlorophyll and assayed both in the dark and in the light at 60-70 μmol photons m^{-2} s^{-1}. NADPH production was measured as discussed above. The O_2 evolution was measured with a PyroScience fiber optic oxygen probe, either an optically isolated minisensor (OXF1100-OI) or microsensor (OXF50-OI). The NADPH

production was measured in a spectrophotometer in a 5mm quartz cuvette at 340 nM. A decrease of O_2 was observed in reaction mixtures that lacked thylakoids, and this was used for a baseline correction of samples.

4.6.5 Oxygen evolution at different light intensities or with and without catalase and SOD

The O_2 evolution was measured at different light intensities with a PyroScience fiber optic oxygen probe, either an optically isolated minisensor (OXF1100-OI) or microsensor (OXF50-OI). The rates were measured in an assay volume of 0.4 mL in a reaction buffer containing: 50 mM HEPES-KOH pH 7.6, 10 mM sodium L-ascorbate, 700 mM sorbitol, 5 mM $MgCl_2$, 5 mM K_2HPO_4, 10 mM KCl, 5 µM of CrFdx1, 3 mM $NADP^+$, 2 mM ADP, either with or without 1.5 µM of catalase, and 52 U mL^{-1} of bovine superoxide dismutase. Thylakoids were added at a total of 10 µg chlorophyll and assayed both in the dark, 30, 60, or 300 µmol photons m^{-2} s^{-1}. There was a decrease in O_2 levels in the dark and this decrease was subtracted from the samples in the light.

4.6.6 Oxygen evolution during Carbon fixation

The O_2 production from thylakoid energy module during the fixation of carbon (by Ccr and Pcc) was measured in an assay volume of 0.5 mL. The reaction mixture was comprised of 50 mM HEPES-KOH pH 7.6, 10 mM sodium L-ascorbate, 700 mM sorbitol, 5 mM $MgCl_2$, 5 mM inorganic phosphate (K_2HPO_4), 10 mM KCl, 5 µM of CrFdx1, 0.6 mM Propionyl-CoA, 1 mM Crotonyl-CoA, 1 mM $NADP^+$, 0.5 mM ADP, 30 nM carbonic anhydrase, 1.5 µM of catalase, 52 U mL^{-1} of bovine superoxide dismutase, 1.3 µM Ccr, and 1.8 µM Pcc, and 30 µM DAPP. Thylakoids were added at a rate of 7.5µg total chlorophyll. The reactions were assayed, both in the dark and illuminated at 60-70 µmol photons m^{-2} s^{-1}. O_2 was measured using the PyroScience fiber optic oxygen probe with either an optically isolated minisensor (OXF1100-OI) or microsensor (OXF50-OI). There was a decrease in O_2 levels in the dark and this was used as a baseline correction. To measure product formation from Pcc or Ccr, samples were taken at 0, 2, and 5 minutes and quenched with formic acid (final concentration of 5%) and analyzed by HPLC-MS using the method described below. Concentrations were calculated using a standard curve prepared in a solution of quenched, unreacted reaction mixture.

4.7. CETCH assays

4.7.1 Assay of CETCH

The initial photoCETCH cycle experiments were performed in 270 µl reaction volume with thylakoids added at 125 µg Chl/mL in a buffer containing: 50 mM HEPES, 330 mM Sorbitol, 10 mM sodium L-ascorbate, 100 µM coenzyme B_{12}, 80 µM propionyl-CoA, 1.25 mM ADP, 2 mM $NADP^+$, 5 mM $MgCl_2$, 5 mM K_2HPO_4, 10 mM KCl, 50 mM $NaH^{13}CO_3$, 1.2 µM catalase, 310 nM superoxide dismutase, 5 µM FdxCr, 1.3 µM Ghr, and the core enzymes from CETCH v6.0 (listed in Materials and Methods Table 1). Samples (30 µL) were taken at 0, 5, 15, 30, 45, 60, 90 and 120 minutes and quenched with formic acid at a final concentration of 5 %. The CoA esters were measured using an Agilent 6550 iFunnel Q-TOF LC-MS as described below. The glycolate produced was derivatized and measured by UPLC-MS/MS (using Agilent 6495B Triple Quad LC/MS) as described below. The glycolate was quantified using a standard curve. Standard solutions were prepared in a quenched, unreacted reaction mixture.

4.7.2 Assay of CETCH v6.0 with Ghr

CETCH cycle v6.0 was reacted in 300 µL with thylakoids added at 125 µg Chl/mL in a buffer containing: 50 mM HEPES-KOH, 330 mM Sorbitol, 10 mM sodium L-ascorbate, 100 µM coenzyme B_{12}, 80 µM propionyl-CoA, 1.25 mM ADP, 2 mM $NADP^+$, 5 mM $MgCl_2$, 5 mM K_2HPO_4, 10 mM KCl, 50 mM $NaH^{13}CO_3$, 1.2 µM catalase, 310 nM superoxide dismutase, 5 µM FdxCr, 1.3 µM Ghr, and the core enzymes from CETCH v6.0 (listed in Materials and Methods Table 1). Samples (30 µL) were taken at 0, 5, 15, 30, 45, 60, 90 and 120 minutes and quenched with formic acid at a final concentration of 5 %. The CoA esters were measured using an Agilent 6550 iFunnel Q-TOF LC-MS as described below. The glycolate produced was derivatized and measured by UPLC-MS/MS (using Agilent 6495B Triple Quad LC/MS) as described below. The glycolate was quantified using standard curve. Solutions were prepared in a quenched, unreacted reaction mixture.

4.7.3 Assay of CETCH v7.0

CETCH cycle v7.0 was reacted in 300 µL with the thylakoid energy module added at 210 µg Chl/mL in a buffer containing: 50 mM HEPES-KOH, 700 mM Sorbitol, 10 mM sodium L-ascorbate, 100 µM coenzyme B_{12}, 85 µM propionyl-CoA, 0.5 mM ADP, 2 mM $NADP^+$, 5 mM $MgCl_2$, 5 mM K_2HPO_4, 10 mM KCl, 50 mM $NaH^{13}CO_3$, 1.2 µM catalase, 310 nM superoxide dismutase, 5 µM FdxCr, 1.3 µM Ghr, and the core enzymes from CETCH v7.0 (listed in Materials and Methods Table 1). Samples (30 µL) were taken at 0, 5, 15, 30, 45, 60, 90 and 120

minutes and quenched with formic acid at a final concentration of 5 %. The CoA esters were measured using an Agilent 6550 iFunnel Q-TOF LC-MS as described below. The glycolate produced was derivatized and measured by UPLC-MS/MS (using Agilent 6495B Triple Quad LC/MS) as described below. The glycolate was quantified using a standard curve. Standard solutions were prepared in a quenched, unreacted reaction mixture.

4.7.4 Optimization of CETCH v7.0 for droplets

CETCH cycle v7.0 was reacted in 300 µL with the thylakoid energy module added at 126 µg Chl/mL in a buffer containing: 50 mM HEPES-KOH, 700 mM Sorbitol, 10 mM sodium L-ascorbate, 85 µM crotonyl-CoA or propionyl-CoA, 0.5 mM ADP, 2 mM $NADP^+$, 5 mM $MgCl_2$, 5 mM K_2HPO_4, 10 mM KCl, 50 mM $NaH^{13}CO_3$, 1.2 µM catalase, 310 nM superoxide dismutase, 5 µM FdxCr, 1.3 µM Ghr, and the core enzymes from CETCH v7.0 (listed in Materials and Methods Table 1). Ecm and Mcm were incubated with 2 µl of a buffered solution of 5 mM coenzyme B_{12} for 30 minutes in the dark and at room temperature prior to adding the enzymes to the reaction mixture. Some samples included the addition of PhaJ (14 µM) and some reactions were incubated for 1 hour prior to illumination. The samples (30 µL) were taken at 0, 5, 15, 30, 45, 60, 90 and 120 minutes and quenched with formic acid at a final concentration of 5 %. The CoA esters were measured using an Agilent 6550 iFunnel Q-TOF LC-MS as described below. The glycolate produced was derivatized and measured by UPLC-MS/MS (using Agilent 6495B Triple Quad LC/MS) as described below. The glycolate was quantified using a standard curve. Standard solutions were prepared in a quenched, unreacted reaction mixture.

4.8. Quantification of reaction Products

4.8.1 High Resolution LC-MS/MS of CoA Esters

Compounds were separated on a RP-18 column (50 mm x 2.1 mm, particle size 1.7 µm, Kinetex EVO C18, Phenomenex) using a mobile phase system comprised of 50 mM ammonium formate pH 8.1 (A) and methanol (B). Chromatographic separation was carried out using the following gradient condition at a flow rate of 250 µL/min: 0 min 2.5% B; 2.5 min 2.5% B; 8 min 23% B; 10 min 80 %B; 11 min 80%; 12 min 2.5% B; 12.5 min 2.5% B. The column oven was set to 40 °C and autosampler was maintained at 10 °C. Standard injection volume was 1 µL.

CoA esters were analyzed using an Agilent 6550 iFunnel Q-TOF LC-MS system equipped with an electrospray ionization source set to positive ionization mode.

Capillary voltage was set at 3.5 kV and nitrogen gas was used as nebulizing (20 psig), drying (13 L/min, 225 °C) and sheath gas (12 L/min, 400°C). The TOF was calibrated using an ESI-L Low Concentration Tuning Mix (Agilent) before measurement (residuals less than 2 ppm for five reference ions) and was recalibrated during a run using 922 m/z as reference mass . The scan range for MS data is 500-1200 m/z.

Alternatively, the CoA esters were detected using an Agilent 6495B Triple Quad LC/MS system equipped with an electrospray ionization source. The source conditions were identical to that of the QTOF conditions. Data were acquired in the positive MRM mode with collision energy, dwell time, and fragmentor voltage set to 35 V, 20 ms, and 380 V respectively. The following MRM transitions were used to quantify the CoA esters : ethylmalonyl-CoA (882 m/z → 428 m/z and 331 m/z), methylsuccinyl-CoA (882 m/z → 428 m/z and 375 m/z), succinyl-CoA (868 m/z → 428 m/z and 361 m/z), methylmalonyl-CoA (868 m/z → 428 m/z and 317 m/z), propionyl-CoA (824 m/z → 428 m/z and 317 m/z), crotonyl-CoA (836 m/z → 428 m/z and 329 m/z), and β- / γ-hydroxybutyryl-CoA (854 m/z → 428 m/z and 347 m/z). To complement the MRM data, CoA esters were also UV detected at 260 nm on an Agilent 1290 Infinity II DAD detector equipped with a Max-Light cartridge cell (60 mm).

LC-MS data were analyzed using MassHunter Qualitative Navigator and QQQ Quantitative analysis software.

4.8.2 UPLC-MS/MS analysis of derivatized glycolate

Glycolate was derivatized according to the method published by Han *et al.*[128]. Briefly described, 50 µl of sample was mixed with 50 µL 150 mM 1-(3-Dimetheylaminopropyl)-3-ethylcarbodiimide (EDC), 50 µl 250 mM 3-nitrophenylhydrazine (3-NPH), and 50 µl of 7.5% pyridine in methanol in a 1.5 ml Eppendorf tube. The reaction was incubated at 30°C for 30 min. After incubation, the samples were centrifuged at 13,000 x *g* for 1 min and the supernatant transferred into HPLC vials.

UPLC-MS/MS analyses were performed on an Agilent 6495B Triple Quad LC/MS system equipped with an electrospray ionization source.

The analytes were separated on a RP-18 column (50 mm x 2.1 mm, particle size 1.8 µm, ZORBAX RRHD Eclipse Plus C18, Agilent) kept at 40 °C using a mobile phase system comprised of 0.1% formic acid in water (A) and acetonitrile (B). The gradient is as follows: 0

min 5% B; 1 min 5% B, 6 min 95% B; 6.5 min 95% B; 7 min 5 %B at a flow rate of 250 µL/min. Samples were held at 15°C and injection volume was 5 µL.

MS/MS data were acquired in negative MRM mode. Capillary voltage was set at 3 kV and nitrogen gas was used as nebulizing (25 psig), drying (11 L/min, 130 °C) and sheath gas (12 L/min, 400°C). The dwell time and fragmentor voltage were 20 ms and 380 V respectively. Optimized collision energy used for the both quantifier (210 *m/z* → 137 *m/z*) and qualifier (210 *m/z* → 152 *m/z*) and was 22 V.

LC-MS data were analyzed and quantified using MassHunter Qualitative Navigator and QQQ Quantitative Analysis softwares (Agilent).

4.8.3 UPLC-MS/MS analysis of ATP, ADP, and AMP

UPLC-MS/MS analyses were performed on an Agilent 6495B Triple Quad LC/MS system equipped with an electrospray ionization source.

The analyte was separated on a HILIC column (50 mm x 2.1 mm, particle size 1.7 µm, 130 Å, BEH Amide, Waters) using a mobile phase system comprised of 95:5 20 mM ammonium acetate pH 9.3 / acetonitrile (A) and acetonitrile (B). The compounds were eluted through the column at a flow rate of 400 µL/min under the following conditions: 0 min 90% B, 1.5 min 40% B, 1.8 min 40% B, 1.9 min 90 %B, 2.5 min 90% B. Samples were held at 15°C and injection volume was 1 µL.

MS/MS data were acquired in negative MRM mode. Capillary voltage was set at 3.5 kV and nitrogen gas was used as nebulizing (20 psig), drying (13 L/min, 225 °C) and sheath gas (12 L/min, 400°C). The dwell time and fragmentor voltage were 50 ms and 380 V respectively. Optimized collision energy used for the analytes were as follows: ATP (506 *m/z* → 408 *m/z*, 25 V, 506 *m/z* → 159 *m/z*, 35 V); ADP (426 *m/z* → 159 *m/z*, 25 V, 426 *m/z* → 79 *m/z*, 35 V); and AMP (346 *m/z* → 134 *m/z*, 35 V, 346 *m/z* → 79 *m/z*, 25 V).

LC-MS data were analyzed and quantified using MassHunter Qualitative Navigator and QQQ Quantitative Analysis softwares (Agilent).

4.9. Microfluidic device fabrication and operation

Dropmaker devices (Supplemental Figure S5) were made of poly(dimethylsiloxane) (PDMS, Sylgard 184) from a SU8-3000 negative photoresist (MicroChem Corp) mold (30 µm depth) produced using a standard soft-lithography procedure [129]. Microfluidic channels were treated

using fluoro-silane (Aquapel, Aquapel) before use. Nemesys syringe pumps (Cetoni) were used to control the flows in the microfluidic channels. Devices were connected to pumps with PTFE tubing (Fischer Scientific, ID 0.3 mm, OD 0.76 mm). Droplets were produced in fluorinated oil (Novec®3000, 3M) and stabilized against coalescence by a perfluoropolyether-polyethyleneglycol block-copolymer surfactant (Fluosurf, Emulseo).

A microfluidic 2D-chamber (Supplemental Figure S5) was assembled as previously described[19]. Briefly, the chamber geometry (35 mm x 10 mm) was cut in a 60 µm-thick double-sided bonding tape (1375, SDAG Adhésifs) using a Graphtech cutting plotter (CE 6000-40). The double-sided bounded template was sandwiched between two microscopy glass slides (76 x 25 x 1mm, Mareinfeld). Holes and glued nanoports on the top glass slide served as inlet/outlet. The chambers were treated using fluoro-silane (Aquapel, Aquapel) before use.

4.10. Thylakoid encapsulation

Independently from final composition, thylakoids suspensions were flowed (100 µL/h) in the dropmaker device and flow-focused with two streams of fluorinated oil containing 3 wt% surfactant (225 µL/h). In typical experiments, 4-bit emulsions were produced by encapsulating four different mixtures in parallel. The 4-bit emulsions were barcoded with sulforhodamine B fluorophore (2, 8, 16, 40 µM). Droplets were collected together in a PTFE tubing and directed to the 2D-chamber. Once the 2D-chamber was fully loaded, flows were stopped and the 2D-chamber closed with caps. Specific assay mixtures can be found in the tables below.

4.11. Time-lapse fluorescence measurements

The 2D-chamber device was mounted on the stage of an inverted microscope equipped with light emitting diodes (Supplemental Figure S5). A 365 nm diode (1150 mW, Thorlabs) combined to an epifluorescence cube composed of an excitation bandpass filter (F39-370, AHF), a beamspliter (F38-409, AHF) and an emission bandpass filter (F39-438, AHF) was used for measuring NADPH fluorescence. A 550 nm diode (CoolLED pE-2) was used for measuring sulforhodamine B fluorescence. A warm white light emitting diode (2000 mW, Thorlabs) mounted on the stage of the microscope was used for the light-activation of the thylakoids. Images were taken with a digital camera (EOS 600, Canon). A labVIEW routine triggering the white LED, the 365 nm LED, and the digital camera was used to perform the time lapse experiments with defined light and imaging patterns.

4.12. Image processing

The home-made image processing algorithm consists of a three-step procedure to automatically extract information from every image captured during the time-lapse experiment (Supplemental Figure S6). (i) A region of interest is drawn on the brightfield image to select the droplets of interest and discard droplets located in the image corners. Using the brightfield image, an intensity threshold is applied in order to discriminate the edges of the droplets to the background of the image. Then, the brightfield image is converted into a binary image where the edges of the droplets are only displayed. From this binary image, droplet boundaries are detected using the Hough transform procedure. The detection of droplets is limited to the range of a low and high radius in order to reduce the time processing. The Hough transform procedure outputs radius and the locations of droplets in the region of interest. The data are saved and the image processing algorithm automatically moves to the coding image. (ii) The coding image is captured at the same location as the brightfield image. Consequently, the droplet location and radius data can be used to find every droplet of interest in the coding image. The fluorescence intensity of each droplet is obtained by listing the intensity value of all pixels composing the droplets tested. The median value of the pixel intensity for each droplet is saved and characterizes the coding intensity of the droplet tested. This process is repeated for every droplet in the imaged region of the interest. Then the image processing algorithm moves to the time lapse images. (iii) Every time lapse image is processed using the same method as the coding image step (ii). Briefly, the median value of the fluorescence intensity of every pixel composing a droplet is saved. Then, this process is iterated for every droplet and image composing the time lapse. The LabVIEW code used for image analysis has been uploaded to a repository on GitHub [83].

4.13. Large-scale experiments

1-bit emulsions (contents outlined below) were produced in large quantities (~500 µL, ~10^8 droplets) and collected in a 2 mL glass vial. The glass vial was continuously rotated and illuminated with warm white LED. 30 µL of emulsion was regularly sampled from the vial and coalesced as follows: the droplets were added to 50 µL of fluorinated oil; 20 µL of 1H, 1H, 2H, 2H-perfluoro-1-octanol was added and the mixture was vortexed and centrifuged; and the aqueous phase was pipetted and quenched with 1% of HCl.

4.13.1 Ccr and Ghr in 1-bit emulsions

Thylakoid energy module powered reactions Ghr and Ccr in droplets were assayed in a buffer containing the following: 100 mM HEPES-KOH, pH 7.8, 330 mM sorbitol, 5 mM K_2HPO_4, 10 mM KCl, 5 mM $MgCl_2$, 10 mM sodium L-ascorbate, 5 μM ferredoxin, 52 U mL^{-1} superoxide dismutase, 1.2 μM catalase, 1.6 mM ADP, 0.8 mM $NADP^+$, 120 μg Chl mL^{-1} of thylakoids, and 8 μM Sulforhodamine B. To assay Ccr: 255 nM Ccr, 33.5 nM carbonic anhydrase, 1 mM Crotonyl-CoA, and 50 mM $NaHCO_3$ was added. To assay Ghr: 214 nM GhrB and 5 mM glyoxylate was added. Droplets were created from a solution with a total volume of 500 μL. Samples were taken after 75 minutes of illumination at 50 μmol photons m^{-2} s^{-1} and quenched as described above. To assess Ccr activity CoA-thioesters were measured by HPLC-MS as described above and quantified using a standard curve. Ghr activity was assessed by measuring glycolate produced by HPLC-MS. The concentration was determined using a standard curve. Standard solutions were prepared in a buffer reflective of assay conditions for accurate concentration calculation.

4.13.2 1-bit emulsions containing CETCH v7.0 and the thylakoid energy module

Droplets containing thylakoid powered CETCH v7.0 were generated from a solution (total volume, 1.8 mL) that contained 70 μg Chl/mL in a buffer that contained 50 mM HEPES-KOH, pH 7.8, 700 mM Sorbitol, 10 mM sodium L-ascorbate, 90 μM crotonyl-CoA, 0.5 mM ADP, 2 mM $NADP^+$, 5 mM $MgCl_2$, 5 mM K_2HPO_4, 10 mM KCl, 50 mM $NaH^{13}CO_3$, 10 mM polyphosphate, 1.2 μM catalase, 310 nM superoxide dismutase, 5 μM FdxCr, 1.3 μM GhrA, 14 μM PhaJ, and the core enzymes from CETCH v7.0 (listed in Materials and Methods Table 1). Ecm and Mcm were incubated with 2 μl of a buffered solution of 5 mM coenzyme B_{12} for 30 minutes in the dark and at room temperature prior to adding the enzymes to the reaction mixture. The samples (30 μL) were taken and quenched as described above. The CoA esters were measured using an Agilent 6550 iFunnel Q-TOF LC-MS and quantified using the integrated UV_{260nm} peak and a standard curve. The glycolate produced was derivatized and measured by UPLC-MS/MS (using Agilent 6495B Triple Quad LC/MS) as described above.

4.13.3 Thylakoid activity in droplets 2, 3, & 4-bit emulsions

4.13.3.1 Controlling TEM in droplets with fluctuating light conditions

The effect of fluctuating light conditions in the droplets was tested (Supplemental Figure S9). Three populations of droplets were created from 0.5 mL solutions that contained: 50 mM

HEPES-KOH, pH 7.8, 330 mM sorbitol, 5 mM K_2HPO_4, 10 mM KCl, 5 mM $MgCl_2$, 10 mM sodium L-ascorbate, 5 µM Ferredoxin, 52 U mL^{-1} superoxide dismutase, 1.2 µM catalase, 0.8 mM ADP, and various concentrations of sulforhodamine B, thylakoids, NADPH, and $NADP^+$. Population 1 contained: 0 µg Chl mL^{-1} of thylakoids, 0.5 mM NADP+, 2 µM sulforhodamine B. Population 2 contained: 11 µg Chl mL^{-1} of thylakoids, 0.5 mM NADP+, 8 µM sulforhodamine B. Population 3 contained: 0 µg Chl mL^{-1} of thylakoids, 0.5 mM NADPH, 40 µM sulforhodamine B. Droplets were prepared and monitored as discussed above.

4.13.3.2 Light intensity

The effect of light intensity in NADPH production on the droplets was assayed using light intensities at 50, 100, 200, 400 and 1200 µmol photons m^{-2} s^{-1} (Supplemental Figure S8). Two populations of droplets were created from solutions of 0.5 mL that contained: 100 mM HEPES-KOH, pH 7.8, 330 mM sorbitol, 3 mM K_2HPO_4, 10 mM KCl, 5 mM $MgCl_2$, 10 mM sodium L-ascorbate, 5 µM Ferredoxin, 52 U mL^{-1} superoxide dismutase, 1.2 µM catalase, 0.75 mM ADP, and various concentrations of sulforhodamine B, thylakoids, NADPH, and $NADP^+$. Population 1 contained: 23 µg Chl mL^{-1} of thylakoids, 0.5 mM NADP+, 2 µM sulforhodamine B. Population 2 contained: 0 µg Chl mL^{-1} of thylakoids, 0.5 mM NADPH, 40 µM sulforhodamine B.

4.13.3.3 Thylakoid consistency in droplets

The consistency between independently prepared droplets was tested using droplets manufactured from four independently pipetted 0.5 mL solutions (Supplemental Figure S6 C & S7 C). The four populations contained: 50 mM HEPES-KOH, pH 7.8, 700 mM sorbitol, 5 mM K_2HPO_4, 10 mM KCl, 5 mM $MgCl_2$, 10 mM sodium L-ascorbate, 5 µM Ferredoxin, 52 U mL^{-1} superoxide dismutase, 1.2 µM catalase, 1.6 mM ADP, and various concentrations of sulforhodamine B, thylakoids, NADPH, and $NADP^+$. Population 1, 2, and 3 contained: 1.0 mM NADP+, 125 µg Chl mL^{-1} of thylakoids, and either 2, 8, 20 µM sulforhodamine B. In population 4, thylakoids were omitted and 1 mM NADPH was used instead of $NADP^+$, for the coding dye 40 µM was used. Droplets were prepared and monitored as discussed above.

4.13.3.4 Controlling droplets

Various enzyme and substrate concentrations were used in multiplexed experiments (4-bit, Figure 18B, 18C). In each case the TEM was coupled to Ghr and either various enzyme and/or

substrate concentrations were assayed. The specific reaction conditions are shown in Table M2. The droplets were manufactured and monitored as discussed above from 0.5 mL solutions.

4.13.3.5 Ghr and Ccr in droplets

Both 330 and 700 mM sorbitol conditions were tested with coupling Ccr and Ghr. In each case, four populations were tested either with 330 or 700 mM sorbitol (Figure 18D & 20B). The specific reaction conditions are shown in Table M3. The droplets were manufactured and monitored as discussed above from 0.5 mL solutions. The contents of each droplet population is indicated and a grey box indicates that component was omitted from that population.

4.13.3.6 Pcs in droplets

The specific reaction conditions to test Pcs coupling is shown in Table M4 (Figure 21). The four populations of droplets were manufactured and monitored as discussed above from 0.5 mL solutions. The contents of each droplet population is shown and a grey box indicates that component was omitted from that population.

4.13.3.7 Time and space control of droplets 2-bit emulsion

As a demonstration of the controllability of droplets, both in time and space, a binary emulsion was created (Figure 19). The two population of droplets were created using 0.5 mL solutions. The two populations contained 50 mM HEPES·KOH, pH 7.8, 700 mM sorbitol, 5 mM K_2HPO_4, 10 mM KCl, 5 mM $MgCl_2$, 10 mM sodium L-ascorbate, 5 μM Ferredoxin, 52 U mL^{-1} superoxide dismutase, 1.2 μM catalase, 1.2 mM ADP, 0.8 mM $NADP^+$, 10 mM glyoxylate, and two different concentrations of GhrA, thylakoids, or sulforhodamine B. Either: 40 nM GhrA, 200 μg Chl mL^{-1} thylakoids, and 2 μM sulforhodamine B or 2.5 nM GhrA, 40 μg Chl mL^{-1} thylakoids, and 8 μM sulforhodamine B.

The 2 populations of droplets were filled into the observation chamber via two inlets. After 2 minutes in the dark, the droplets were exposed to 50 μmol photons m^{-2} s^{-1} light. The light was turned off again after 60 minutes.

4.13.3.8 Thylakoid Stability

Thylakoid stability was assayed (Figure 17C). Four populations of droplets were created from 0.4 mL solutions that contained 50 mM HEPES-KOH, pH 7.8, 330 mM sorbitol, 5 mM K_2HPO_4, 10 mM KCl, 5 mM $MgCl_2$, 10 mM sodium L-ascorbate, 1.0 mM NADPH, and various concentrations of sulforhodamine B, GhrB, GhrA, and Coenzyme B_{12}. Population 1 contained:

1.3 μM GhrA, 0 μM coenzyme B_{12}, 2 μM sulforhodamine B. Population 2 contained: 1.3 μM GhrA, 100 μM coenzyme B_{12}, 8 μM sulforhodamine B. Population 3 contained: 53.5 nM GhrB, 100 μM coenzyme B_{12}, 16 μM sulforhodamine B. Population 4 contained: 53.5 nM GhrB, 100 μM coenzyme B_{12}, 40 μM sulforhodamine B. Droplets were prepared and monitored as discussed above.

4.13.3.9 CETCH in droplets

Four-bit reaction conditions for droplets containing CETCH v6.0 and 7.0 that were monitored in the 2D array chamber described in Table M5 (Figure 26B, 26C, 25A & 25B). Three experiments are shown and droplets were created from 500 μL solutions. The contents of each droplet population is shown and a grey box indicates that component was omitted from that population.

Table M1.
Enzyme concentrations used in CETCH experiments.

CETCH Cycle v6.0 and 7.0 enzyme composition

Enzyme full name	Organism	Name	Enzyme abbreviation	Concentration added (nM)
propionyl-CoA carboxylase	*M. extorquens*	PccAB	Pcc	*2310*
emC/mmC epimerase	*R. sphaeroides*	Epi	Epi	*20*
methylmalonyl-CoA mutase	*R. sphaeroides*	Mcm	Mcm	*360*
succinyl-CoA reductase	*C. kluyveri*	SucD	Scr	*194*
succinic semialdehyde reductase	*H. sapiens*	AKR7a2	Ssr	*670*
4-hydroxybutyryl-CoA synthetase	*N. maritimus*	Nmar0206	Hbs	*5890*
4-hydroxybutyryl-CoA dehydratase	*N. maritimus*	Nmar0207	Hbd	*560*
crotonyl-CoA carboxylase/reductase	*M. extorquens*	Ccr	Ccr	*580*
ethylmalonyl-CoA mutase	*R. sphaeroides*	Ecm	Ecm	*550*
methylsuccinyl-CoA oxidase	*R. sphaeroides.*	Mco	Mco	*21410*
methylsuccinyl-CoA dehydrogenase	*R. sphaeroides*	Mcd	Mcd	*3000*
electron transport flavoprotein	*R. sphaeroides*	Etf A/B	Etf	*1000*
Etf ubiquinone oxidoreductase	*P. migulae*	Etf:QO	Etf:QO	*8000*
mesaconyl-CoA hydratase	*R. sphaeroides*	Mch	Mch	*30*
β-methylmalyl-CoA lyase	*R. sphaeroides*	Mcl1	Mcl1	*2720*
glyoxylate reductase	*E. coli*	GhrA	Ghr	*1300*
enoyl-CoA hydratase	*P. aeruginosa*	PhaJ	PhaJ	*14000*

The enzyme highlighted in blue is Mco that was used in CETCH v6.0, and those highlighted in orange are those used in CETCH v7.0. The last two enzymes, highlighted in green, are used in the cycle but are not part of the core reactions.

Table M2.
Detailed pipetting schemes of multiplexed Ghr coupling experiments. Some internal components were varied (either enzyme concentration or substrate concentration). In each experiment, four populations were multiplexed and analyzed simultaneously. Grey boxes indicate the component was omitted, and concentrations of components that were varied are indicated.

		Protein concentration				**Substrate concentration**			
		Droplet population				Droplet population			
Component	Concentration	1	2	3	4	1	2	3	4
HEPES·KOH, pH 7.8	100 mM								
Sorbitol	330 mM								
K_2HPO_4	3 mM								
KCl	10 mM								
$MgCl_2$	5 mM								
Sodium L-ascorbate	10 mM								
Catalase	0.1 mg/mL								
Ferredoxin	5 µM								
Superoxide Dismutase	52 U/mL								
ADP	0.75 mM								
$NADP^+$	0.5 mM				-				-
NADPH	0.5 mM	-	-	-		-	-	-	
Glyoxylate	mM	-	0.5	0.5	-	-	0.5	1.5	-
GhrA	nM	50	50	1000	50	1000	1000	1000	1000
Thylakoids	µg mL^{-1}	65	65	65	-	150	150	150	-
Sulforhodamine B	µM	2	8	20	40	2	8	20	40

Table M3.
Detailed pipetting schemes of single enzyme coupling experiments. Ccr and Ghr were coupled in parallel two times either with 700 or 330 mM sorbitol. Grey boxes indicate the component was omitted, and concentrations of components that were varied are indicated.

330 or 700mM Sorbitol Ccr and GhrB Coupling

		Droplet population			
Component	Concentration	1	2	3	4
HEPES·KOH	100 mM				
Sorbitol	700 or 330 mM				
K_2HPO_4	5 mM				
KCl	10 mM				
$MgCl_2$	5 mM				
Sodium L-ascorbate	10 mM				
Catalase	0.1 mg mL^{-1}				
Ferredoxin	5 µM				
Superoxide Dismutase	52 U mL^{-1}				
Ccr	41.8 nM				
GhrB	53.5 nM				
Carbonic anhydrase	33.5 nM				
Crotonyl-CoA	5.0 mM				
Glyoxylate	5.0 mM				
$NaHCO_3$	50 mM				
ADP	1.6 mM				
$NADP^+$	0.8 mM				
NADPH	0.8 mM				
Thylakoids	120 µg Chl mL^{-1}				
Sulforhodamine B	µM	2	8	16	40

Table M4.
Detailed pipetting schemes of Pcs coupling experiments. Grey boxes indicate the component was omitted, and concentrations of components that were varied are indicated.

Pcs Coupling

		Droplet population			
Component	Concentration	1	2	3	4
HEPES·KOH, pH 7.8	50 mM				
Sorbitol	330 mM				
K_2HPO_4	3 mM				
KCl	10 mM				
$MgCl_2$	5 mM				
Sodium L-ascorbate	10 mM				
Catalase	0.1 mg mL^{-1}				
Ferredoxin	5 µM				
Superoxide Dismutase	52 U mL^{-1}				
Pcs	100 nM			■	■
CoA	5 mM				
3-Hydroxypropionate	5 mM				
ADP	1.2 mM		■		
ATP	1.2 mM	■		■	■
$NADP^+$	0.8 mM				■
NADPH	0.8 mM	■	■	■	
Thylakoids	80 µg Chl mL^{-1}				■
Sulforhodamine B	µM	2	4	20	40

Table M5.
Detailed pipetting schemes of individual multiplexed CETCH experiments. Grey boxes indicate the component was omitted, and concentrations of components that were varied are indicated.

		Figure 25 A				Figure 25 B				Figure 26 B-C			
		Droplet population				Droplet population				Droplet population			
Component	Concentration	1	2	3	4	1	2	3	4	1	2	3	4
HEPES·KOH, pH 7.8	100 mM												
Sorbitol	700 mM												
K_2HPO_4	5 mM												
KCl	10 mM												
$MgCl_2$	5 mM												
Sodium L-ascorbate	10 mM												
Catalase	1.2 µM												
Ferredoxin	5 µM												
Superoxide Dismutase	52 U/mL												
mcd	3 µM												
etf	8 µM												
etf:QO	1 µM												
mco	21.4 µM												
Ccr	580 nM												
Other CETCH core enzymes, see Table S3													
Ppk	1.6 µM												
polyphosphate	10 mM												
Carbonic anhydrase	33.5 nM												
Crotonyl-CoA	250 µM												
phaJ	14 µM												
GhrA	1.3 µM												
$NaHCO_3$	50.0 mM												
CoA	0.5 mM												
ADP	mM	1.6	1.6	1.6	1.6	1.6	1.6	1.6	1.6	1.2	1.2	1.2	1.2
$NADP^+$	0.8 mM												
NADPH	0.8 mM												
Thylakoids	µg Chl mL^{-1}	70	70	70		70	70	70		60	60	60	
Sulforhodamine B	µM	2	8	16	40	2	8	16	40	2	8	16	40

Table M6
List of vectors used in this work.

Vector	Relevant features	Source or reference
pET28a-PPK	pET28a, SMc02148 (codon optimized Ppk2), kan^r	Nocek *et al.*, 2008 PNAS[130]
Nmar0206	pET16b, nmar0206, amp^r	Könneke *et al.* 2014, PNAS[131]
p2BP1	pLIC-SGC1, akr7a2, amp^r	Addgene plasmid #39130
pBB541	*E. coli* Chaperones GroEL, GroES, spectinomycin^r	Marco *et al.* 2007, BMC Biotechnology[132], Addgene plasmid #27394
pRKisc	*E. coli* ORF2-iscS-iscU-iscA-hscB-hscA-fdx-0RF3 Gene Cluster Involved in the Assembly of Fe-S Clusters, tet^r	Nakamura *et al.* 1999, J. Biochemistry [125]
pMCH_RS_JZ06	pET16b, mch, amp^r	Zarzycki *et al.* 2008, J. Bacteriol[133]
pMCL1_RS_JZ03	pET16b, mcl1, amp^r	Erb *et al.* 2010 J. Bacteriol[134]
JW5656	pCA24N,tiaE, cam^r, ASKA collection	Kitagawa *et al.* 2005, DNA Res[135]
JW5146	pCA24N, ycdW, cam^r, ASKA collection	Kitagawa *et al.* 2005, DNA Res[135]
JW1721	pCA24N, katE, cam^r, ASKA collection	Kitagawa *et al.* 2005, DNA Res[135]
JW3879	pCA24N, SodA, cam^r, ASKA collection	Kitagawa *et al.* 2005, DNA Res[135]
JW1648	pCA24N, SodB, cam^r, ASKA collection	Kitagawa *et al.* 2005, DNA Res[135]
pET21a(+)-fdh$_{D221A}$	pET21, fdh (D221A), amp^r	Hoelsch *et al.* 2013, Appl. Microbiol. Biotechnol.[136]
pTE22	pET16b, mcd, amp^r	Erb *et al.* 2009, Mol. Microbiol.[137]
pTE33A	pET16b, ecm, amp^r	Erb *et al.* 2008, JBC.[138]
pTE45	pET16b, epi, amp^r	Erb *et al.* 2008, JBC.[138]
pTE46	pET16b, mcm, amp^r	Schwander *et al.* 2016, Science[38]
pTE71	pET16b, ccr, amp^r	Rosenthal *et al.* 2014 Nat. Chem. Biol.[52]
pTE1012	pSEVA 471, Propionyl-CoA synthetase (*Erythrobacter* sp. Nap-1) optimized for *E. coli*	Bernhardsgrütter *et al.* 2019, JACS[122]
pTE701	pET28a, His-phaJ from *P. aeruginosa* (codon optimized), kan^r	Schwander *et al.* 2016, Science[38]
pTE2101	pET28a, ETF:QO from *P. migulae*, codon optomized, kan^r	this work, BaseClear
pTE380	pCDFDuet-1, 6xHis-sucD, yihU, streptomycin^r	Schwander *et al.* 2016, Science[38]
pTE392	pCDFDuet-1, His-etfA, etfB, *R. sphaeroides,* streptomycin^r	Schwander *et al.* 2016, Science[38]
pTE393	pRSET B, nmar0207 (codon optimized), amp^r	Schwander *et al.* 2016, Science[38]
pTE801	pET16b, mcd, amp^r	Schwander *et al.* 2016, Science[38]
pTE826	pTE16b, "pco" acx4_opt (T134I), amp^r	Schwander *et al.* 2016, Science[38]
pTE813	pET16b, "mco" mcd (T317G, W315F, E377N), amp^r	Schwander *et al.* 2016, Science[38]
pASK-IBA7-FNRCr	pASK-IBA7, n-term strep tag, FNR *C. reinhardtii*, transit peptide removed, amp^r	Rumpel *et al.*, 2014, Energy & Environmental Science[121]
pTE2001	pEX-A2-Fdx, petF *C. reinhardtii* (codon optimized), transit peptide removed, amp^r	Eurofins MWG
pTE2002	pET16b, petF *C. reinhardtii* (codon optimized), transit peptide removed, n-term strep tag, amp^r	This work
pTE2003	pEX-A2-3_Fdx, Fdx1 *S. oleracea* , Fdx2 spinach, Fdx2 *A. thaliana,* codon optimized, transit peptides removed, amp^r	Eurofins MWG
pTE2004	pET16b, Fdx1 *S. oleracea* (codon optimized), transit peptide removed, n-term strep tag, amp^r	This work

pTE2005	pET16b, petF *S. oleracea* (codon optimized), transit peptide removed, n-term strep tag, amp^r	This work
pTE2006	pEX-A2_FNRSp, FNR Spinach (codon optimized), transit peptide removed, n-term strep tag, amp^r	Eurofins MWG
pTE2007	pASK-IBA7, n-term strep tag, FNR spinach (codon optimized), transit peptide removed, amp^r	This work
pTE2008	pET16b, ETF:QO from *R. sphaeroides 2.4.1*, amp^r	This work

Table M7.
DNA sequence of the codon optimized genes used in this work

Gene name	Codon optimized DNA sequence
FdxCr (petF) from *C. reinhardtii*	TACAAGGTCACCCTGAAAACCCCTAGCGGCGATAAAACGATTGAGTGCCCAGCCGACACTTACATTTTGGA TGCTGCTGAAGAGGCGGGGCTGGACCTGCCGTATTCGTGTCGCGCGGGTGCCTGCTCTTCATGCGCGGGC AAAGTGGCCGCAGGCACCGTGGATCAAAGCGACCAGTCATTCTTAGACGATGCGCAGATGGGTAACGGTT TTGTGCTGACGTGTGTAGCTTATCCGACGAGTGATTGCACTATCCAAACACATCAGGAAGAAGCGCTGTAT TAA
FdxSp1 (Fdx1) from *S. oleracea*	GCAGCATATAAAGTGACGCTGGTGACTCCGACCGGTAACGTAGAATTTCAGTGTCCTGATGACGTCTATAT CCTTGATGCTGCTGAAGAGGAAGGCATCGATTTACCATACTCCTGTCGCGCCGGTTCGTGCTCAAGCTGCG CCGGTAAACTGAAGACGGGATCATTGAACCAAGACGATCAGAGCTTCCTGGACGACGACCAGATTGATGAA GGGTGGGTTCTGACATGCGCGGCGTACCCGGTGAGCGATGTTACCATTGAGACCCATAAGGAAGAAGAAC TCACCGCGTAA
FdxSp2 (petF) from *S. oleracea*	GCGACTTACAAAGTCACCTTAGTTACACCATCTGGTTCACAAGTTATTGAATGTGGTGACGATGAATATATC TTGGACGCCGCGGAAGAGAAAGGTATGGATCTGCCGTACTCCTGTCGCGCGGGCGCATGCTCGTCGTGCG CAGGTAAAGTAACTTCAGGCTCGGTGGACCAGAGCGATCAGAGCTTTTTGGAAGATGGACAGATGGAAGA AGGCTGGGTGCTCACATGCATAGCCTATCCGACCGGCGATGTGACGATCGAAACCCATAAGGAGGAAGAG TTGACCGCCTAA
FNRSp (FNR) from *S. oleracea*	ATGGCTAGCTGGAGTCATCCGCAATTTGAGAAAATCGAAGGTCGCCAGATTGCATCTGATGTGGAAGCCCC ACCACCCGCTCCGGCGAAAGTGGAGAAACATAGCAAAAAAATGGAAGAAGGCATCACAGTTAATAAATTTA AACCAAAAACACCTTATGTTGGACGATGCTTGTTGAATACCAAGATCACCGGCGATGACGCCCCTGGTGAG ACTTGGCACATGGTCTTCTCCCACGAAGGCGAGATCCCTTACCGTGAGGGCCAATCGGTTGGGGTCATTCC GGATGGCGAAGATAAAAATGGTAAACCGCACAAACTGAGGCTGTACTCAATAGCCAGTAGCGCATTAGGG GATTTCGGGGATGCAAAGTCCGTCTCACTGTGCGTTAAACGCCTGATTTATACTAATGACGCTGGTGAAAC CATCAAAGGCGTATGCTCGAATTTTTTATGTGATCTGAAACCGGGCGCAGAGGTAAAGTTAACGGGCCCGG TGGGTAAAGAAATGCTGATGCCGAAGGACCCCAACGCAACCATTATTATGCTCGGTACTGGGACGGGCATT GCTCCGTTTCGTTCTTTTCTTTGGAAAATGTTTTTTGAGAAACACGATGATTATAAATTCAACGGTCTCGCC TGGCTATTCCTCGGTGTCCCGACGTCCTCATCGCTGCTGTACAAGGAAGAGTTCGAGAAAATGAAGGAAAA AGCTCCGGACAACTTCCGCCTTGATTTCGCGGTGAGCCGTGAGCAGACCAACGAAAAAGGCGAAAAAATGT ATATCCAGACCCGGATGGCGCAGTACGCGGTGGAACTGTGGGAAATGTTGAAAAAGGACAACACCTATTTT TATATGTGTGGTCTGAAAGGGATGGAGAAGGGCATTGATGACATTATGGTGAGTCTTGCCGCGGCGGAAG GAATTGACTGGATCGAATACAAGCGCCAGCTGAAAAAAGCGGAACAGTGGAACGTGGAAGTGTATTGA
ETF:QO$_{pm}$ (Etf:QO) from *P. migulea*	ATGGAGCGTGAGTACATGGAATTTGATGTCGTAATTGTTGGGGCTGGTCCTGCTGGTCTTTCTGCGGCGTG TCGCTTAAAGCAAAAAGCCGCAGAGGCTGGGAAAGAAATCAGCGTATGTGTTGTTGAAAAGGGGAGTGAG GTGGGTGCTCATATCTTATCTGGTGCTGTTTTTGAGCCACGCGCCCTGAATGAGCTGTTCCCTGACTGGAA GGAACTGGGAGCCCCTCTTAACACTCCTGTAACTCGCGATGATATCTTTGTGTTGAAAAATGCGGATTCAG CACAAAAAATTCCAGACCTTTTTGTTCCAAAGACCATGCACAACGAGGGCAACTACATTATCTCCCTGGGAA ATCTGTGTCGTTGGTTGGCCCAACAAGCAGAAAACTTAGGTGTAGAGATCTACCCGGGATTTGCTGCGCAG GAGGCTCTGTTTGATGAAAATGGAGTAGTCCGTGGTATCATTACTGGGGATTTAGGTGTAGACCGTGAGG GACATCCCAAGGAGGGATTGTATACACCGGGTATGGAGTTACGTGGCAAGTATACGTTGTTCGCAGAAGG CTGCCGCGGTCATATTGGAAAACAATTGATTAAACGCTTCAACCTTGACTCGGAAGCTGATGCCCAACACT ATGGTATTGGACTTAAAGAAATCTGGGAGATCGATCCAGCCAAACATCAGCCCGGGCTGGTCGTGCACACG GCGGGCTGGCCTTTAGACATCATGGGAACTGAGAACACAGGGGGTTCGTTTTTATATCATCTTGAGAACAA CCAGGTTGTCGTCGGTTTGATCGTTGACCTTTCATACTCCAACACGTATCTGTCCCCCTTTGATGAGTTTCA GCGTTTGAAGCATCACCCTGTTCTGAAGCAGTATCTGGAGGGTGGTAAACGTATCTCGTATGGTGCACGCG CGATCTGCAAAGGCGGCCTGAACTCGCTGCCTAAAATGGTATTCAAGGGTGGTGCCCTTATCGGCTGCGAT CTTGGAACTTTAAATTTCGCGAAGATCAAAGGATCACACACCGCCATGAAGAGCGGGATGTTGGCGGCAGA AAGCGTGGCTGAGGCGCTTTTTGCGGAGAAGGATGGAACTGAGGAATTGACCACGTATGTCGATGCGTTT AAAAAATCGTGGCTTTATGACGAGTTGTTCGCCTCGCGTAATTTTGGGCCGGCTATTCACAAGTTCGGGGC CATTGTCGGTGGGGGCTTTAACTGGCTTGACCAGAATATCTTCGGAGGAAAACTTCCCTTCACGTTACACG ACACTAAGCCCGACTACGCCTGCTTGAAACTTGCAGCGGATTGTAAGAAAATCGATTATCCAAAGCCCGAC GGTAAAATCTCTTTTGACAAACTGTCTAGCGTCTTTATTTCGGGTACGAATCACGAGGAAGAACAGCCTTG TCATCTGAAATTGACCGATCCCTCCATCCCCATCGCAAAAAATTTACCCATGTACGACGAACCTGCCCAGCG CTACTGTCCCGCGGGGGTTTACGAAGTCGTGACGAAGGAGGACGGGGAGAAACGTTTCCAAATCAATGCC CAGAACTGTGTTCATTGCAAAACGTGCGACATTAAGGATCCTGCTCAGAACATCACGTGGGTAGCGCCTGA AGGTGCTGGTGGCCCAACATACCCAAATATGTAA

5. References

1 Schrödinger, E. *What is Life?: The Physical Aspect of the Living Cell.* (The University Press, 1945).

2 Mazzarello, P. A unifying concept: the history of cell theory. *Nature Cell Biology* **1**, E13-E15 (1999).

3 Koshland, D. E. The Seven Pillars of Life. *Science* **295**, 2215-2216 (2002).

4 Schwille, P. *et al.* MaxSynBio: Avenues Towards Creating Cells from the Bottom Up. *Angewandte Chemie* **57**, 13382-13392 (2018).

5 Arnold, F. H. Design by Directed Evolution. *Accounts of Chemical Research* **31**, 125-131 (1998).

6 Gleizer, S. *et al.* Conversion of *Escherichia coli* to Generate All Biomass Carbon from CO_2. *Cell* **179**, 1255-1263.e1212 (2019).

7 Adli, M. The CRISPR tool kit for genome editing and beyond. *Nature Communications* **9**, 1911 (2018).

8 Hannon, G. J. RNA interference. *Nature* **418**, 244-251 (2002).

9 Qi, L. S. *et al.* Repurposing CRISPR as an RNA-guided platform for sequence-specific control of gene expression. *Cell* **152**, 1173-1183 (2013).

10 Glass, J. I. *et al.* Essential genes of a minimal bacterium. *Proceedings of the National Academy of Sciences of the USA* **103**, 425-430 (2006).

11 Luisi, P. L. Toward the engineering of minimal living cells. *The Anatomical Record* **268**, 208-214 (2002).

12 Purnick, P. E. M. & Weiss, R. The second wave of synthetic biology: from modules to systems. *Nature Reviews Molecular Cell Biology* **10**, 410-422 (2009).

13 Rasmussen, S. *et al.* Transitions from Nonliving to Living Matter. *Science* **303**, 963-965 (2004).

14 *Frankenstein, or, The Modern Prometheus*. 1st Edition edn, (Lackington, Hughes, Harding, Mavor, & Jones, 1818).

15 Feng, X., Jia, Y., Cai, P., Fei, J. & Li, J. Coassembly of Photosystem II and ATPase as Artificial Chloroplast for Light-Driven ATP Synthesis. *ACS Nano* **10**, 556-561 (2016).

16 Lee, K. Y. *et al.* Photosynthetic artificial organelles sustain and control ATP-dependent reactions in a protocellular system. *Nature Biotechnology* **36**, 530-535 (2018).

17 Staufer, O., Schröter, M., Platzman, I. & Spatz, J. P. Bottom-Up Assembly of Functional Intracellular Synthetic Organelles by Droplet-Based Microfluidics. *Small* **16**, 1906424 (2020).

18 Monreal Santiago, G., Liu, K., Browne, W. R. & Otto, S. Emergence of light-driven protometabolism on recruitment of a photocatalytic cofactor by a self-replicator. *Nature Chemistry* **12**, 603-607 (2020).

19 Beneyton, T. *et al.* Out-of-equilibrium microcompartments for the bottom-up integration of metabolic functions. *Nature Communications* **9**, 2391 (2018).

20 Gumsley, A. P. *et al.* Timing and tempo of the Great Oxidation Event. *Proceedings of the National Academy of Sciences of the USA* **114**, 1811-1816 (2017).

21 Berkner, L. V. & Marshall, L. C. On the Origin and Rise of Oxygen Concentration in the Earth's Atmosphere. *Journal of the Atmospheric Sciences* **22**, 225-261 (1965).

22 Keeling, P. J. Diversity and evolutionary history of plastids and their hosts. *American Journal of Botany* **91**, 1481-1493 (2004).

23 Moore, K. R. *et al.* An Expanded Ribosomal Phylogeny of Cyanobacteria Supports a Deep Placement of Plastids. *Frontiers in Microbiology* **10** (2019).

24 Mareš, J., Strunecký, O., Bučinská, L. & Wiedermannová, J. Evolutionary Patterns of Thylakoid Architecture in Cyanobacteria. *Frontiers in Microbiology* **10** (2019).

25 Kramer, D. M. & Evans, J. R. The importance of energy balance in improving photosynthetic productivity. *Plant physiology* **155**, 70-78 (2011).

26 Hahn, A., Vonck, J., Mills, D. J., Meier, T. & Kühlbrandt, W. Structure, mechanism, and regulation of the chloroplast ATP synthase. *Science* **360**, eaat4318 (2018).

27 Kramer, D. M., Avenson, T. J. & Edwards, G. E. Dynamic flexibility in the light reactions of photosynthesis governed by both electron and proton transfer reactions. *Trends in Plant Science* **9**, 349-357 (2004).

28 Danielsson, R., Albertsson, P.-Å., Mamedov, F. & Styring, S. Quantification of photosystem I and II in different parts of the thylakoid membrane from spinach. *Biochimica et Biophysica Acta (BBA) - Bioenergetics* **1608**, 53-61 (2004).

29 Nishiyama, Y. *et al.* Oxidative stress inhibits the repair of photodamage to the photosynthetic machinery. *The EMBO Journal* **20**, 5587-5594 (2001).

30 Barth, C. & Krause, G. H. Study of tobacco transformants to assess the role of chloroplastic NAD(P)H dehydrogenase in photoprotection of photosystems I and II. *Planta* **216**, 273-279 (2002).

31 Munekage, Y. *et al.* PGR5 Is Involved in Cyclic Electron Flow around Photosystem I and Is Essential for Photoprotection in Arabidopsis. *Cell* **110**, 361-371 (2002).

32 Munekage, Y. *et al.* Cyclic electron flow around photosystem I is essential for photosynthesis. *Nature* **429**, 579-582 (2004).

33 Strand, D. D., Fisher, N. & Kramer, D. M. The higher plant plastid NAD(P)H dehydrogenase-like complex (NDH) is a high efficiency proton pump that increases ATP production by cyclic electron flow. *Journal of Biological Chemistry* **292**, 11850-11860 (2017).

34 Strand, D. D., Fisher, N. & Kramer, D. M. *Distinct Energetics and Regulatory Functions of the Two Major Cyclic Electron Flow Pathways in Chloroplasts*., 89-100 (Caister Academic Press, 2016).

35 Cruz, J. A. *et al.* Plasticity in light reactions of photosynthesis for energy production and photoprotection. *Journal of Experimental Botany* **56**, 395-406 (2004).

36 Allen, J. F. Photosynthesis of ATP—Electrons, Proton Pumps, Rotors, and Poise. *Cell* **110**, 273-276 (2002).

37 Zhu, X.-G., Long, S. P. & Ort, D. R. Improving Photosynthetic Efficiency for Greater Yield. *Annual Reviews in Plant Biology* **61**, 235-261 (2010).

38 Schwander, T., Schada von Borzyskowski, L., Burgener, S., Cortina, N. S. & Erb, T. J. A synthetic pathway for the fixation of carbon dioxide in vitro. *Science* **354**, 900-904 (2016).

39 Bassham, J. A., Benson, A. A. & Calvin, M. The path of carbon in photosynthesis. *The Journal of Biological Chemistry* **185**, 781-787 (1950).

40 Berg, I. A. Ecological Aspects of the Distribution of Different Autotrophic CO_2 Fixation Pathways. *Applied Environmental Microbiology* **77**, 1925-1936 (2011).

41 Sharkey, T. Estimating the rate of photorespiration in leaves. *Physiologia Plantarum* **73**, 147-152 (1988).

42 Cui, Y., Schubert, B. A. & Jahren, A. H. A 23 m.y. record of low atmospheric CO_2. *Geology* **48**, 888-892 (2020).

43 Rumble, J. R. & Rumble, J. *CRC Handbook of Chemistry and Physics, 98th Edition*. (CRC Press LLC, 2017).

44 Hanson, M. R., Lin, M. T., Carmo-Silva, A. E. & Parry, M. A. J. Towards engineering carboxysomes into C3 plants. *The Plant Journal* **87**, 38-50 (2016).

45 Kebeish, R. *et al.* Chloroplastic photorespiratory bypass increases photosynthesis and biomass production in Arabidopsis thaliana. *Nature Biotechnology* **25**, 593-599 (2007).

46 Trudeau, D. L. *et al.* Design and *in vitro* realization of carbon-conserving photorespiration. *Proceedings of the National Academy of Sciences of the USA* **115**, E11455-E11464 (2018).

47 Lefebvre, S. *et al.* Increased Sedoheptulose-1,7-Bisphosphatase Activity in Transgenic Tobacco Plants Stimulates Photosynthesis and Growth from an Early Stage in Development. *Plant Physiology* **138**, 451-460 (2005).

48 Negi, S. *et al.* Light regulation of light-harvesting antenna size substantially enhances photosynthetic efficiency and biomass yield in green algae. *The Plant Journal* **103**, 584-603 (2020).

49 RAINES, C. A. Transgenic approaches to manipulate the environmental responses of the C3 carbon fixation cycle. *Plant, Cell & Environment* **29**, 331-339 (2006).

50 Flamholz, A. I. *et al.* Revisiting Trade-offs between Rubisco Kinetic Parameters. *Biochemistry* **58**, 3365-3376 (2019).

51 Bar-Even, A., Noor, E., Lewis, N. E. & Milo, R. Design and analysis of synthetic carbon fixation pathways. *Proceedings of the National Academy of Sciences of USA* **107**, 8889-8894 (2010).

52 Rosenthal, R. G. *et al.* Direct evidence for a covalent ene adduct intermediate in NAD(P)H-dependent enzymes. *Nature Chemical Biology* **10**, 50-55 (2014).

53 Erb, T. J. *et al.* Synthesis of C_5-dicarboxylic acids from C_2-units involving crotonyl-CoA carboxylase/reductase: The ethylmalonyl-CoA pathway. *Proceedings of the National Academy of Sciences of the USA* **104**, 10631-10636 (2007).

54 Erb, T. J., Brecht, V., Fuchs, G., Müller, M. & Alber, B. E. Carboxylation mechanism and stereochemistry of crotonyl-CoA carboxylase/reductase, a carboxylating enoyl-thioester reductase. *Proceedings of the National Academy of Sciences of the USA* **106**, 8871- 8876 (2009).

55 Erb, T. J., Fuchs, G. & Alber, B. E. (2S)-Methylsuccinyl-CoA dehydrogenase closes the ethylmalonyl-CoA pathway for acetyl-CoA assimilation. *Molecular Microbiology* **73**, 902-1008 (2009).

56 Freeman Rosenzweig, E. S. *et al.* The Eukaryotic CO_2-Concentrating Organelle Is Liquid-like and Exhibits Dynamic Reorganization. *Cell* **171**, 148-162.e119 (2017).

57 Kerfeld, C. A., Aussignargues, C., Zarzycki, J., Cai, F. & Sutter, M. Bacterial microcompartments. *Nature Reviews Microbiology* **16**, 277-290 (2018).

58 Carlton, J. G., Jones, H. & Eggert, U. S. Membrane and organelle dynamics during cell division. *Nature Reviews Molecular Cell Biology* **21**, 151-166 (2020).

59 Theberge, A. B. *et al.* Microdroplets in Microfluidics: An Evolving Platform for Discoveries in Chemistry and Biology. *Angewandte Chemie International Edition* **49**, 5846-5868 (2010).

60 Caen, O. *et al.* High-throughput multiplexed fluorescence-activated droplet sorting. *Microsystems & Nanoengineering* **4**, 33 (2018).

61 Brouzes, E. *et al.* Droplet microfluidic technology for single-cell high-throughput screening. *Proceedings of the National Academy of Sciences of the USA* **106**, 14195-14200 (2009).

62 Lu, H. *et al.* High throughput single cell counting in droplet-based microfluidics. *Scientific Reports* **7**, 1366 (2017).

63 Weiss, M. *et al.* Sequential bottom-up assembly of mechanically stabilized synthetic cells by microfluidics. *Nature Materials* **17**, 89-96 (2018).

64 Beneyton, T., Love, C., Girault, M., Tang, T.-Y. D. & Baret, J.-C. High-Throughput Synthesis and Screening of Functional Coacervates Using Microfluidics. *ChemSystemsChem* (2020).

65 Shah, R. K. *et al.* Designer emulsions using microfluidics. *Materials Today* **11**, 18-27 (2008).

66 Deng, N.-N., Yelleswarapu, M. & Huck, W. T. S. Monodisperse Uni- and Multicompartment Liposomes. *Journal of the American Chemical Society* **138**, 7584-7591 (2016).

67 Deshpande, S., Caspi, Y., Meijering, A. E. C. & Dekker, C. Octanol-assisted liposome assembly on chip. *Nature Communications* **7**, 10447 (2016).

68 Yu, B., Lee, R. J. & Lee, L. J. in *Methods in Enzymology* Vol. 465 129-141 (Academic Press, 2009).

69 Baret, J.-C. Surfactants in droplet-based microfluidics. *Lab on a chip* **12**, 422-433 (2012).

70 Li, M. *et al.* A versatile platform for surface modification of microfluidic droplets. *Lab on a chip* **17**, 635-639 (2017).

71 Mason, C. B., Bricker, T. M. & Moroney, J. V. A rapid method for chloroplast isolation from the green alga Chlamydomonas reinhardtii. *Nature protocols* **1**, 2227-2230 (2006).

72 Mason, C. B., Matthews, S., Bricker, T. M. & Moroney, J. V. Simplified Procedure for the Isolation of Intact Chloroplasts from *Chlamydomonas reinhardtii*. *Plant Physiology* **97**, 1576-1580 (1991).

73 Sager, R. & Ishida, M. R. Chloroplast DNA in *Chlamydomonas*. *Proceedings of the National Academy of Sciences of the USA* **50**, 725-730 (1963).

74 Seigneurin-Berny, D., Salvi, D., Joyard, J. & Rolland, N. Purification of Intact Chloroplasts from Arabidopsis and Spinach Leaves by Isopycnic Centrifugation. *Current Protocols in Cell Biology* **40**, 3.30.31-33.30.14 (2008).

75 Galván, F., Márquez Antonio, J. & Fernández, E. Physicochemical Properties of Ferredoxin from Chlamydomonas reinhardii. *Zeitschrift fur Naturforschung. Section C, Biosciences* **40**, 373 (1985).

76 Murakami, S. & Strotmann, H. Adenylate kinase bound to the envelope membranes of spinach chloroplasts. *Archives of Biochemistry and Biophysics* **185**, 30-38 (1978).

77 Lienhard, G. E. & Secemski, I. I. P1,P5-Di(adenosine-5')pentaphosphate, a Potent Multisubstrate Inhibitor of Adenylate Kinase. *Journal of Biological Chemistry* **248**, 1121-1123 (1973).

78 Miyake, C. & Asada, K. Thylakoid-Bound Ascorbate Peroxidase in Spinach Chloroplasts and Photoreduction of Its Primary Oxidation Product Monodehydroascorbate Radicals in Thylakoids. *Plant and Cell Physiology* **33**, 541-553 (1992).

79 Nakano, Y. & Asada, K. Purification of Ascorbate Peroxidase in Spinach Chloroplasts; Its Inactivation in Ascorbate-Depleted Medium and Reactivation by Monodehydroascorbate Radical. *Plant and Cell Physiology* **28**, 131-140 (1987).

80 Ukeda, H., Maeda, S., Ishii, T. & Sawamura, M. Spectrophotometric Assay for Superoxide Dismutase Based on Tetrazolium Salt 3′-{1-[(Phenylamino)-carbonyl]-3,4-tetrazolium}-bis(4-methoxy-6-nitro)benzenesulfonic Acid Hydrate Reduction by Xanthine–Xanthine Oxidase. *Anal. Biochem.* **251**, 206-209 (1997).

81 Javier, F. P., Estela, M. V. & Carrillo, N. Oxidative Stress Causes Ferredoxin-NADP$^+$ Reductase Solubilization from the Thylakoid Membranes in Methyl Viologen-Treated Plants. *Plant Physiology* **115**, 1721-1727 (1997).

82 Zhang, J., Frerman, F. E. & Kim, J.-J. P. Structure of electron transfer flavoprotein-ubiquinone oxidoreductase and electron transfer to the mitochondrial ubiquinone pool. *Proceedings of the National Academy of Sciences of the USA* **103**, 16212-16217 (2006).

83 Miller, T. E. *et al.* Data and computational codes for: Light-powered CO_2 fixation in a chloroplast mimic with natural and synthetic parts. https://doi.org/10.5281/zenodo.3724502. *Zenodo* (2020).

84 Sokol, K. P. *et al.* Bias-free photoelectrochemical water splitting with photosystem II on a dye-sensitized photoanode wired to hydrogenase. *Nature Energy* **3**, 944-951 (2018).

85 Nuñez, M. F., Pellicer, M. T., Badia, J., Aguilar, J. & Baldoma, L. Biochemical characterization of the 2-ketoacid reductases encoded by ycdW and yiaE genes in Escherichia coli. *The Biochemical Journal* **354**, 707-715 (2001).

86 Nazhat, N. B., Golding, B. T., Johnson, G. R. A. & Jones, P. Destruction of vitamin B12 by reaction with ascorbate: The role of hydrogen peroxide and the oxidation state of cobalt. *Journal of Inorganic Biochemistry* **36**, 75-81 (1989).

87 Dewhirst, R. A. & Fry, S. C. The oxidation of dehydroascorbic acid and 2,3-diketogulonate by distinct reactive oxygen species. *The Biochemical Journal* **475**, 3451-3470 (2018).

88 Fukui, T., Shiomi, N. & Doi, Y. Expression and Characterization of (*R*)-Specific Enoyl Coenzyme A Hydratase Involved in Polyhydroxyalkanoate Biosynthesis by *Aeromonas caviae*. *Journal of Bacteriology* **180**, 667-673 (1998).

89 Sun, J., Jeffryes, J. G., Henry, C. S., Bruner, S. D. & Hanson, A. D. Metabolite damage and repair in metabolic engineering design. *Metabolic engineering* **44**, 150-159 (2017).

90 Jensen, K. H. & Zwieniecki, M. A. Physical Limits to Leaf Size in Tall Trees. *Physical Review Letters* **110**, 018104 (2013).

91 Berhanu, S., Ueda, T. & Kuruma, Y. Artificial photosynthetic cell producing energy for protein synthesis. *Nature Communications* **10**, 1325 (2019).

92 Berhanu, S., Ueda, T. & Kuruma, Y. Artificial photosynthetic cell producing energy for protein synthesis. *Nature Communications* **10**, 1325 (2019).

93 Kawakami, K. & Shen, J.-R. in *Methods in Enzymology* Vol. 613 (ed Fraser Armstrong) 1-16 (Academic Press, 2018).

94 Treves, H. *et al.* The mechanisms whereby the green alga Chlorella ohadii, isolated from desert soil crust, exhibits unparalleled photodamage resistance. *New Phytologist* **210**, 1229-1243 (2016).

95 Hodgman, C. E. & Jewett, M. C. Cell-free synthetic biology: Thinking outside the cell. *Metabolic engineering* **14**, 261-269 (2012).

96 Kulesa, A., Kehe, J., Hurtado, J. E., Tawde, P. & Blainey, P. C. Combinatorial drug discovery in nanoliter droplets. *Proceedings of the National Academy of Sciences of the USA* **115**, 6685-6690 (2018).

97 Svensson, C.-M. *et al.* Coding of Experimental Conditions in Microfluidic Droplet Assays Using Colored Beads and Machine Learning Supported Image Analysis. *Small* **15**, 1802384 (2019).

98 Singh, R. K. *et al.* Insights into Cell-Free Conversion of CO_2 to Chemicals by a Multienzyme Cascade Reaction. *ACS Catalysis* **8**, 11085-11093 (2018).

99 Shi, T., Liu, S. & Zhang, Y.-H. P. J. CO_2 fixation for malate synthesis energized by starch via in vitro metabolic engineering. *Metabolic engineering* **55**, 152-160 (2019).

100 Schada von Borzyskowski, L. *et al.* Marine Proteobacteria metabolize glycolate via the β-hydroxyaspartate cycle. *Nature* **575**, 500-504 (2019).

101 Adamala, K. P., Martin-Alarcon, D. A., Guthrie-Honea, K. R. & Boyden, E. S. Engineering genetic circuit interactions within and between synthetic minimal cells. *Nature Chemistry* **9**, 431-439 (2017).

102 Gardner, P. M., Winzer, K. & Davis, B. G. Sugar synthesis in a protocellular model leads to a cell signalling response in bacteria. *Nature Chemistry* **1**, 377-383 (2009).

103 Fanalista, F. *et al.* Shape and Size Control of Artificial Cells for Bottom-Up Biology. *ACS Nano* **13**, 5439-5450 (2019).

104 Dora. Tang, T. Y., van Swaay, D., deMello, A., Ross Anderson, J. L. & Mann, S. In vitro gene expression within membrane-free coacervate protocells. *Chemical Communications* **51**, 11429-11432 (2015).

105 Sokolova, E. *et al.* Enhanced transcription rates in membrane-free protocells formed by coacervation of cell lysate. *Proceedings of the National Academy of Sciences of the USA* **110**, 11692-11697 (2013).

106 O'Flaherty, D. K. *et al.* Copying of Mixed-Sequence RNA Templates inside Model Protocells. *Journal of the American Chemical Society* **140**, 5171-5178 (2018).

107 Tayar, A. M., Karzbrun, E., Noireaux, V. & Bar-Ziv, R. H. Synchrony and pattern formation of coupled genetic oscillators on a chip of artificial cells. *Proceedings of the National Academy of Sciences of the USA* **114**, 11609-11614 (2017).

108 Yelleswarapu, M. *et al.* Sigma Factor-Mediated Tuning of Bacterial Cell-Free Synthetic Genetic Oscillators. *ACS Synthetic Biology* **7**, 2879-2887 (2018).

109 Rivas, G., Vogel, S. K. & Schwille, P. Reconstitution of cytoskeletal protein assemblies for large-scale membrane transformation. *Current Opinion in Chemical Biology* **22**, 18-26 (2014).

110 Kurihara, K. *et al.* A recursive vesicle-based model protocell with a primitive model cell cycle. *Nature Communications* **6**, 8352 (2015).

111 Srinivas, N., Parkin, J., Seelig, G., Winfree, E. & Soloveichik, D. Enzyme-free nucleic acid dynamical systems. *Science* **358**, eaal2052 (2017).

112 Dudley, Q. M., Karim, A. S. & Jewett, M. C. Cell-free metabolic engineering: Biomanufacturing beyond the cell. *Biotechnology Journal* **10**, 69-82 (2015).

113 Noireaux, V. & Libchaber, A. A vesicle bioreactor as a step toward an artificial cell assembly. *Proceedings of the National Academy of Sciences of the USA* **101**, 17669-17674 (2004).

114 Elani, Y., Law, R. V. & Ces, O. Vesicle-based artificial cells as chemical microreactors with spatially segregated reaction pathways. *Nature Communications* **5**, 5305 (2014).

115 Godfray, H. C. J. *et al.* Food Security: The Challenge of Feeding 9 Billion People. *Science* **327**, 812-818 (2010).

116 *"World Bank. 2007. World Development Report 2008 : Agriculture for Development. Washington, DC. © World Bank. https://openknowledge.worldbank.org/handle/10986/5990 License: CC BY 3.0 IGO."*.

117 Gattuso, J.-P. *et al.* Contrasting futures for ocean and society from different anthropogenic CO_2 emissions scenarios. *Science* **349**, aac4722 (2015).

118 Lindsey, A. S. & Jeskey, H. The Kolbe-Schmitt Reaction. *Chemical Reviews* **57**, 583-620 (1957).

119 Ciamician, G. The Photochemistry of the future. *Science* **36**, 385-394 (1912).

120 Peter, D. M., Vögeli, B., Cortina, N. S. & Erb, T. J. A Chemo-Enzymatic Road Map to the Synthesis of CoA Esters. *Molecules* **21**, 517-517 (2016).

121 Rumpel, S. *et al.* Enhancing hydrogen production of microalgae by redirecting electrons from photosystem I to hydrogenase. *Energy & Environmental Science* **7**, 3296-3301 (2014).

122 Bernhardsgrütter, I. *et al.* Awakening the Sleeping Carboxylase Function of Enzymes: Engineering the Natural CO_2-Binding Potential of Reductases. *Journal of the American Chemical Society* **141**, 9778-9782 (2019).

123 Tagawa, K. & Arnon, D. I. Oxidation-reduction potentials and stoichiometry of electron transfer in ferredoxins. *Biochimica et Biophysica Acta (BBA) - Bioenergetics* **153**, 602-613 (1968).

124 Shin, M. (3rd ed.) *Methods in Enzymology* Vol. 23 440-447 (Academic Press, 1971).

125 Nakamura, M., Saeki, K. & Takahashi, Y. Hyperproduction of Recombinant Ferredoxins in Escherichia coli by Coexpression of the ORF1-ORF2-iscS-iscU-iscA-hscB-hscA-fdx-ORF3 Gene Cluster1. *Journal of Biochemistry* **126**, 10-18 (1999).

126 Usselman, R. J. *et al.* Impact of Mutations on the Midpoint Potential of the [4Fe-4S]+1,+2 Cluster and on Catalytic Activity in Electron Transfer Flavoprotein-ubiquinone Oxidoreductase (ETF-QO). *Biochemistry* **47**, 92-100 (2008).

127 Porra, R. J. The chequered history of the development and use of simultaneous equations for the accurate determination of chlorophylls a and b. *Photosynthesis Research* **73**, 149-156 (2002).

128 Han, J., Gagnon, S., Eckle, T. & Borchers, C. H. Metabolomic analysis of key central carbon metabolism carboxylic acids as their 3-nitrophenylhydrazones by UPLC/ESI-MS. *Electrophoresis* **34**, 2891-2900 (2013).

129 Beneyton, T., Coldren, F., Baret, J.-C., Griffiths, A. D. & Taly, V. CotA laccase: high-throughput manipulation and analysis of recombinant enzyme libraries expressed in E. coli using droplet-based microfluidics. *Analyst* **139**, 3314-3323 (2014).

130 Nocek, B. *et al.* Polyphosphate-dependent synthesis of ATP and ADP by the family-2 polyphosphate kinases in bacteria. *Proceedings of the National Academy of Sciences of the USA* **105**, 17730-17735 (2008).

131 Könneke, M. *et al.* Ammonia-oxidizing archaea use the most energy-efficient aerobic pathway for CO_2 fixation. *Proceedings of the National Academy of Sciences of the USA* **111**, 8239-8244 (2014).

132 de Marco, A., Deuerling, E., Mogk, A., Tomoyasu, T. & Bukau, B. Chaperone-based procedure to increase yields of soluble recombinant proteins produced in E. coli. *BMC Biotechnology* **7**, 32 (2007).

133 Zarzycki, J. *et al.* Mesaconyl-Coenzyme A Hydratase, a New Enzyme of Two Central Carbon Metabolic Pathways in Bacteria. *Journal of Bacteriology* **190**, 1366-1374 (2008).

134 Erb, T. J., Frerichs-Revermann, L., Fuchs, G. & Alber, B. E. The Apparent Malate Synthase Activity of *Rhodobacter sphaeroides* Is Due to Two Paralogous Enzymes, (3*S*)-Malyl-Coenzyme A (CoA)/β-Methylmalyl-CoA Lyase and (3*S*)- Malyl-CoA Thioesterase. *Journal of Bacteriology* **192**, 1249-1258 (2010).

135 Kitagawa, M. *et al.* Complete set of ORF clones of Escherichia coli ASKA library (A Complete S et of *E. coli* K -12 ORF A rchive): Unique Resources for Biological Research. *DNA Research* **12**, 291-299 (2005).

136 Hoelsch, K., Sührer, I., Heusel, M. & Weuster-Botz, D. Engineering of formate dehydrogenase: synergistic effect of mutations affecting cofactor specificity and chemical stability. *Applied Microbiology and Biotechnology* **97**, 2473-2481 (2013).

137 Erb, T. J., Fuchs, G. & Alber, B. E. (2S)-Methylsuccinyl-CoA dehydrogenase closes the ethylmalonyl-CoA pathway for acetyl-CoA assimilation. *Molecular Microbiology* **73**, 992-1008 (2009).

138 Erb, T. J., Rétey, J., Fuchs, G. & Alber, B. E. Ethylmalonyl-CoA Mutase from Rhodobacter sphaeroides Defines a New Subclade of Coenzyme B12-dependent Acyl-CoA Mutases. *Journal of Biological Chemistry* **283**, 32283-32293 (2008).

139 Kalberer, P. P., Buchanan, B. B. & Arnon, D. I. Rates of Photosynthesis by Isolated Chloroplasts. *Proceedings of the National Academy of Sciences of the USA* **57**, 1542-& (1967).

140 Heber, U., Egneus, H., Hanck, U., Jensen, M. & Köster, S. Regulation of photosynthetic electron transport and photophosphorylation in intact chloroplasts and leaves of Spinacia oleracea L. *Planta* **143**, 41-49 (1978).

141 Reeves, S. G. & Hall, D. O. The stoichiometry (ATP/2e– ratio) of non-cyclic photophosphorylation in isolated spinach chloroplasts. *Biochimica et Biophysica Acta (BBA) - Bioenergetics* **314**, 66-78 (1973).

142 Avron, M. & Gibbs, M. Carbon Dioxide Fixation in the Light and in the Dark by Isolated Spinach Chloroplasts. *Plant Physiology* **53**, 140-143 (1974).

143 Heber, U. Stoichiometry of reduction and phosphorylation during illumination of intact chloroplasts. *Biochimica et Biophysica Acta (BBA) - Bioenergetics* **305**, 140-152 (1973).

144 Heineke, D., Stitt, M. & Heldt, H. W. Effects of inorganic phosphate on the light dependent thylakoid energization of intact spinach chloroplasts. *Plant physiology* **91**, 221-226 (1989).

145 Stitt, M. Limitation of Photosynthesis by Carbon Metabolism : I. Evidence for Excess Electron Transport Capacity in Leaves Carrying Out Photosynthesis in Saturating Light and CO_2. *Plant physiology* **81**, 1115-1122 (1986).
146 Yacoby, I. *et al.* Photosynthetic electron partitioning between [FeFe]-hydrogenase and ferredoxin:NADP+-oxidoreductase (FNR) enzymes in vitro. *Proceedings of the National Academy of Sciences of the USA* **108**, 9396-9401 (2011).

6. Supplemental material

6.1. Supplementary figures

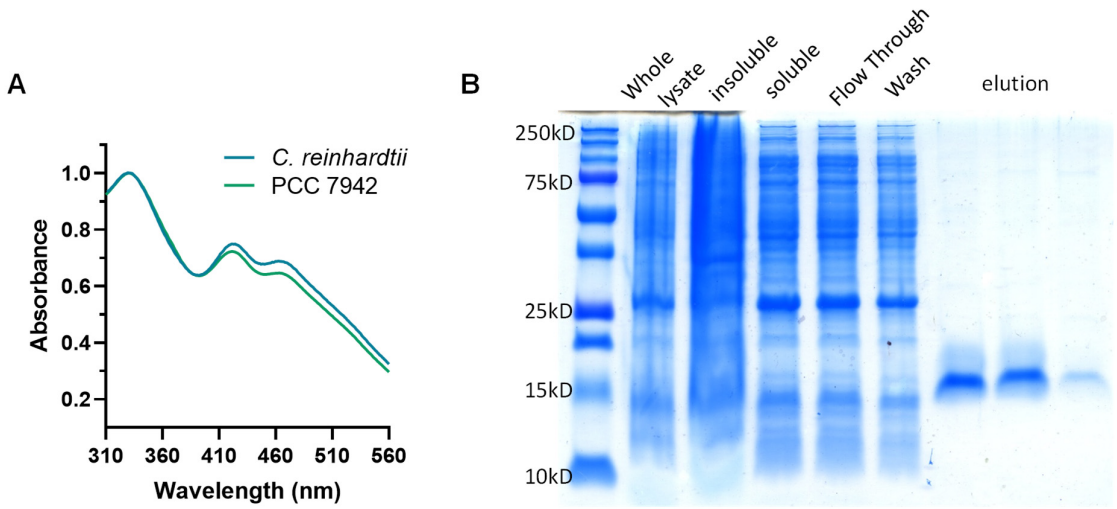

Figure S1. Ferredoxin (A) Ferredoxin absorption spectra of two fdx normalized to the maximum at 330 nM. The typical peaks for 2Fe-2S are apparent, indicating an intact iron sulphur cluster **(B)** SDS-page from a typical Fdx purification. Shown is PETF from *C. reinhardtii*.

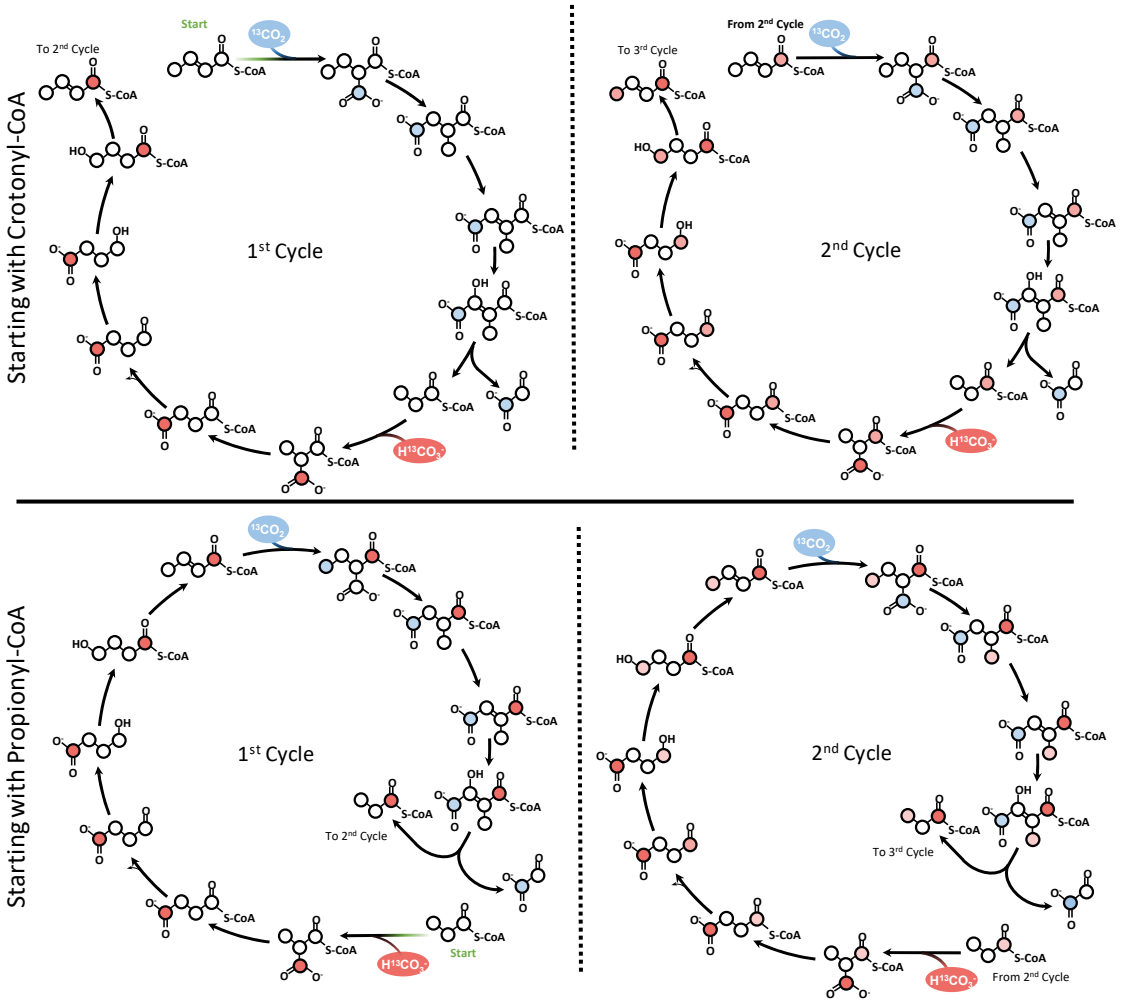

Figure S2. Expected $^{13}CO_2$ isotopic labelling pattern in the CETCH cycle: Shown is the expected labelling pattern for the four turns of the CETCH cycle starting at either crotonyl-CoA or propionyl-CoA using isotopic labelling with ^{13}C-bicarbonate. The cycle features two CO_2-incorporation steps per turn catalyzed by Ccr (shown in blue) and Pcc (shown in red). ^{13}C-labeled carbon incorporated into the C4-acceptor crotonyl-CoA by Ccr remain with the output molecule glyoxylate when β-methylmalyl-CoA is split by Mcl into propionyl-CoA and glyoxylate (position and migration of the ^{13}C-label is shown in blue). The carbon incorporated into the C3-acceptor propionyl-CoA (shown in red), stays with the acceptor molecule during each turn of the cycle (position and migration of the ^{13}C-label is indicated by different shades of red). Note that the CETCH cycle includes carbon skeleton-rearranging steps catalyzed by mutases, resulting in a complex labelling pattern.

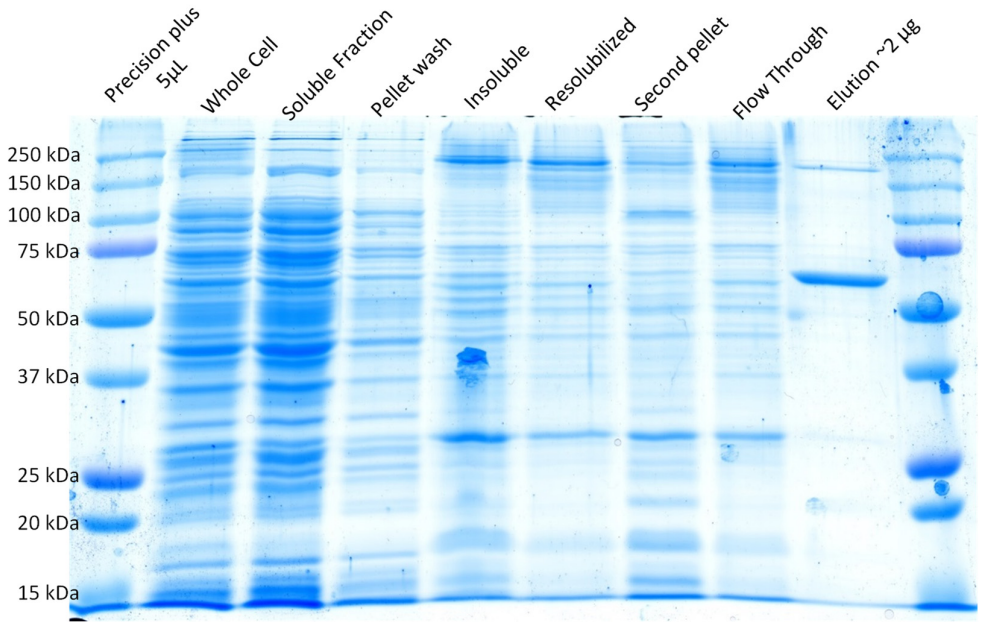

Figure S3. SDS-PAGE from a typical Etf:QO purification. Samples were loaded from each purification step. The elution band was loaded with approximately 2 µg of protein. The elution sample was not boiled.

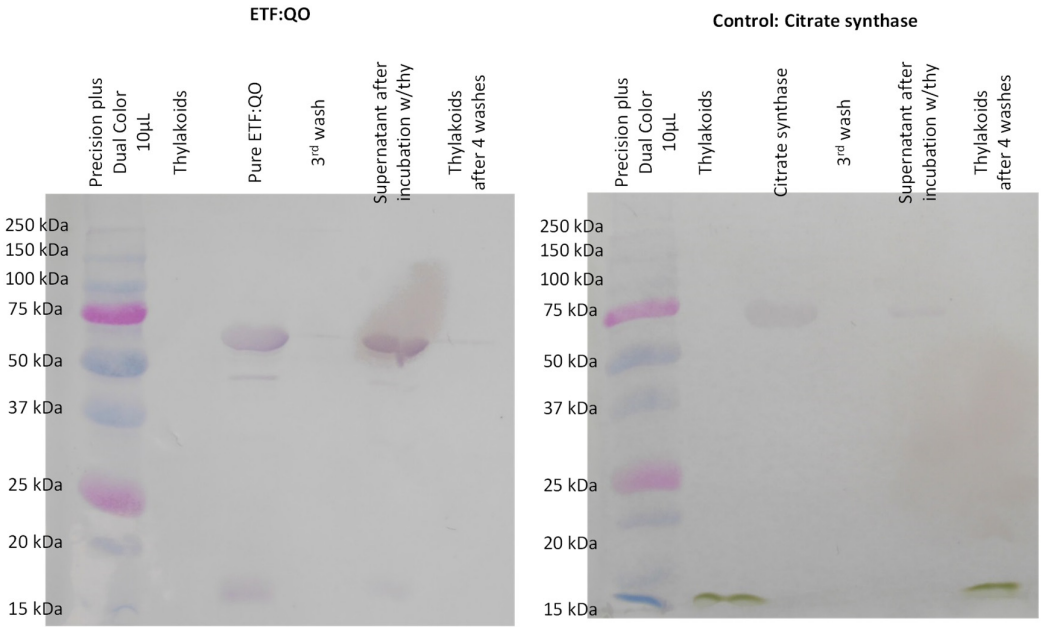

Figure S4. Etf:QO interacts with the thylakoid membrane. Etf:QO and citrate synthase were incubated with thylakoid membranes and washed. Samples were taken and blotted with an anti-his antibody. A small band is visible in samples incubated with Etf:QO and not in the control with citrate synthase.

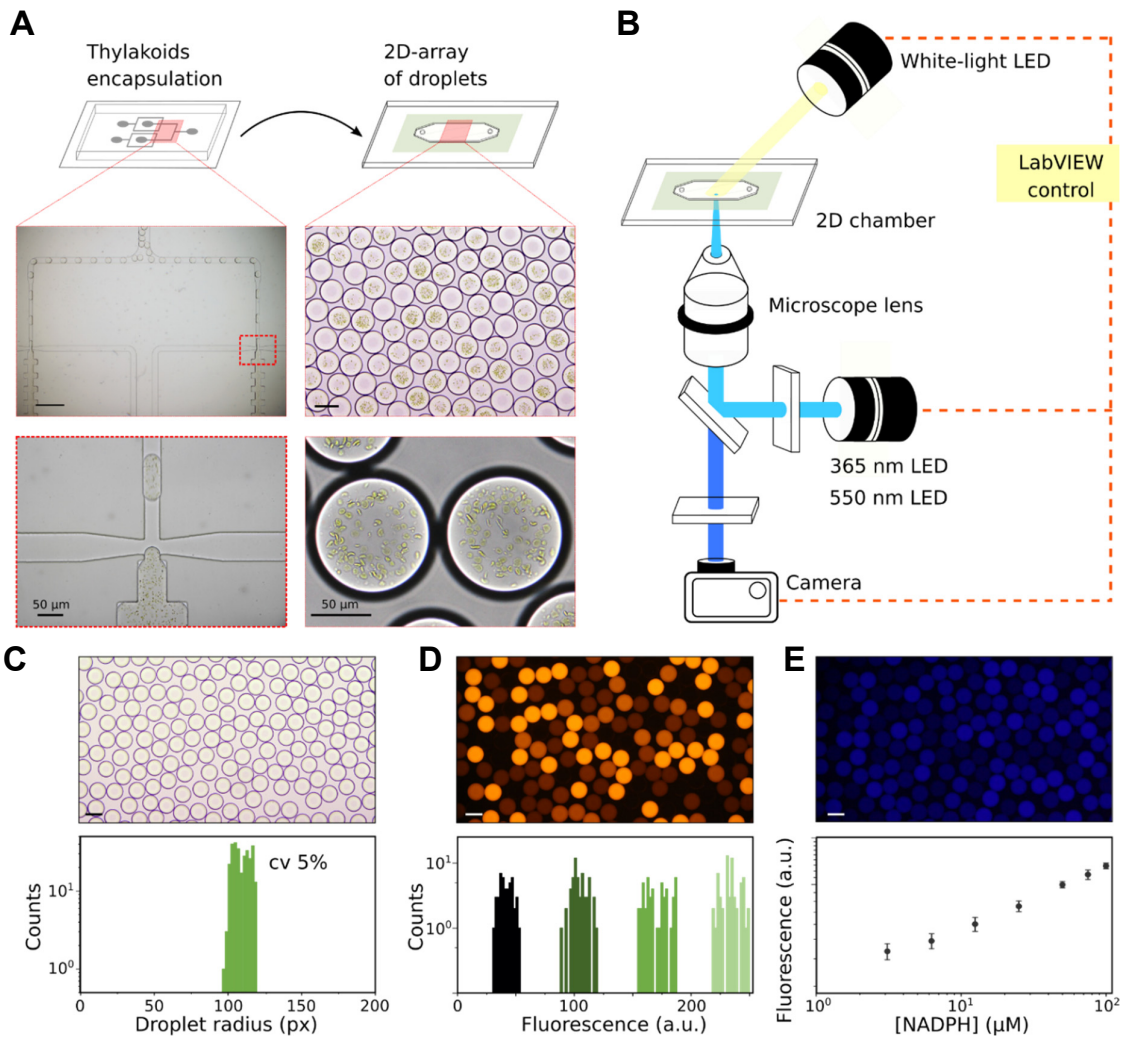

Figure S5. Description of the microfluidic platform. (**A**) Microfluidic workflow. Thylakoids are encapsulated in 300 pL water-in-oil (w/o) droplets using a dropmaker device with two parallel production nozzles (30x30 µm). Two devices are used in parallel to produce 4-bit emulsions. Droplets are then flowed into an incubation chamber and stored as a 2D-array for light activation and time-lapse microscopy imaging. (**B**) Optical setup. The 2D-incubation chamber is integrated on the stage of an inverted microscope equipped with a 10x objective. A white-light LED and a 365 nm LED are used for the light activation of the thylakoids and the NADPH fluorescence excitation, respectively. The two LEDs are triggered together with the camera using a home-made LabVIEW routine to perform automated time-lapse fluorescence imaging with defined light/dark cycles. A 550 nm LED is used for the sulforhodamine B fluorescence excitation (barcoding). (**C**) Bright-field image of a 4-bit emulsion and droplet radius distribution. (**D**) 550 nm (barcoding) fluorescence image and droplet fluorescence distribution. (**E**) 365 nm (NADPH) fluorescence image. Linear relationship between NADPH concentration and 365 nm fluorescence. Scale bars are 100 µm unless specified.

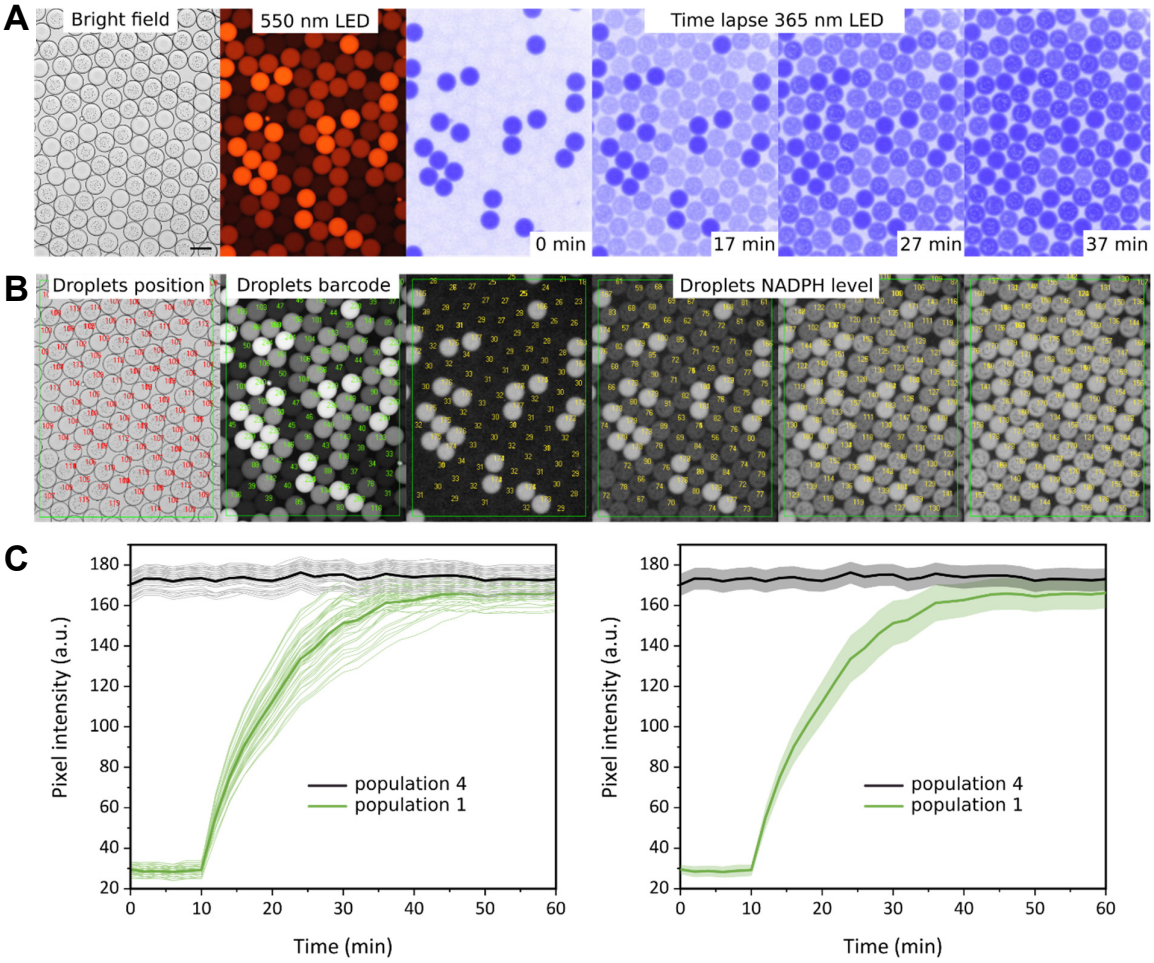

Figure S6. Image processing workflow. (**A**) Typical sequence of processed images: bright-field, 550 nm LED and 365 nm LED time-lapse images (0, 17, 27 and 37 min). Scale bars are 100 µm. (**B**) Image processing of the sequence. A region of interest is defined. Droplet positions and radii are extracted from the bright-field image. The 4-bit droplet barcoding is extracted from 550 nm fluorescence image. The NADPH level of each droplet over time is extracted from the 365 nm fluorescence time-lapse imaging. (**C**) Dynamics of NADPH concentration at the single droplet level are shown by, 365 nm fluorescence versus time for each individual droplet. The mean for each population is indicated in bold. In a typical experiment, N = 50 for each population. For more clarity, only population 1 and population 4 are shown here. On the right, the average of the same populations is shown with the corresponding standard deviation indicated by the shaded area.

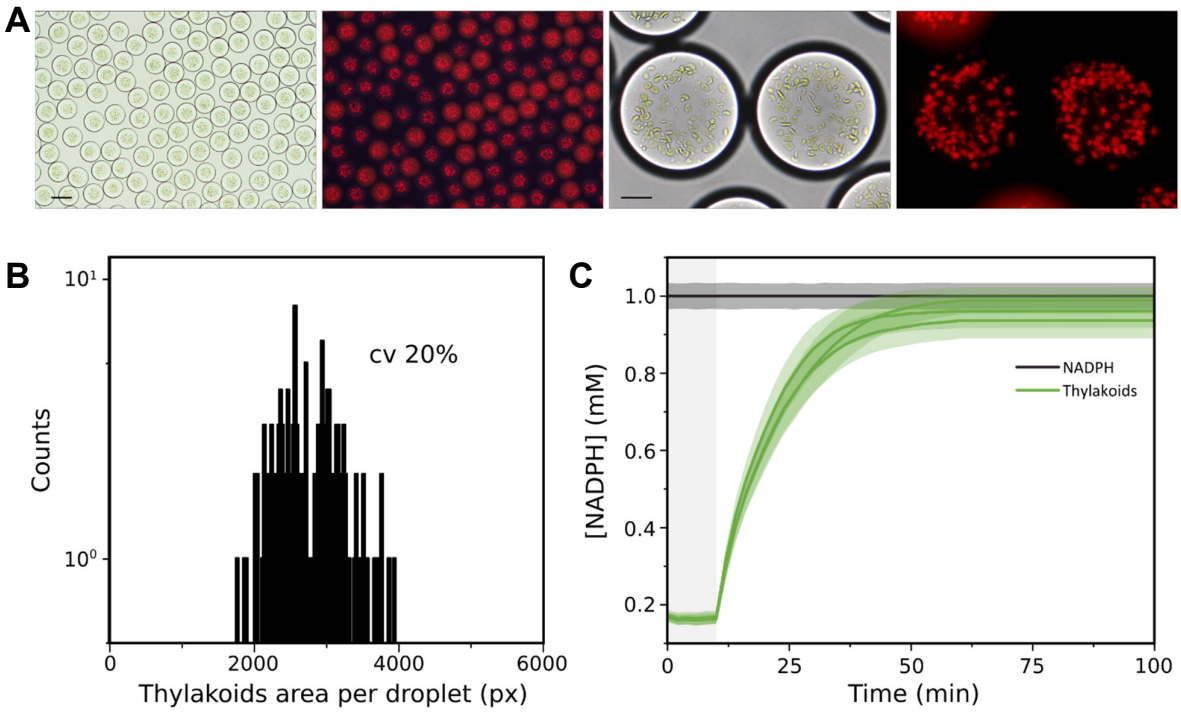

Figure S7. TEM encapsulation. (A) Bright-field and chlorophyll fluorescence images of thylakoids within 300 pL w/o droplets. Scale bars are 100 µm. **(B)** Distribution of the thylakoids: area per droplet estimated using image processing. Briefly, similar to the time-lapse algorithm, the Hough transform procedure is used on binary images to detect droplet boundaries. Then, a local threshold intensity allows the detection of thylakoids in the droplet. This step is suitable to distinguish thylakoids with a low intensity from the image background. Finally, the pixels identified as thylakoids in the droplet are summed. This process is iterated for every droplet. **(C)** NADPH production consistency. NADPH concentration over time for three different droplets populations prepared with the same initial quantity of added thylakoids normalized by total chlorophyll (125 µg Chl mL^{-1}) and containing 1 mM $NADP^+$ under continuous illumination (50 µmol photons m^{-2} s^{-1}). NADPH concentration of all populations was corrected for the non-catalytic oxidation observed in the NADPH-only control. The average measurements are indicated by a bold line with corresponding shading indicating the ± standard deviation (N = 50).

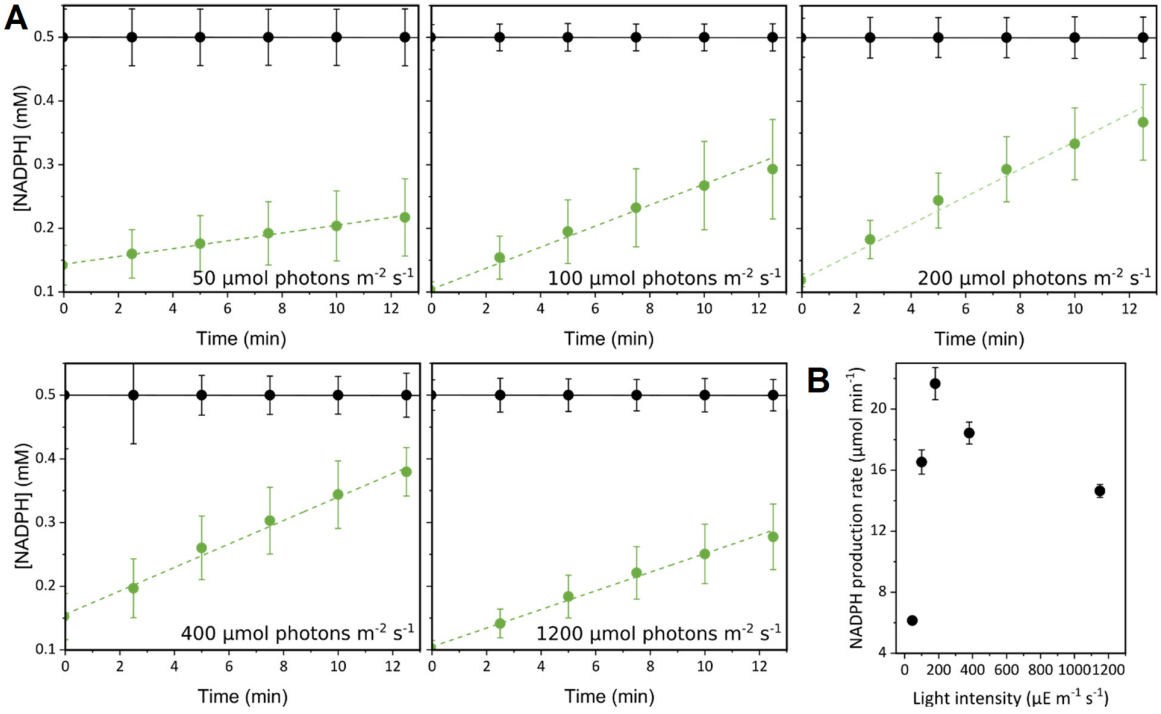

Figure S8. Effect of light intensity on NADPH production of the thylakoid energy module encapsulated in droplets. (**A**) NADPH production rates (green points) of 130 µg Chl/mL TEM encapsulated in microdroplets under continuous illumination using 50, 100, 200, 400 or 1200 µmol photons m^{-2} s^{-1} and 0.5 mM $NADP^+$. Black lines show 0.5 mM NADPH in microdroplets lacking thylakoids. (**B**) NADPH production rate versus light intensity. Maximum NADPH production of around 200 µmol photons m^{-2} s^{-1} is achieved. However, we opted to operate the TEM at 50-60 µmol photons m^{-2} s^{-1} in order to limit the production of ROS that would damage the TEM. Depicted are the mean values with error bars that correspond to ± standard deviation (*N = 50*).

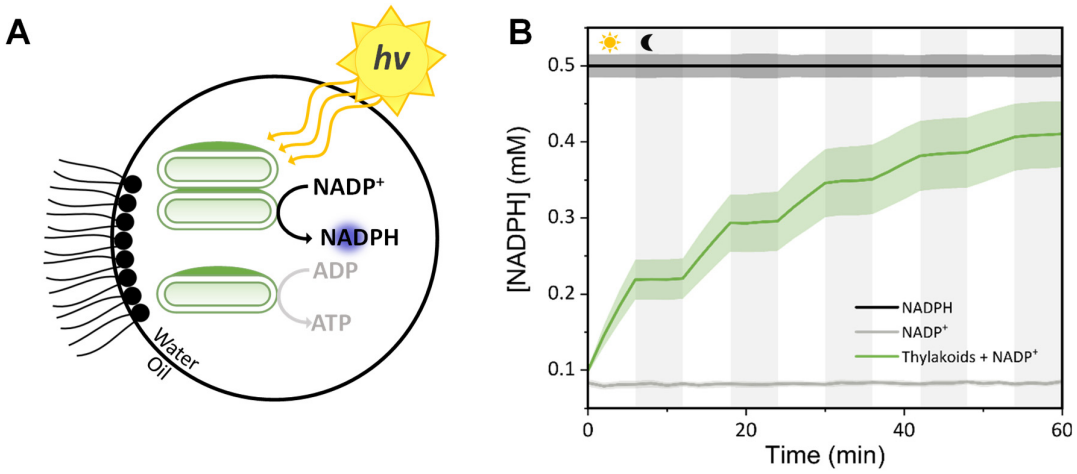

Figure S9. Control of NADPH production by thylakoids encapsulated in droplets through light-dark cycles. (**A**) Scheme of the thylakoid energy module system in microdroplets. Light triggers thylakoid activity to produce ATP and NADPH. NADPH production is monitored through fluorescence measurements. (**B**) NADPH concentration over time under programmed light-dark cycles (50 µmol photons m^{-2} s^{-1}/dark) using thylakoids (65 µg Chl mL^{-1}) and 0.5 mM $NADP^+$ (green line). NADPH production stops almost immediately when the light is turned off. Controls: 0.5 mM NADPH in droplets (black line), 0.5 mM $NADP^+$ in droplets (grey line) and TEM (65 µg Chl mL^{-1}) with 0.5 mM NADPH (green line). NADPH concentration of all populations was corrected for the non-catalytic oxidation observed in the NADPH-only control (0.5 mM NADPH in droplets, black line). This demonstrates that the energy status of the droplets can be controlled using light as an external signal. The average measurements are indicated by a bold line with corresponding shading indicating the standard deviation ($N = 50$).

Table S1.
Carbon fixation and ATP and NADPH regeneration rates of natural and synthetic systems compared to rates achieved in this study (normalized per mg chlorophyll).

Listed are CO_2-fixation, ATP and NADPH generation rates of isolated chloroplasts and thylakoids, other synthetic systems and the system of this study. For single-enzyme CO_2-fixing reactions (Ccr and Pcc), our integrated system is capable of fixing CO_2 at 124 µmoles mg Chl^{-1} h^{-1}, which is within the range of natural systems (38-280 µmoles mg Chl^{-1} h^{-1}). In bulk experiments with isolated thylakoids, NADPH and ATP regeneration rates are better than previously reported, yet lower than those measured with intact chloroplasts. In droplets, the regeneration of NADPH is of similar magnitude. Note that these rates are dependent on light intensity and could be improved by using higher light intensities. Furthermore, for the CETCH cycle operation, thylakoids are added in amounts so that cofactor regeneration is not limiting. Limiting the thylakoids would improve the rates on a per chlorophyll basis.

		Reported rates (µmoles/mg Chl/hour)		**Calculated or measured rates (µmoles/mg Chl/hour)**		
	Measurement	Carbon fixation rate	O_2 evolution	ATP	NADPH	Source
Natural	Isolated chloroplasts	50	--	--	--	Kalberer, et al. 1967[139]
	Isolated chloroplasts	130-280	--	--	--	Heber et al. 1978[140]
	Isolated chloroplasts	40-60	--	--	--	Reeves and Hall 1973[141]
	Isolated chloroplasts (Spinach)	38	--	--	--	Avron and Gibbs, 1974[142]
	Isolated chloroplasts	--	55	165*	110*	Heber, 1973[143]
	Isolated chloroplasts	--	122	367*	245*	Heineke et al., 1989[144]
	Isolated chloroplasts	--	231	693*	462*	Stitt, 1986[145]
	Isolated thylakoid membranes *(in vitro)*	--	--	--	27 ± 3	Yacoby et al., 2011[146]
Synthetic	Reconstituted photosynthetic system			0.9	--	Feng et al., 2015[15]
This work	ATP & NADPH measurements bulk	--	71.5‡	65	143	This work (Fig. 4A, 5A)
	Thylakoids in droplets	--	11.8‡	--	23.5	This work (Fig 17C)
	Ccr in droplets	6.4†	--	--	--	This work (measured values, Ccr 1-bit experiment)
	Pcc and Ccr reaction in bulk	124	30.5‡	62**	61**	This work (Fig. 9B)
	CETCH in bulk	0.55†	>2.2‡‡	--	--	This work (Fig. 14D)
	CETCH in Droplets	0.21†	>0.84‡‡	--	--	This work (CETCH v7.0 in droplets)
	ATP & NADPH measurements bulk	--	71.5‡	65	143	This work (Fig. 4A, B, and D)

* Calculated from the O_2 evolution assuming for every 1 O_2 generated there are 2 NADPH and 3 ATP produced ** From the carbon fixation rates in bulk of single carboxylation reactions † Thylakoids were added in excess. On a per Chl or PSII basis, we expect higher rates when thylakoids are limiting. ‡ Calculated with the NADPH production or from the NADPH dependent reaction, assuming a 2:1 ratio NADPH:O_2 ‡‡ Calculated with NADPH dependent reactions, 4 NADPH consumed per glycolate formed, assuming a 2:1 ratio NADPH:O_2

Table S2.
Comparison of carbon fixation and ATP regeneration rates of natural and synthetic systems compared to rates achieved in this study normalized to the chromophore

Reported CO_2-fixation rates of natural and synthetic systems compared to rates achieved in this study. As above, rates of thylakoid-powered single CO_2 fixation reactions (68,600 molecules $PSII^{-1}$ h^{-1}) are comparable to rates in natural systems (21,100-155,500 molecules $PSII^{-1}$ h^{-1}). Compared to other synthetic systems, we achieve 2 to 3 orders of magnitude higher ATP generation rates and single CO_2-fixation reactions. For all calculations, 617 chlorophylls per PS II were assumed[28], except for the system described by Lee et al. that was calculated using 35 chromophores per PS II[16].

Molecules / PSII reaction center / hour

	Measurement	Carbon fixation rate	ATP	O_2 evolution	Source
Natural	Isolated chloroplasts	27,800	--		Kalberer, et al. 1967[139]
	Isolated chloroplasts	72,200-155,500	--		Heber et. al. 1978[140]
	Isolated chloroplasts	22,200-33,300	--		Reeves and Hall, 1973[141]
	Isolated chloroplasts (Spinach)	21,100	--		Avron and Gibbs 1974[142]
Synthetic or Hybrid	CO_2 Fixation-single reaction	34*			Lee et al., 2018[16]
	ATP production		29*		Lee et al., 2018[16]
	ATP Production		500		Feng et al., 2015[15]
	O_2 evolution			9000	Sokol et al., 2018[84]
This work	ATP production		36000		This work (Fig. 5A)
	Ccr in droplets	3600†			This work (measured values, Ccr 1-bit experiment)
	Ghr in droplets	21300† **			This work (measured values, Ghr 1-bit experiment)
	O_2 evolution			26600	This work (Fig. 8B, calculated from first 2 minutes)
	Pcc and Ccr reaction in bulk	68600			This work (Fig. 14D, CETCH v6.0 in bulk)
	CETCH in bulk	303†			This work (CETCH v7.0 in droplets)
	CETCH in Droplets	119†			This work (measured values)

* Calculated using 35 chromophore per PS II[16] ** Reaction rate, not a carbon fixation rate. † thylakoids were added in excess. On a per Chl or PSII basis, we expect higher rates when thylakoids are limiting.

6.3. Supplementary movies

Movie S1.

Time-lapse of $NADP^+$ photoreduction in droplets containing various concentrations of thylakoids (experiment shown in **Figure 17B**). Images show NADPH fluorescence, excited using a 365 nm diode, images taken every 2.5 minutes.

Movie S2.

Time-lapse of NADPH oscillations in light/dark cycles of droplets containing the Ghr reaction (experiment shown in **Figure 18D**). Images show NADPH fluorescence, excited using a 365 nm diode, images taken every 2.5 minutes.

Movie S3.

Time-lapse of NADPH fluorescence of experiment demonstrating how the metabolic activity of droplets can be controlled in time and space (experiment shown in **Figure 19**). Images show NADPH fluorescence, excited using a 365 nm diode. After 2 minutes in the dark, the droplets were exposed to 50 µmol photons m^{-2} s^{-1} light. The light was turned off again after 60 minutes. The images were taken every minute for the first 5 minutes, at 7.5 minutes, then every 5 minutes until 125 minutes, and taken every 10 minutes after that.

Movie S4.

Time-lapse of the NADPH fluorescence of droplets encapsulated with variations of the full CETCH cycle (experiment shown in **Figure 26B & C,** detailed droplet contents can be found in Table S7). Images show NADPH fluorescence, excited using a 365 nm diode. The images are taken every 2.5 minutes.

7. List of abbreviations

ATP	Adenosine triphosphate
Cat	Catalase
CETCH cycle	Crotonyl-CoA Ethylmalonyl-CoA 4-hydroxybutyryl-CoA cycle
DAPP	Diadenosine triphosphate
E. coli	*Escherichia coli*
FAD	flavin adenine dinucleotide
Fdx	Ferredoxin
FNR	Ferredoxin:$NADP^+$ reductase
R. sphaeroides	*Rhodobacter sphaeroides* 2.4.1
Spinach	*Spinacia oleracea*
DMSO	dimethyl sulfoxide
DNA	deoxyribonucleic acid
DNase	deoxyribonuclease
Ecm	ethylmalonyl-CoA mutase
Hbd	4-hydroxybutyryl-CoA dehydratase
Hbs	4-hydroxybutyryl-CoA synthetase
HEPES	4-(2-hydroxyethyl)-1-piperazineethanesulfonic acid
HPLC-MS	high performance liquid chromatography coupled massspectrometry
IPTG	isopropyl β-D-1-thiogalactopyranoside
LB	lysogeny broth
Mcl	β-methylmalonyl-CoA mutase
Mcm	methylmalonyl-CoA mutase
Mco	methylsuccinyl-CoA oxidase
MOPS	3-(N-morpholino)propanesulfonic acid
NADH	Nicotinamide adenine dinucleotide
NADPH	nicotinamide adenine dinucleotide phosphate
NPT	nitro blue tetrazolium
Pcc	propionyl-CoA carboxylase
Pco	propionyl-CoA oxidase
Pcs	propionyl-CoA synthase
PMF	proton motive force
RuBisCO	ribulose-1,5-bisphosphate carboxylase/oxygenase
Sod	Superoxide dismutase
SucD	succinyl-CoA reductase

TaCo pathway	tartronyl-CoA pathway
Tris	tris(hydroxymethyl)aminomethane
w/o	water-in-oil
wt	wildtype

8. Acknowledgements

Reaching the end of this chapter required an astonishing amount of support from my friends, colleagues, family, and mentors. They have continually challenged me to be better. I am often pretty cheesy, but I would like to take a moment and go "full cheese" and to tell some of the people that helped me through this time how much their support has meant to me. They have made my journey a more fulfilling and rich experience! Overall, they made the road a little smoother when the road was rocky, and simply more enjoyable for the whole journey.

First, and foremost, thank you **Tobi** for believing in me and giving me a project that I could make my own. You gave me the means to freely explore and make this work something novel. Your support through this time was fundamental.

Furthermore, thank you to the members of my Thesis Advisory Committee, **Stefan Rensing**, **Martin Thanbichler**, and **Felix Willmund**. Your input and support has been invaluable throughout this process. I am grateful that I have had your knowledge and support to lean on.

I would like to thank **Jean-Christophe Baret** and **Thomas Beneyton** for giving me a second lab, teaching me, and taking this work to another level. I am impressed by your knowledge, creativity, and approach to science. I will always look up to you. Thank you to all of the members of the Baret group for making me feel welcome and helping me with my work.

I would like to thank **Thomy** for being there, teaching me the art of cycling, and trusting me to continue your legacy. Your achievements were a huge goal to live up to. I hope that I did the CETCH cycle some justice and shed a bit of **light** on it.

Thank you **Jan,** for helping me get where I am today, literally and figuratively, from encouraging me to *physically* move across the ocean, to encouraging me to put things on paper. You are a wonderful friend.

I would like to give a special shout out to **Dr. DD Strand** for letting me be stupid but, bluntly and kindly correcting me and patiently teaching me. You were there for the stuff my own lab didn't know about. Thank you for going on this German adventure with me.

I would like to thank **Dr. Work** for helping me believe in myself and listening to my woes and worries. This last year challenged me in ways I haven't experienced before and you were there to listen.

I would like to thank **Basti** for his ability to sound like a clock and remind me Tic-tock! I have been grateful for our discussions that challenged me and made me think. Your curiosity is an inspiration. I am very grateful for your friendship and support.

Thank you, **Simon**. I do not think that I could have done this without you. You are an amazing friend and an amazing scientist. You have helped me despite me challenging your patience (*in reality that statement can probably apply to anyone on this list*). Thank you for our Quod-versations that spanned the entire spectrum of topics from science to philosophy, from an atom to the universe.

Gabo, I would like to thank you for giving me CoA-esters. Also, for some other stuff; thank you for helping me smile when I was having a tough day, teaching me about Italy, and letting me unleash the cutest of memes.

Simon and **Gabo**, thank you for essential Δ nights, we had some really great discussions about FNR, along with pretty good food, and amazing laughs!

Thank you **Iria**, for your unconditional friendship, kindness, and level headedness. You have been a delightful colleague and have taught me so much. I appreciate your support on this journey. Thank you for always lending me an ear.

Nina, you are always the best photographer, thank you for capturing the most candid moments. **Kyra,** thank you for always being in those photos and taking a trip to grandma's house with me. I look forward to future adventures with you both.

Thank you **Marieke**, for encouraging me to do my initial thylakoid experiments, despite me not believing in them. Thank you for being with me through this journey, for your friendship, and support.

Thank you **Chris**, thank you for cycling with me, your engineering brain, and your support.

Thank you **Lenny**, for great conversations and your support, especially in the home stretch. Your input has been invaluable and your perspective is appreciated. Thank you for your ability to tell stories and for the comments that kept us on our toes. And of course for your *fearlessness*!

Thank you **Tan-guy**, for teaching me the history of France, your support, your perspective, and one good hand for pipetting.

Now, **"Hanna!!!," Kristen, Manuel, Stefano, Marc, & Francisco** you made my Marburg experience better in so many ways. Your friendship and support was essential to this whole process. I look up to all of you and I am inspired by your journey and the work that you do. I appreciate that our journeys overlapped here and I look forward to our future escapades across the globe.

I would like to thank my little sister, **Jazzmyn** for her love and support. And my big one, **Alicia**, for giving me a home. Thank you to the rest of my family for helping me get where I am today and supporting my pursuit of becoming a scientist. I love you.

Thank you to all of the past and current members of the Erb lab that I have may have missed in this list, you are amazing, and you are smart, caring, and kind. You are always there to help and up to having a challenging discussion. Furthermore, thank you to all my friends, family, and to my mentors, past and present, that have encouraged me and believed in me. It helped me to keep going when I did not necessarily believe in myself.

My Marburg family and Marburg itself will always have a place in my heart. It is a place where we could laugh and cry, be completely weird and unfiltered. I am sad to see this chapter end but, excited for what is next. As Ms. Frizzle said, **"Hit it Liz!"**